ENVIRONMENTAL RESEARCH PAPERS, NO. 991

An Infrared Spectral Radiance Code for the Auroral Thermosphere (AARC)

J.R. WINICK
R.H. PICARD
R.A. JOSEPH
R.D. SHARMA
P.P. WINTERSTEINER

24 November 1987

INFRARED TECHNOLOGY DIVISION PROJECT 2310
AIR FORCE GEOPHYSICS LABORATORY
HANSCOM AFB, MA 01731

This technical report has been reviewed and is approved for publication

RICHARD S. PICARD
Author

ROBERT R. O'NEIL, Chief
Infrared Dynamics Branch

FOR THE COMMANDER

RANDALL E. MURPHY, Director
Infrared Technology Division

Qualified requestors may obtain additional copies from the Defense Technical Information Center. All others should apply to the National Technical Information Service.

If your address has changed, or if you wish to be removed from the mailing list or if the addressee is no longer employed by your organization, please notify AFGL/DAA, Hanscom AFB, MA 01731. This will assist us in maintaining a current mailing list.

Do not return copies of this report unless contractual obligations or notices on a specific document requires that it be returned.

Unclassified
SECURITY CLASSIFICATION OF THIS PAGE

REPORT DOCUMENTATION PAGE

1a. REPORT SECURITY CLASSIFICATION Unclassified	1b. RESTRICTIVE MARKINGS
2a. SECURITY CLASSIFICATION AUTHORITY	3. DISTRIBUTION/AVAILABILITY OF REPORT Approved for public release; Distribution unlimited.
2b. DECLASSIFICATION/DOWNGRADING SCHEDULE	
4. PERFORMING ORGANIZATION REPORT NUMBER(S) AFGL-TR-87-0334 ERP, No. 991	5. MONITORING ORGANIZATION REPORT NUMBER(S)
6a. NAME OF PERFORMING ORGANIZATION Air Force Geophysics Laboratory 6b. OFFICE SYMBOL (If applicable) LSI	7a. NAME OF MONITORING ORGANIZATION
6c. ADDRESS (City, State, and ZIP Code) Hanscom AFB Massachusetts, 01731-5000	7b. ADDRESS (City, State, and ZIP Code)
8a. NAME OF FUNDING/SPONSORING ORGANIZATION AF Office of Scientific Research 8b. OFFICE SYMBOL (If applicable) NC	9. PROCUREMENT INSTRUMENT IDENTIFICATION NUMBER
8c. ADDRESS (City, State, and ZIP Code) AFOSR/NC Bolling AFB, DC 20332	10. SOURCE OF FUNDING NUMBERS PROGRAM ELEMENT NO. 61102F; PROJECT NO. 2310; TASK NO. G5; WORK UNIT ACCESSION NO. 02

11. TITLE (Include Security Classification)
An Infrared Spectral Radiance Code for the Auroral Thermosphere (AARC)

12. PERSONAL AUTHOR(S)
Winick, J.R., Picard, R.H., Joseph, R.A., Sharma, R.D., Wintersteiner, P.P.*

13a. TYPE OF REPORT	13b. TIME COVERED	14. DATE OF REPORT (Year, Month, Day)	15. PAGE COUNT
Scientific Interim	FROM ____ TO ____	1987 November 24	238

16. SUPPLEMENTARY NOTATION
*Arcon Corporation, 260 Bear Hill Road, Waltham, MA 02154

17. COSATI CODES			18. SUBJECT TERMS (Continue on reverse if necessary and identify by block number)
FIELD	GROUP	SUB-GROUP	
04	01		Infrared Spectroscopy; Thermosphere
20	06		Atmospheric emission; Energy deposition
			Aurora; Spectral radiance

19. ABSTRACT (Continue on reverse if necessary and identify by block number)

A first-principles scientific model for predicting the spectral radiance from the auroral thermosphere seen by an earthlimb observer is described. This model, and the resulting Auroral Atmospheric Radiance Code (AARC), describe the energy deposition in the thermosphere by primary auroral electrons and the ensuing effects. The latter include electron production and production of nonequilibrium concentrations of vibrationally and electronically excited states, by photochemical means, and by energy transfer. Relaxation of the states by collisions and radiation is described, and the transmission of the infrared radiation emitted from these states is treated. Currently, the model considers four radiators: the nitric oxide vibrational fundamental and first overtone at 2.8 and 5.3μm, the NO^+ fundamental at 4.3μm, and the CO_2 asymmetric-stretch (ν-3 mode) emission at 4.3μm. The prompt optically thin emitters (NO and NO^+) are treated in terms of stored, precalculated tables of efficiencies (photons per ion-pair). On the other hand, the CO_2 ν-3

(Continued)

20. DISTRIBUTION/AVAILABILITY OF ABSTRACT ☐ UNCLASSIFIED/UNLIMITED ☒ SAME AS RPT ☐ DTIC USERS	21. ABSTRACT SECURITY CLASSIFICATION UNCLASSIFIED
22a. NAME OF RESPONSIBLE INDIVIDUAL R.H. Picard	22b. TELEPHONE (Include Area Code) (617) 377-2222 22c. OFFICE SYMBOL LST

DD FORM 1473, 84 MAR 83 APR edition may be used until exhausted. All other editions are obsolete.

SECURITY CLASSIFICATION OF THIS PAGE
UNCLASSIFIED

Continuation of Block 19:

emission is both time-delayed and optically thick. Consequently, AARC includes both the finite time response of the CO_2 excited-state density to the auroral electrons and the calculation of radiative-transfer effects through a line-by-line transport code.

The resulting code is user-friendly and menu-driven. Standard output consists of the total radiance in a molecular band and of the spectra observed by a spectrometer of user-prescribed spectral resolution and lineshape.

Preface

This report discusses the results of recent research on modeling the infrared emission from the earth's upper atmosphere under auroral dosing conditions. One outgrowth of basic research into the radiative properties of the terrestrial thermosphere has been the issuance of a first-principles, user-friendly scientific model known as AARC (Auroral Atmospheric Radiance Code). This report serves as both a discussion of the scientific foundations of the model, as well as a user's guide to AARC. Scientists and engineers wishing a copy of the code should communicate with the authors. It is the hope of the authors that the reader will find the model both useful for scientific applications and easy to interact with (and modify, if necessary).

This research was supported by the Air Force Office of Scientific Research (AFOSR) through Project 2310. We are grateful to Donald Ball of AFOSR and to Randall Murphy and Robert O'Neil of AFGL, for their support and encouragement. We are also grateful to A.T. Stair, Jr., for his encouragement to start work on this infrared auroral model. We benefited greatly from discussions with E.R. Hegblom and W.F. Grieder during the early phases of this work, and the structure of the resulting code shows their influence. The final version of the AURGRAF plotting program included as part of AARC was written by Armand Paboojian. We appreciate a careful reading of the manuscript by David Sparrow.

Contents

Contents (contd)

Illustrations

Tables

An Infrared Spectral Radiance Code for the Auroral Thermosphere (AARC)

1. INTRODUCTION AND OVERVIEW

The deposition of electron energy in the thermosphere during an auroral event is accompanied by the emission of copious optical radiation. The emission occurs throughout a broad spectral region ranging from the extreme ultraviolet to the infrared. Radiation of major band systems in the infrared region of the spectrum accounts for a large fraction of the total energy deposited, representing more than 20 percent of

(Received for Publication 23 November 1987)

the deposition under some circumstances.[1-3] The infrared radiation from the thermosphere plays an important role in the thermospheric heat budget,[4,5] can be used to remotely sense thermospheric state and composition[6], and may be seen as background by infrared surveillance sensors. Consequently, it is of great importance to understand how auroral activity alters the thermospheric infrared environment.

A number of experiments have been carried out at AFGL and elsewhere with this goal in mind. They involved rocketborne and satellite-borne probes[2,7-10] and, to a lesser extent, ground-based[11-13] and aircraft-based[14] instruments.

---

1. Whalen, J.A., O'Neil, R.R., and Picard R.H. (1985) "The Aurora," Chapter 12 of Handbook of Geophysics and the Space Environment, ADA 167000, A.S. Jursa, Editor. Air Force Geophysics Laboratory, Hanscom AFB, Massachusetts, pp. 12-1 to 12-42.

2. Stair, A.T., Jr., Ulwick, J.C., Baker, K.D., and Baker, D.J. (1975) Rocketborne observations of atmospheric infrared emissions in the auroral region, in Atmospheres of Earth and the Planets, B.M. McCormac, Editor. D. Reidel Publishing Co., Dordrecht, p. 335.

3. Gordiets, B.F., and Markov, M.N. (1977) Infrared radiation in the energy balance of the upper atmosphere, Kosm. Issled. 15: 725-35 [transl: (1978) Cosm. Res. 15: 633-41].

4. Kockarts, G. (1980) Nitric oxide cooling in the terrestrial thermosphere, Geophys. Res. Lett. 7: 137-40.

5. Gordiets, B.F., Kulikov, Yu.N., Markov, M.N., and Marov, M.Ya. (1982) Numerical modeling of the thermospheric heat budget, J. Geophys. Res. 87: 4504-14.

6. Zachor, A.S., and Sharma, R.D. (1985) Retrieval of non-LTE vertical structure from a spectrally resolved infrared limb radiance profile, J. Geophys. Res. 90: 467-75.

A number of open-literature, scientific models have been generated that describe the ultraviolet and visible radiation emitted by the aurorally dosed thermosphere, given the dosing conditions.[15-19] Such models analyze the chemistry, the radiation transport, and occasionally the dynamics that follow upon auroral energy deposition and

7. Baker, K.D., Baker, D.J., Ulwick, J.C., and Stair, A.T. Jr., (1977) Measurements of 1.5- to 5.3-μm infrared enhancements associated with a bright auroral breakup, J. Geophys. Res. 82: 3518.

8. Rawlins, W.T., Caledonia, G.E., Gibson, J.J., and Stair, A.T., Jr.(1981) Infrared emission from NO(Δv = 1) in an aurora: Spectral analysis and kinetic interpretation of HIRIS measurements, J. Geophys. Res. 86: 1313.

9. Reidy, W.P., Degges, T.C., Hurd, A.G., Stair, A.T., Jr., and Ulwick, J.C. (1982) Auroral nitric oxide concentration and infrared emission, J. Geophys. Res. 87: 3591-8.

10. Stair, A.T., Jr., Pritchard, J., Coleman, I., Bohne, C., Williamson, W., Rogers, J., and Rawlins, W.T. (1983) Rocketborne cryogenic (10° K) high-resolution interferometer spectrometer flight HIRIS: auroral and atmospheric IR emission spectra, Appl. Opt. 22: 1056.

11. Vallance Jones, A., and Gattinger, R.L. (1971) Infrared spectrum of aurora, in The Radiating Atmosphere, B.M. McCormac, Editor. D. Reidel, Dordrecht, pp. 176-84.

12. Baker, D., Pendleton, W., Jr., Steed, A., and Huppi, R. (1977) Near-infrared spectrum of an aurora, J. Geophys. Res. 82: 1601-9.

13. Gattinger, R.L., and Vallance Jones, A. (1981) Quantitative spectroscopy of the aurora. V. The spectrum of strong aurora between 10 000 and 16 000 Å, Can. J. Phys. 59: 480-7.

14. Huppi, R.J., and Stair, A.T., Jr. (1979) Aurorally enhanced infrared emissions, Appl. Opt. 18: 3394.

15. Vallance Jones, A. (1975) A model for the excitation of optical aurora and some of its applications, Can. J. Phys. 53: 2267-84.

determine the characteristics of the observable photon emission. Ideally, they are easy for the experienced and inexperienced user to interact with and include tools to enable a scientist or engineer to run them under a wide variety of conditions.

There is a need for an open-literature scientific model that will extend the capability to do first-principles radiance modeling in a user-friendly environment into the infrared portion of the spectrum, where many of the models available to date have tended to be of an empirical nature or systems-oriented. Among the more fundamentally oriented early codes, one should pay special notice to the ARCTIC[20] and OPTAUR/QCARC[21] codes, which were applied to the analysis of the ICECAP[2] data.

---

16. Rees, M.H. (1975) Processes and emissions associated with electron precipitation, in Atmospheres of Earth and the Planets, B.M. McCormac, Editor. D. Reidel Publishing Co., Dordrecht, pp. 323-33.

17. Meier, R.R., Conway, R.R., Feldman, P.D., Strickland, D.J., and Gentieu, E.P. (1982) Analysis of nitrogen and oxygen far UV auroral emissions, J. Geophys. Res. 87: 2444.

18. Strickland, D.J., Jasperse, J.R., and Whalen, J.A. (1983) Dependence of auroral FUV emissions on the incident electron spectrum and neutral atmosphere, J. Geophys. Res. 88: 8051-62.

19. Degen, V. Private communication.

20. Tarr, P.W., Archer, D.H., and Utterback, N.G. (1974) Studies of Auroral Simulation, DNA Report No. 3297F.

21. Hurd, A.G., Carpenter, J.W., Degges, T.C., Grieder, W.F., Reidy, W.P., Shepherd, O., Stair, A.T., Jr., O'Neil, R.R., Ulwick, J.C., Baker, D.J., and Baker, K.D. (1977) Comparison of ICECAP and EXCEDE rocket measurements with computer code predictions, AFGL-TR-77-0060, AD-A047526.

A number of aids are available in developing such a first-principles scientific model. First, as alluded to earlier, ICECAP and other AFGL experiments, as well as experiments elsewhere, have demonstrated that the radiance from several infrared molecular vibration-rotation band systems is enhanced markedly under conditions of moderate and strong dosing.[2,1] In particular, the FWI experiment, launched from Poker Flat, Alaska, into a moderate aurora in April 1983, has yielded a rich data set on the radiative properties of the auroral thermosphere in the 2 to 7 μm spectral region. The experimental data from FWI has been analyzed and modeled to increase our understanding of the aurorally dosed thermosphere.[22] This infrared data base is available as a guide in choosing the processes to include in an infrared auroral model and as a test data set with which to compare the model predictions. Secondly, a number of theoretical papers are available describing some of the basic processes, including electron-induced chemistry and radiation transport, resulting from auroral dosing of the atmosphere and required by such a first-principles model.[23-26]

22. Picard, R.H., Winick, J.R., Sharma, R.D., Zachor, A.S., Espy, P.J., and Harris, C.R. (1987) Interpretation of infrared measurements of the high-latitude thermosphere from a rocketborne interferometer, Adv. Space Res., 7(No. 10):23-30

23. Roble, R.G., and Rees, M.H. (1977) Time-dependent studies of the aurora: Effects of particle precipitation on the dynamic morphology of ionospheric and atmospheric properties, Planet. Space Sci. 25: 991-1010.

24. Kumer, J.B. (1977) Theory of the CO_2 4.3 μm aurora and related phenomena, J. Geophys. Res. 82: 2203.

25. Caledonia, G.E., and Kennealy, J.P. (1982) NO infrared radiation in the upper atmosphere, Planet. Space Sci. 30: 1043-56.

Finally, a number of laboratory spectroscopic and chemical-kinetic investigations, including those conducted at AFGL's LABCEDE and COCHISE facilities, contain useful data to incorporate into the desired infrared model.[26-29]

The current work describes a program undertaken at AFGL to develop such an auroral model. The AARC (Auroral Atmospheric Radiance Code) model has been developed as a first-principles, scientific model of the infrared behavior of the nighttime auroral thermosphere. It is easy to use and, at the same time, incorporates the latest understanding of auroral energy deposition, electron-deposition-induced chemistry, and infrared radiation transport. AARC fills the gap between scientifically well-grounded models of the visible and ultraviolet radiance from aurora, on the one hand, and empirical models of the infrared auroral radiance based on measured efficiencies, on the other. It uses the best available theoretical methods, consistent

26. Sharma, R.D., Siani, R.D., Bullitt, M.K., and Wintersteiner, P.P. (1983) A computer code to calculate emission and transmission of infrared radiation through non-equilibrium atmospheres, AFGL-TR-83-0168, ADA137162.

27. Kennealy, J.P., Del Greco, F.P., Caledonia, G.E., and Green, B.D. (1978) Nitric oxide chemiexcitation occurring in the reaction between metastable nitrogen atoms and oxygen molecules, J. Chem. Phys. 69: 1574-84.

28. Smith, M.A., Bierbaum, V.M., and Leone, S.R. (1983) Infrared chemiluminescence from vibrationally excited NO^+: product branching in the $N^+ + O_2$ ion-molecule reation, Chem. Phys. Lett. 94:398-403.

29. Green, B.D., Caledonia, G.E., Blumberg, W.A.M., and Cook, F.H. (1984) Absolute production rates and efficiencies of NO in electron-irradiated N_2/O_2 mixtures, J. Chem. Phys. 80: 773-8.

with the requirements of reasonable execution speed and computer storage, and uses available laboratory, field, and calculated inputs for chemical, spectroscopic, and aeronomic parameters.

1.1 Scientific Overview

Auroral energy deposition resulting in infrared radiance seen by a radiometer or a spectrometer is a complex process involving a number of different processes. Consequently, an infrared auroral model such as AARC requires a number of distinct elements to describe the observed radiance properly. A typical block diagram showing some of these processes and elements is shown in Figure 1. All of these elements are dealt with in some fashion by AARC, and the manner in which this is done is described in the rest of this section.

In its current implementation, AARC is basically a short-wave to medium-wave infrared model, covering the spectral range from 5000 to 1400 cm^{-1} (2 to 7 μm). The important long-wave infrared region is not covered for two related reasons: (1) There is no conclusive data showing enhancements of infrared radiation under auroral dosing conditions in the long-wave region between 1100 and 600 cm^{-1}. Some evidence for enhancements by an order-of-magnitude on the 1040-cm^{-1} ν_3 band of ozone and the 667-cm^{-1} ν_2 band of CO_2 was found in the HIRIS experiment, but the data are flawed by the tumbling of the payload and the broad angle of acceptance of the untelescoped sensor, which viewed the aurora in a half-limb geometry.[8,10] Hopefully, data from the recently launched SPIRIT interferometric probe, which is currently being

INFRARED AURORAL MODELING

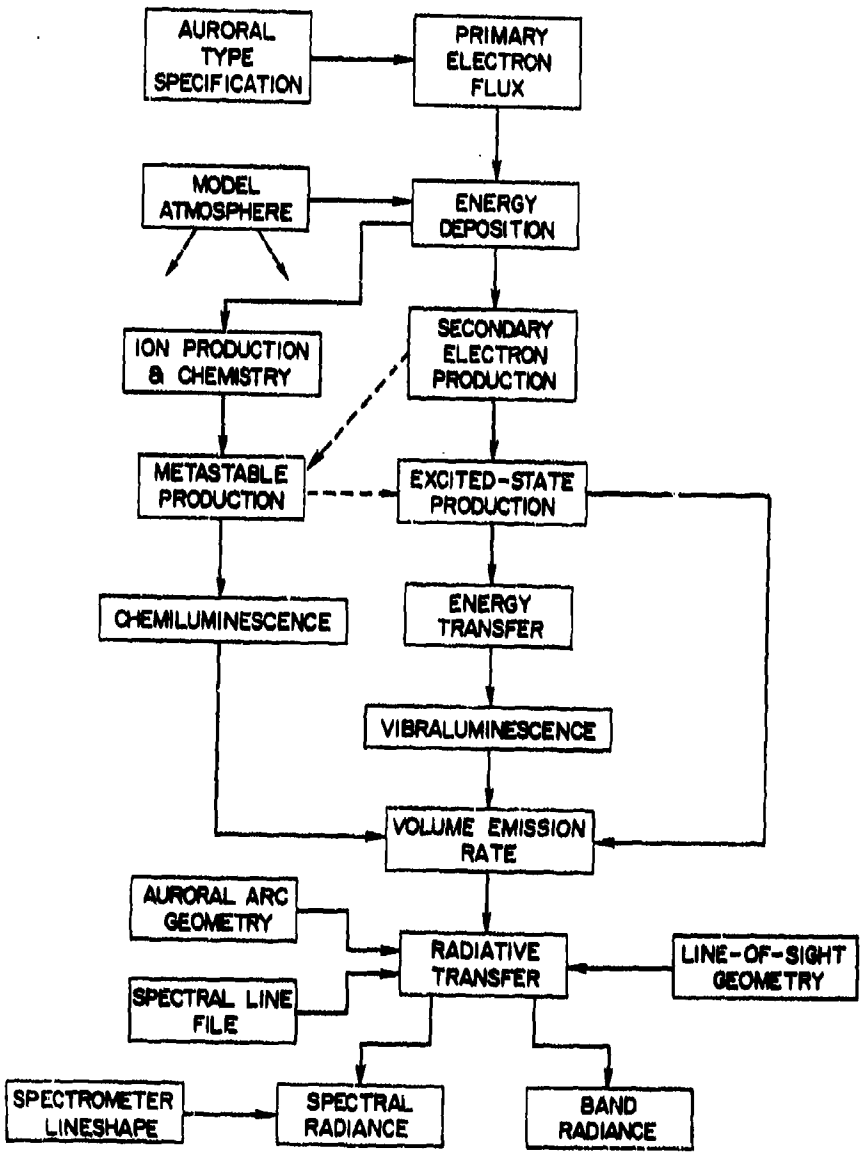

Figure 1. Schematic of the Logical Structure of Infrared Auroral Model.

analyzed, will fill this gap. (2) There is no established mechanism, with reasonably well-known rate constants and other parameters, for enhancing the long-wave radiance through auroral activity.

The altitude range of interest in AARC is 90 to 160 km. This is the main region where infrared-radiation enhancements due to auroral electrons are seen by infrared detectors. Below 90 km there is very little deposition by the typical electrons of characteristic energy ≈30 keV associated with an IBC class III^+ or IV aurora. Above 160 km, on the other hand, the infrared radiance observed in the zenith or the earthlimb is too faint to be seen by typical infrared detectors.

The main auroral radiators in the spectral range covered by AARC are the 1876-cm^{-1} (5.3-μm) fundamental bands and the 3724-cm^{-1} (2.7-μm) overtone bands of NO and the ν_3-mode fundamental bands of CO_2 near 2349 cm^{-1} (4.3 μm). These radiators are included in the AARC code, along with the weaker 2344-cm^{-1} fundamental bands of NO^+, which share the 4.3-μm region with CO_2. In the limit of zero dosing, AARC includes radiance from two radiators observed in the background atmosphere, namely the NO $v'=1 \rightarrow v''=0$ fundamental and the CO_2 ν_3 bands. Radiators in the quiescent nighttime atmosphere that are not enhanced during aurora are omitted from the code at the present time. Notably, these include the ν_1 and ν_3 modes of H_2O near 3830 cm^{-1} (2.7 μm) and its ν_2 mode near 1650 cm^{-1} (6 μm), as well as the OH fundamental Meinel bands near 3738 cm^{-1} (2.7 μm).

The AARC model includes a model atmosphere, read in from an external file. Insofar as possible the species profiles supplied have

been chosen from the 1976 U.S. Standard Atmosphere[30] (USSA 76), but the model is so structured that the user can easily replace any profile with one of his own. In one instance, namely nitric oxide, the model incorporates two species profiles with the choice between them left to the user.

Since many of the past, present, and planned experiments and many possible surveillance systems involve a limb-viewing geometry, the current issued version of AARC is set up to calculate the spectral radiance for a limb view. The altitude, latitude, and longitude of the observer are specified, as well as the azimuth and nadir angle of the line-of-sight (LOS). Zenith-viewing geometry is available in working codes used to analyze the FWI field data and will be incorporated in the next version of the code issued.

The auroral electrons are assumed to impinge on the earth's atmosphere in a discrete arc, with uniform dosing within the arc and no dosing outside the arc. The case of the isolated, discrete arc is the most important because it is the case where the largest enhancements of infrared emissions above quiescent thermospheric backgrounds are observed. At the present time, the geometry assumed for the arc boundaries is extremely simple; the boundaries are along lines of constant geographic or geomagnetic coordinates (latitude and longitude, or magnetic latitude and magnetic local time, respectively).

30. U.S. Standard Atmosphere, 1976, NOAA-S/T 76-1562. National Oceanic and Atmospheric Administration, Washington, D.C.

Energy deposition is treated by the simple, yet surprisingly accurate, semiempirical range model of Rees and Grün[31,32] starting from a specification of the primary electron spectral flux density at the top of the atmosphere. AARC also includes three precalculated and stored energy deposition profiles corresponding to typical IBC class II, III, and III$^+$ auroras. Following energy deposition, the energy degradation of the primary electrons, resulting in the production of secondary electrons, is calculated by AARC. This is necessary since secondary electrons are a very important source of molecular nitrogen in vibrationally excited states [$N_2(v)$], and the $N_2(v)$ controls the 4.3-μm radiance from CO_2 by transferring its vibrational excitation to ground-state CO_2.

In addition to electron precipitation, other phenomena occur during geomagnetically disturbed times whose effect on the infrared radiative properties should be considered. Electron precipitation is accompanied by proton and other positive-ion precipitation. However, since the protons can diffuse away from a field line due to their participation in charge-exchange reactions, the proton precipitation tends to be diffuse and not associated with discrete bright arcs where the major infrared enhancements occur. Hence, AARC neglects proton precipitation. Of more interest is Joule heating of the auroral

31. Rees, M.H. (1964) Auroral ionization and excitation by incident energetic electrons, Planet. Space Sci. 11: 1209-18.

32. Grün, A.E. (1957) Lumineszenz-photometrische Messungen der Energieabsorption im Strahlungsfeld von Elektronenquellen Eindimensionaler Fall im Luft, Z. Naturforsch. 12a: 89-95.

thermosphere due to perpendicular electric fields, which accelerate electrons and ions.[33] The resulting Pedersen currents heat the neutral atmosphere through collisions. Column-integrated Joule heating rates can equal heating rates due to particle precipitation during geomagnetically disturbed times. Thus Joule heating can modify all kinetic temperatures appreciably, alter excited-level populations, and result in increased infrared emissions. Nevertheless, there is no provision for Joule heating in the current version of the model.

The chemistry, photon emission, and radiative transfer that follow electron dosing have been handled in two different ways, depending on the radiating species. The radiating species included in AARC fall into two distinct groups. The first group (group A) consists of NO $\Delta v=1$ and $\Delta v=2$ and NO^+ $\Delta v=1$. These are species that have the following two characteristics: (1) Their chemiluminescent emission is prompt, since the time constant for the chemistry, collisional relaxation, and photon emission following energy deposition is short, say a second or less. (2) The radiation in the molecular lines is optically thin. This means that one can sum local volume emission rates to obtain total path radiance without regard for radiative transfer effects.

As a result of these characteristics of the radiating species, the following simplifications are possible. (1) The electron-deposition-induced chemistry that produces the radiating excited states is treated by a steady-state photochemical model involving ten ionic and

33. Rees, M.H. (1975) Magnetospheric substorm energy dissipation in the atmosphere, Planet. Space Sci. 23: 1589-1596.

metastable species. The vibrational relaxation of these states by collisions and radiation is also handled in a steady-state approximation. In the present version of AARC, the production and relaxation models are not issued as part of the code, but the results of the calculation are incorporated into tables of efficiencies for emission on a particular vibrational band of a radiating species -- for example, the $v'=5 \rightarrow v''=3$ NO overtone transition -- as a function of altitude. (2) No radiative transfer calculation need be done to obtain the total path radiance, and AARC simply obtains the total band radiance by adding the local emission rates, weighted by the local element of path length. For these radiators the band radiance is apportioned over lines in accordance with an effective band radiance temperature, which is calculated in the model along with the band radiance.

The second group of radiators (group B) currently consists of the most important radiating states of the CO_2 ν_3 mode, including isotopic and hot bands. The radiation from these states has the following distinguishing characteristics: (1) In contrast to the states of group A, the radiation from the states of group B is delayed. The main auroral process contributing to the CO_2 ν_3 radiance is excitation of N_2 vibration by secondary auroral electrons, followed by energy transfer from N_2 vibration to CO_2. Due to the long $N_2(v)$ - CO_2 transfer time, which can be many minutes in the altitude range of interest, the 4.3-μm CO_2 vibraluminescent emission does not follow the dosing, but lags behind it. The consequence is that a time-dependent calculation of the CO_2 vibrationally excited-state population result-

ing from thermospheric dosing must be carried out. (2) Many of the lines radiated by the group-B states are optically thick. Thus calculation of the CO_2 radiance seen by an observer requires inclusion of the effect of radiation transport. This is done in AARC by a line-by-line radiation transport computation using a modification of the NLTE code, developed originally for the case of a quiescent, spherically symmetric atmosphere.[26,34]

Transport of electrons and neutrals outside of the region where they are deposited or produced results from neutral winds, electric fields, and turbulent and molecular diffusion processes. Such transport is ignored in the AARC model.

The standard output of the model for both group A and group B radiators consists of (a) band radiances, (b) line radiances, and (c) radiance spectra. For both groups, the model makes use of a file of line positions and strengths slightly modified from the format of the AFGL Atmospheric Absorption Line Parameters Compilation, otherwise known as the HITRAN data base.[35-37] For the group-B radiators, in

34. Wintersteiner, P.P., and Sharma, R.D. (1985) Update of an Efficient Computer Code (NLTE) to Calculate Emission and Transmission of Radiation Through Non-Equilibrium Atmospheres, AFGL-TR-85-0240, AD A172556.

35. Rothman, L.S., Gamache, R.R., Barbe, A., Goldman, A., Gillis, J.R., Brown, L.R., Toth, R.A., Flaud, J.-M., and Camy-Payret, C. (1983) AFGL atmospheric absorption line parameters compilation: 1982 edition, Appl. Opt. 22: 2247.

36. Rothman, L.S., Goldman, A., Gillis, J.R., Gamache, R.R., Pickett, H.M., Poynter, R.L., Husson, N., and Chedin, A. (1982) AFGL trace gas compilation: 1982 version, Appl. Opt. 22: 1616-627.

addition to the integrated individual line radiances, the spectral profiles for individual lines are also calculated in the course of running the model, but no provision is made for examining them. It is assumed that the user has a spectrometer of only moderate resolution -- with a response function width of, say, > 0.1 cm^{-1} -- so that the much narrower molecular lines, which have Doppler widths of only 10^{-3} - 10^{-4} cm^{-1}, are, to all appearances, monochromatic radiators. A choice of spectrometer response functions is provided within the model to use in computing the radiance spectrum. In calculating the instrument-broadened spectra, the widths of the atmospheric lines are ignored, and their lineshapes are considered to be Dirac delta functions, or unit impulses, in wavenumber.

In the current issue of AARC, there is no provision internally for radiometer output. However, the user interested in simulating a radiometer observation need only provide his own routine for reading the line-radiance file and computing the sum, weighted by the spectral response function of his radiometer.

1.2 Structure of Code

The actual code for AARC, a block diagram for which is shown in Figure 2, consists of three main program modules. Module DAARC is a driver which sets up the deposition and observation conditions and

37. Rothman, L.S., Gamache, R.R., Goldman, A., Brown, L.R., Toth, R.A., Pickett, H.M., Poynter, R.L., Flaund, J.-M., Camy-Payret, C., Barke, A., Husson, N., Rinsland, C.P., and Smith, M.A.H. (1987) The HITRAN database: 1986 edition, Appl. Opt. 26: 4058-4097.

FLOW CHART - AARC

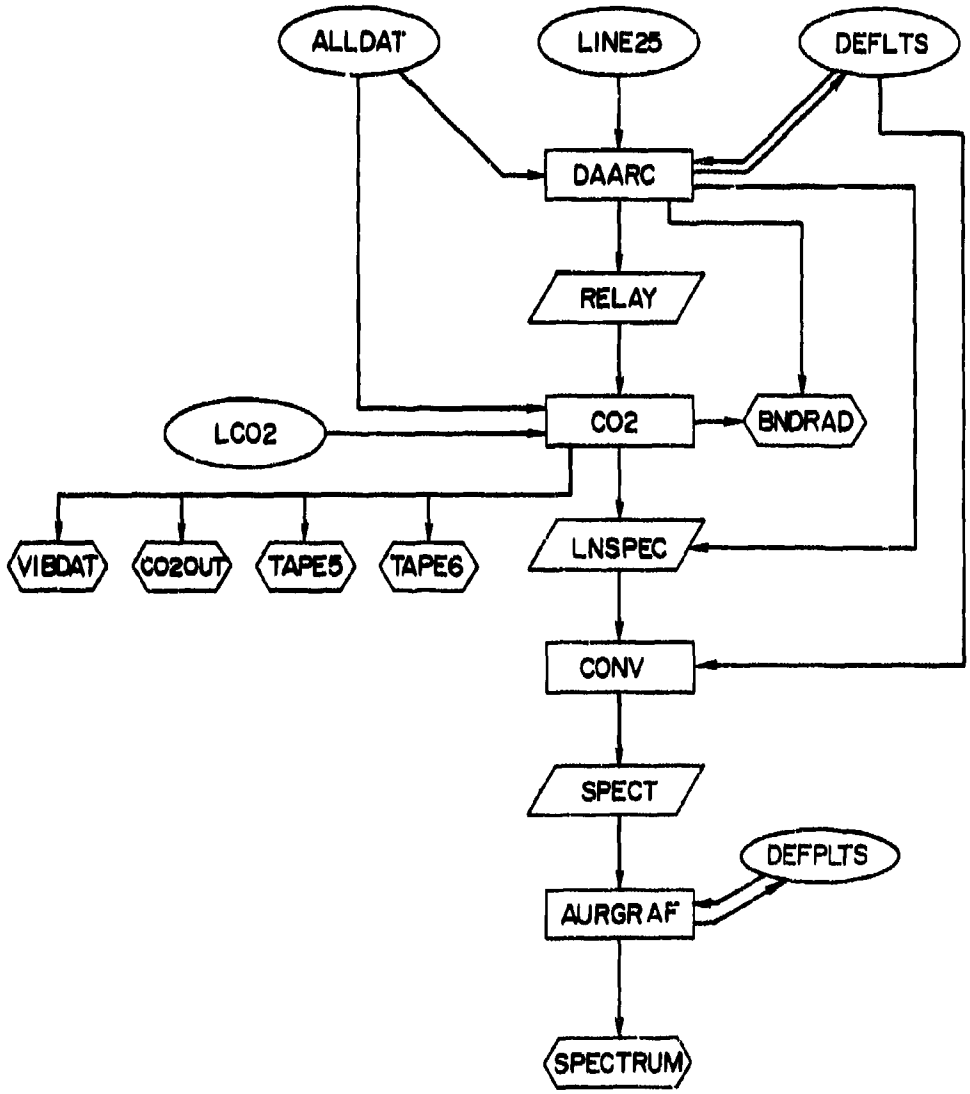

Figure 2. Flow Chart for the Auroral Atmospheric Radiance Code. Rectangular boxes enclose executable program modeules; ovals enclose input data files; parallelograms enclose intermediate output that is input to other segments; hexagons enclose final output.

calculates the band and line radiances for the group-A radiators. Module CO2 calculates the corresponding quantities for the group-B radiators. Finally, module CONV convolves the line radiances with a spectrometer response function and calculates the radiance spectrum. A fourth machine-specific module, AURGRAF, is also available to plot the resulting spectrum using modified CALCOMP library routines on AFGL's CYBER 180-860, or any other computer where they are available. Alternatively, any other available plotting package may be used.

Program DAARC contains a menu-driving routine that asks the user if he wishes to change the conditions of the calculation and allows him to input new values of the most commonly changed parameters. These values are stored in a file called DEFLTS, which provides default values of parameters for the next run and is automatically updated when any changes are made. These parameters include location of observer and orientation of LOS, electron flux spectrum at the top of the atmosphere, boundaries of dosed region, duration of dosing and time after start of dosing when observation is made, spectrometer lineshape, range over which spectrum is to be computed, and spacing of spectral points. In addition, DAARC communicates with two other input files: ALLDAT contains the model atmosphere and other tabular data, while LINE25 contains the tables of spectral line positions and transition probabilities for NO and NO^+.

The calculation of radiance from group-B radiators, specifically CO_2 ν_3, is carried out in module CO2. Module CO_2 reads line positions and strengths from file LCO2 and the model atmosphere from ALLDAT.

Both DAARC and CO2 write band radiance information on file BNDRAD and line radiances on file LNSPEC. All output files, including BNDRAD and LNSPEC, include a header of about 100 lines containing the conditions and parameter values for the computation.

If the user desires to obtain the spectral radiance seen by an observer, he may then run module CONV, which reads the line radiances on LNSPEC convolves them with the chosen spectrometer response function, and writes the output spectra on file SPECT. File SPECT is available for input to another user-supplied program, such as a plotting routine. If the AFGL plotting calls are available, the user may use the program AURGRAF, which is supplied as part of the AARC code, to do the plotting. AURGRAF is supplied with a menu driver patterned after the one in DAARC. Also like DAARC, the default values of axis lengths and the plotting ranges, on both the wavenumber and spectral-radiance axes, are taken from a file, in this case the file DEFPLTS. DEFPLTS is updated using any changes to these values and saved for the next run.

1.3 Outline

In the following sections we develop the scientific foundations of the AARC model and describe the structure and use of the code in more detail. Section 2 describes the model, starting with a brief discussion of the model atmosphere in Section 2.1. The deposition of energy in the thermosphere by precipitating electrons is discussed in Section 2.2 and secondary-electron production in Section 2.3. The photochem-

istry following energy deposition is presented in Section 2.4, and collisional energy-transfer processes are discussed in Section 2.5. Sections 2.6 and 2.7 deal with geometry, the first with the geometry of the auroral arc and the second with that of the LOS. Finally, Section 2.8 deals with the generation of synthetic spectra.

The structure and usage of the AARC code is presented in Section 3, and some examples of its application are given in Section 4. Several appendixes present a description of each of the program subroutines, as well as sample input and output files.

2. THE AARC MODEL

2.1 Model Atmosphere

A simple model atmosphere is provided internally within the AARC model. The atmospheric density ρ (gm/cm^3), mean molecular mass m (amu), neutral temperature T_n (K), and number densities of neutral species required by the program are read in as functions of altitude z from a data file. Data read include profiles for the densities of the neutral species N_2, O_2, and O. The altitude range of the data is 30 to 300 km. The mixing ratios of CO_2 are also supplied between 90 and 140 km. The limb radiance from CO_2 is negligible above this altitude with sensors of typical sensitivity. In all cases but one, discussed further below, the profiles are fixed, and no choice is allowed. However, the file is clearly structured so that the user may easily

replace a profile by one of his own.

The atmospheric density ρ, mean molecular mass m, neutral temperature T_n, and number densities of N_2, O_2, and O above 86 km are all taken directly from the 1976 U.S. Standard Atmosphere.[30] Below 86 km, the number densities of N_2 and O_2 are calculated from ρ and M, assuming a uniform volume mixing ratio of 0.78084 and 0.209476, respectively, for N_2 and O_2. The nighttime atomic oxygen concentration profile below 86 km decreases rapidly to zero, consistent with photochemical models. Profiles of temperature, mass density, and concentration of major species are shown in Figure 3.

Measurements of atomic-oxygen concentration above 80 km have indicated that the density is highly variable. A summary of recent measurements has been given by Offermann et al.[38] Some of the variability is thought to be real, the atomic oxygen density appearing to depend on time of day, season, and dynamics.[39] Infrared airglow emissions from the quiescent thermosphere above 110 km altitude, notably the 5.3-μm 1-0 band of NO and the 15-μm ν_2 band of CO_2, depend strongly on atomic-oxygen density. This is because of its dominant role in collisional excitation and quenching. Nevertheless, studies have shown that many auroral emissions -- for example, aurorally produced NO vibration[25] resulting from the $N(^2D) + O_2$ reaction -- are not very

38. Offermann, D., Friedrich, V., Ross, P., and Von Zahn, U. (1981) Neutral gas composition measurements between 80 and 120 km, Planet. Space Sci. 24: 747.

39. Sharp, W.E. (1985) Upper limits to [O] in the lower thermosphere from airglow, Planet. Space Sci. 33: 571.

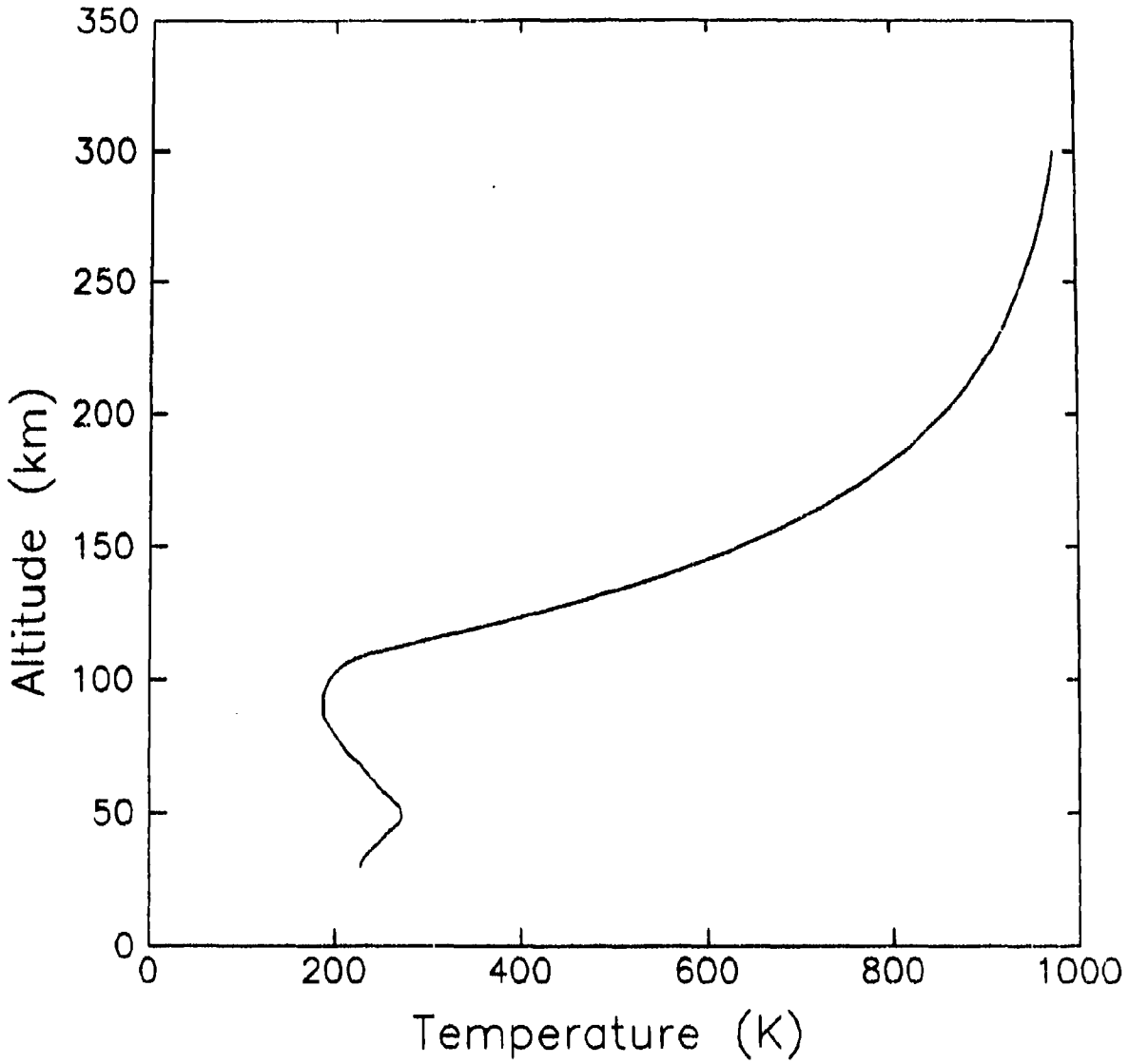

Figure 3a. Temperature Profile Supplied in ALLDAT for AARC.

sensitive to the O density. (See Section 2.4.2 and Figure 9a.)

Because NO is produced in the aurorally dosed atmosphere by the $N(^2D) + O_2$ reaction and it is a long-lived species, NO densities can reach quite large values at high latitudes during periods of auroral

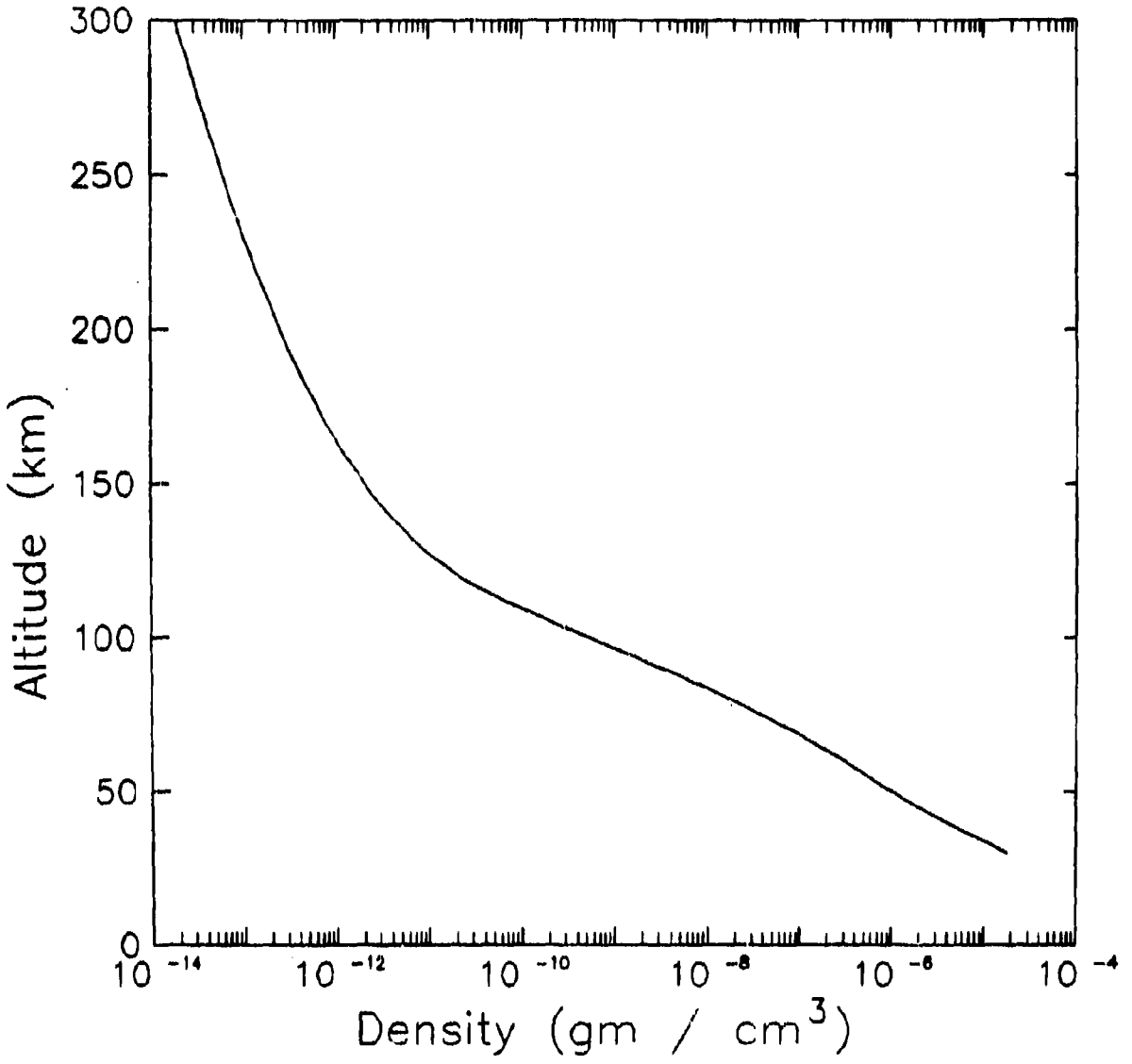

Figure 3b. Density Profile (g/cm^{-3}) Supplied in ALLDAT for AARC.

activity. Consequently, there is great variability observed in the NO density, and there can easily be an order-of-magnitude variation in the NO density observed in the auroral zone. For this reason, two NO profiles[25] are provided in the model, a medium profile appropriate to

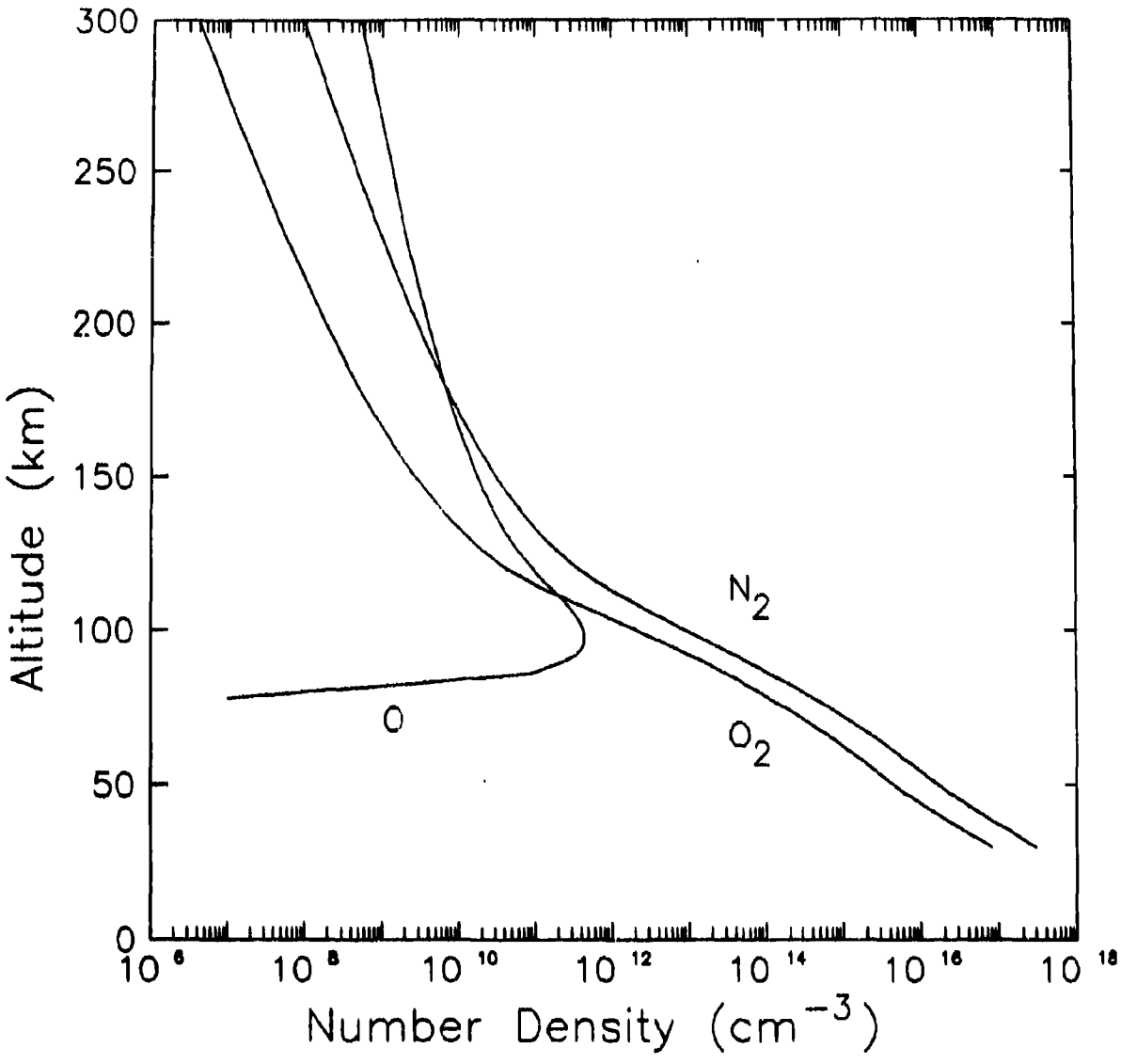

Figure 3c. Density (cm^{-3}) of Major Consituents in AARC. Note the fall off in atomic oxygen for the nighttime conditions of the model.

a quiescent atmosphere and a higher profile appropriate to an atmosphere that has been subjected to a period of strong auroral predosing. These profiles are shown in Figure 4.

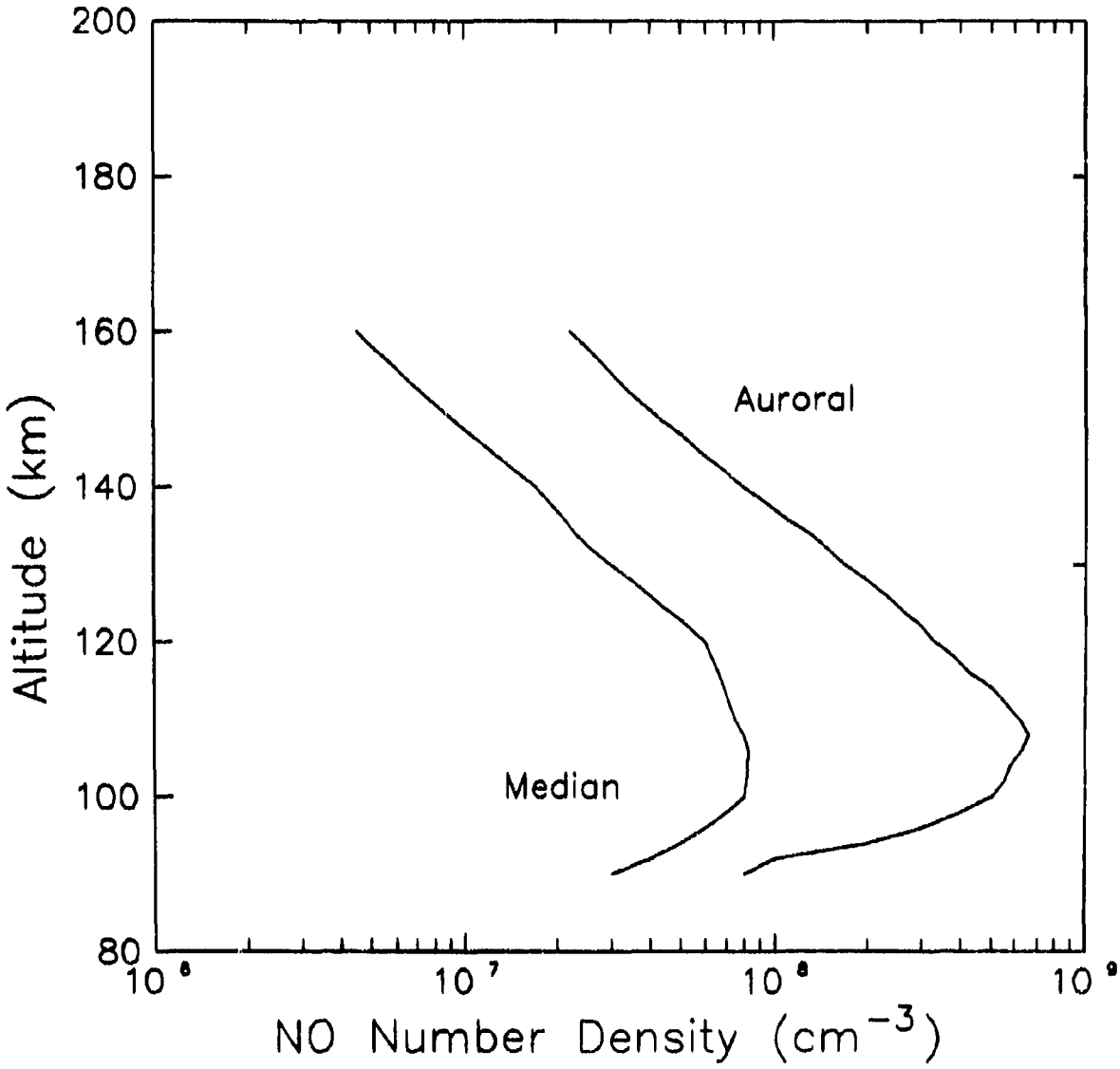

Figure 4. Density Profile for Nitric Oxide (NO). The high profile is representative of densities in active auroral arc, and the medium profile is representative of high latitude conditions outside of an active arc.

The temperature T_e of the ambient thermal electrons and the ion temperature T_i are assumed to be equal to T_n in this version of the

code; the model does not solve the electron and ion energy equations, and heating by precipitating particles or Joule heating is not considered. (See also the discussion in Section 1.1.)

2.2 Energy Deposition by Primary Auroral Electrons

2.2.1 OVERVIEW OF ENERGY-DEPOSITION CALCULATION METHODS

The problem of calculating the transport of energetic electrons in matter has received a great deal of attention for many years. Early work includes that of Bethe and co-workers,[40,41] Lewis,[42] and Spencer.[43] Chamberlain[44] surveyed early work on atmospheric energy deposition by kilovolt auroral electrons. The various approaches used can be categorized as semi-empirical, range-theoretic, Monte-Carlo, and transport-theoretic.[45]

The range-theoretic formulations most often use Bethe's formula

40. Bethe, H. (1930) Zur Theorie des Durchgangs schneller Korpuskularstrahlen durch Materie, Ann. Phys. (Leipzig) 15: 325-400.

41. Bethe, H., and Heitler, W. (1934) On the stopping of fast particles and on the creation of positive electrons, Proc. Roy. Soc. (London) A146: 83-112.

42. Lewis, H.W. (1950) Multiple scattering in an infinite medium, Phys. Rev. 178: 526-9.

43. Spencer, L.V. (1955) Theory of electron penetration, Phys. Rev. 198: 1597-1615.

44. Chamberlain, J.W. (1961) Physics of the Aurora and Airglow, Academic Press, New York, pp. 284-92.

45. Jasperse, J.R., and Strickland, D.J. (1981) Approximate Analytic Solutions for the Primary Auroral Electron Flux and Related Quantities, AFGL-TR-81-0069, ADA102905.

for the stopping power[45,46] and express the continuous electron energy loss in terms of a loss function.[47,48] Monte-Carlo calculations[49-51] have been used to calculate altitude profiles of energy deposition, back-scattering coefficients, and energy spectra for energetic electrons in the atmosphere.

Transport models are potentially more versatile and accurate and have received considerable attention in recent years. Walt et al[52] solved the Fokker-Planck equation to obtain energy-deposition profiles and pitch-angle distributions for auroral electrons within the constraints of small-angle scattering and the continuous-energy-loss ap-

46. Bethe, H. (1933) "Quantenmechanik der Ein- und Zwei-Elektronenprobleme," Chapter 3 of Handbuch der Physik, Vol. 24/1, H. Geiger and K. Scheel, Editors. Springer-Verlag, Berlin, pp. 273-560.

47. Green, A.E.S., and Barth, C.A. (1965) Calculations of ultraviolet molecular nitrogen emissions from the aurora, J. Geophys. Res. 170:1083-92.

48. Peterson, L.R., Sawada, T., Bass, J.N., and Green, A.E.S. (1973) Electron energy deposition in a gaseous mixture, Comp. Phys. Commun. 15: 239-62.

49. Maeda, K. (1965) Diffusion of low-energy auroral electrons in the atmosphere, J. Atm. Terr. Phys. 127: 259.

50. Berger, M.J., Seltzer, S.M., and Maeda, K. (1970) Energy deposition by auroral electrons in the atmosphere, J. Atm. Terr. Phys. 132: 1015-45.

51. Berger, M.J., Seltzer, S.M., and Maeda, K. (1974) Some new results on electron transport in the atmosphere, J. Atm. Terr. Phys. 136: 591-617.

52. Walt, M., MacDonald, W.M., and Francis, W.E. (1967) "Penetration of auroral electrons into the atmosphere," in Physics of the Magnetosphere, R.L. Carovillano, J.F. McClay, and H.R. Radoski, Editors. D. Reidel Publishing Company, Dordrecht, Netherlands, p. 354.

proximation. Banks et al[53] combined the Fokker-Planck method for electron energies greater than 0.5 keV with an approximate two-stream approach for low energy electrons due to Banks and Nagy[54] capable of accounting for discrete energy loss. Numerical treatments of auroral electron transport using the linearized Boltzmann equation have been proposed and elaborated by Strickland et al.[55] and by Stamnes.[56,57] The latter treatments are not restricted to near-forward scattering and allow for discrete energy loss. An analytic solution to the linear auroral-electron transport equation was carried out by Jasperse and Strickland,[45] assuming small-angle scattering, an average-discrete-energy-loss approximation, and a pseudoparticle scattering approach.

53. Banks, P.M., Chappell, C.R., and Nagy, A.F. (1974) A new model for the interaction of auroral electrons with the atmosphere: Spectral degradation, backscatter, optical emission, and ionization, J. Geophys. Res. 179: 1459-70.

54. Banks, P.M., and Nagy, A.F. (1970) Concerning the influence of elastic scattering upon photoelectron transport and escape, J. Geophys. Res. 175: 1902.

55. Strickland, D.J., Book, D.L., Coffey, T.P., and Fedder, J.A. (1976) Transport equation techniques for the deposition of auroral electrons, J. Geophys. Res. 181: 2755-64.

56. Stamnes, K. (1980) Analytic approach to auroral electron-transport and energy degradation, Planet. Space Sci. 28:427-441.

57. Stamnes, K. (1981) On the two-stream approach to electron transport and thermalization, J. Geophys. Res. 86:2405-2410.

2.2.2 ENERGY DEPOSITION IN AARC

One of the earliest, simplest, and most fruitful approaches to the auroral-electron energy-deposition problem has been the semi-empirical approach pioneered by Rees.[31] Rees's model is used in AARC to describe electron energy deposition. It has also been used in a number of other codes predicting auroral emissions from atomic and molecular electronic transitions[15] and infrared vibrational transitions.[21]

Rees's approach is based on luminescence measurements of energy deposition from a point source of collimated electrons in laboratory air by Grün.[32] For primary electron energies E_0 from 5 to 54 keV and for a monodirectional incident flux, Grün obtained three-dimensional energy deposition profiles, as well as the stopping power, or rate of electron energy loss (eV cm^2/gm electron)

$$\alpha(Z, E_0) = - \frac{dE_0}{dZ} , \qquad (2\text{-}1)$$

Here α is expressed as a function of Z, the integrated column mass density (gm/cm^2)

$$Z(z) = \int_z^\infty dz' \ \rho(z') \ \frac{ds}{dz'} , \qquad (2\text{-}2)$$

where z is the altitude, ρ is the mass density, and ds is the element of electron path length. Later Grün's results were refined and extended down to 2 keV by Cohn and Caledonia,[58] who found very good

58. Cohn, A., and Caledonia, G. (1970) Spatial distribution of the fluorescent radiation emission caused by an electron beam, J. Appl. Phys. 141: 3767-75.

agreement with the earlier work.

Grün discovered that the energy-loss profile had very definite scaling properties and could be represented in terms of a universal energy-dissipation function $\lambda(X)$ through the relation

$$\alpha(Z, E_0) = \frac{E_0}{R} \lambda\left(\frac{Z}{R}\right) . \tag{2-3}$$

Here E_0 (keV) is the initial primary electron energy, R is Bethe's electron range[46] (gm/cm^2), defined by

$$R(E_0) = \int_{E_0}^{0} \frac{dE}{dE/dZ} , \tag{2-4}$$

and the integral of λ is normalized to unity,

$$\int_{-\infty}^{\infty} dX \; \lambda(X) = 1, \tag{2-5}$$

since $\alpha(Z, E_0)$ integrates to E_0. The range can be assumed to follow a power-law distribution as a function of E_0.

$$R = C \; E_0^{n} , \tag{2-6}$$

where C and n are empirically determined constants. Grün found that the values

$$\begin{aligned} n &= 1.75 , \\ C &= 4.57 \times 10^{-6} \; gm/cm^2\text{-}keV^{1.75} , \end{aligned} \tag{2-7}$$

provided the best fit to the data. Equations (2-6) and (2-7) follow from application of the first Born approximation to Bethe's relativis-

tic stopping-power formula,[46] according to which dE/ds is proportional to lnE/E. If we approximate lnE by $E^{1/3}$ to $E^{1/4}$ over a limited range of E, then dE/ds varies as $E^{-2/3}$ to $E^{-3/4}$. The value of R is then obtained from Eq. (2-4), which yields $R \sim E^{5/3}$ to $E^{7/4}$, in agreement with Grün's result, Eq. (2-6). While Grün presented $\lambda(X)$ as a numerically defined function, Lazarev[59] attempted to derive an analytic expression for it. The expression he obtained agrees very well with Grün's data for $X \leq 1.2$.

Rees used Grün's expression between 0.4 and 300 keV, thus extending beyond the region over which Grün, and Cohn and Caledonia had validated it at both the high-energy and the low-energy ends of the range. Barrett and Hays[60] have examined the range-energy relation for electrons of energy down to 300 eV by N_2^+ 0-0 band emission photometry and have found significant deviations from the Rees extrapolation. They propose a three-term range-energy relation,

$$R = C_1 + C_2 E_0^{n_2} - C_3 E_0^{n_3} \quad , \qquad (2\text{-}8)$$

and find, with R in gm/cm^2 and E_0 in keV, that

59. Lazarev, V.I. (1967) Absorption of the energy of an electron beam in the upper atmosphere, Geomag. Aeron. 17: 219-23.

60. Barrett, J.L., and Hays, P.B. (1976) Spatial distribution of energy deposited in nitrogen by electrons, J. Chem. Phys. 164: 743-50.

$$C_1 = 4.30 \times 10^{-7} \ ,$$

$$C_2 = 5.20 \times 10^{-5} \ , \qquad n_2 = 1.67 \ , \tag{2-9}$$

$$C_3 = 3.82 \times 10^{-6} \ , \qquad n_3 = -0.7 \ .$$

For energies $\geq$ 1 keV, the first and third terms become negligible, and the expression agrees approximately with the Grün-Rees formula.

We have calculated energy deposition using the Barrett-Hays range-energy relation, Eq. (2-8), in place of Eq. (2-6). However, the low-energy electrons of energies < 1 keV are deposited at such high altitudes ($\sim$ 200 km) that they have negligible effect on the most important infrared auroral emissions, which are confined to altitudes $z \leq 160$ km. Consequently, AARC uses the original Grün range-energy relation [Eqs. (2-6) and (2-7)] throughout.

Rees integrated Grün's three-dimensional isophotes, or energy-deposition contours, over pitch angle for a monodirectional incident beam, assuming three different electron pitch-angle distributions, and used the results to define normalized energy-dissipation functions $\lambda(Z/R)$ for these distributions.

Letting the electron specific intensity (electrons/cm^2 sec sr) be I, we have

$$\frac{dI(E_0, \mu_0)}{dE_0} = \frac{d^3P}{dA \ \mu_0 \ d\Omega \ dE_0} = \frac{dF(E_0)}{dE_0}\eta(\mu_0) \ , \tag{2-10}$$

where $\mu_0 = \cos\theta_0$, θ_0 is the pitch angle of the electron velocity

vector v relative to the magnetic field intensity B (assumed vertical), P is the total flux (electrons/sec), dA is an element of area perpendicular to the velocity vector, dE_0 is the element of initial particle energy, and $d\Omega$ is the element of solid angle. The electron spectral number flux density (electrons/cm^2 sec keV) is dF/dE_0, and the pitch-angle distribution is denoted by $\nu(\mu_0)$, which is normalized so that its integral over the downward hemisphere is unity,

$$\int_0^1 d\mu_0 \, \eta(\mu_0) = 1 \quad .$$

Rees's three assumed pitch-angle distributions can then be written:[61]

(a) Isotropic

$$\eta(\mu_0) = C \quad (0^\circ \leq \theta_0 \leq 90^\circ) \; , \tag{2-11}$$

(b) Inverse cosine (0° - 80°)

$$\begin{aligned} \eta(\mu_0) &= C/\mu_0 \quad (0^\circ \leq \theta_0 \leq 80^\circ) \\ &= 0 \qquad (\theta_0 > 80^\circ) \; , \end{aligned} \tag{2-12a}$$

61. Note, however, that Rees[31] calls distributions (b) and (c) "isotropic" while calling distribution (a) "cosine-dependent," as pointed out by Berger et al (1970).[49] Apparently, Rees defined isotropy, not as constant electron specific intensity Φ, but rather as constant angular flux $\Phi \cos\theta_0$. The angular flux falls in proportion to the projected area dA $\cos(\theta_0)$ as θ_0 increases, and consequently the source intensity must be increased with increased pitch angle to keep the angular flux constant. For case (b), the source intensity increases by a factor of 6 between pitch angles of 0° and 80°.

(c) Inverse cosine (0° - 70°)

$$\eta(\mu_0) = C/\mu_0 \quad (0° \leq \theta_0 \leq 70°)$$
$$= 0 \quad (\theta_0 > 70°) \quad . \tag{2-12b}$$

In these relations C is a normalization constant.

In AARC we use the energy-dissipation function corresponding to an inverse-cosine (0° - 80°) pitch-angle distribution; this function is plotted in Figure 5. Note that the portion of the curve at negative Z/R, whose area represents 17 percent of the total and incorporates the contribution of the backscattered electron flux, has not been drawn because it does not contribute when using a range-energy relation of the type of Eq. (2-6), except by reducing the energy available for deposition in the forward hemisphere. The backscattered portion of the electron flux is also responsible for energy deposition at the conjugate point, which is ignored in the current model.

The energy deposition rate (energy/cm^3 sec) is given by

$$W(z) = \rho(z)\int_0^\infty dE_0(R)\ \frac{dF[E_0(R)]}{dE_0(R)}\ \alpha[z,\ E_0(R)]\ , \tag{2-13}$$

where $\rho(z)$ is the atmospheric mass density (gm/cm^3) and $E_0(R)$ is the inverse of Eq. (2-4) or (2-6). Production of an ion pair by electrons of energy greater than a few hundred eV stopped in matter requires a constant specific energy $\Delta E_{ion} \approx 0.035$ keV, nearly independent of the energy of the primary electrons[62] and the composition of the

62. Valentine, J.M., and Curran, S.C. (1958) Average energy expenditure per ion pair in gases and gas mixtures, Rep. Progr. Phys. 21: 1.

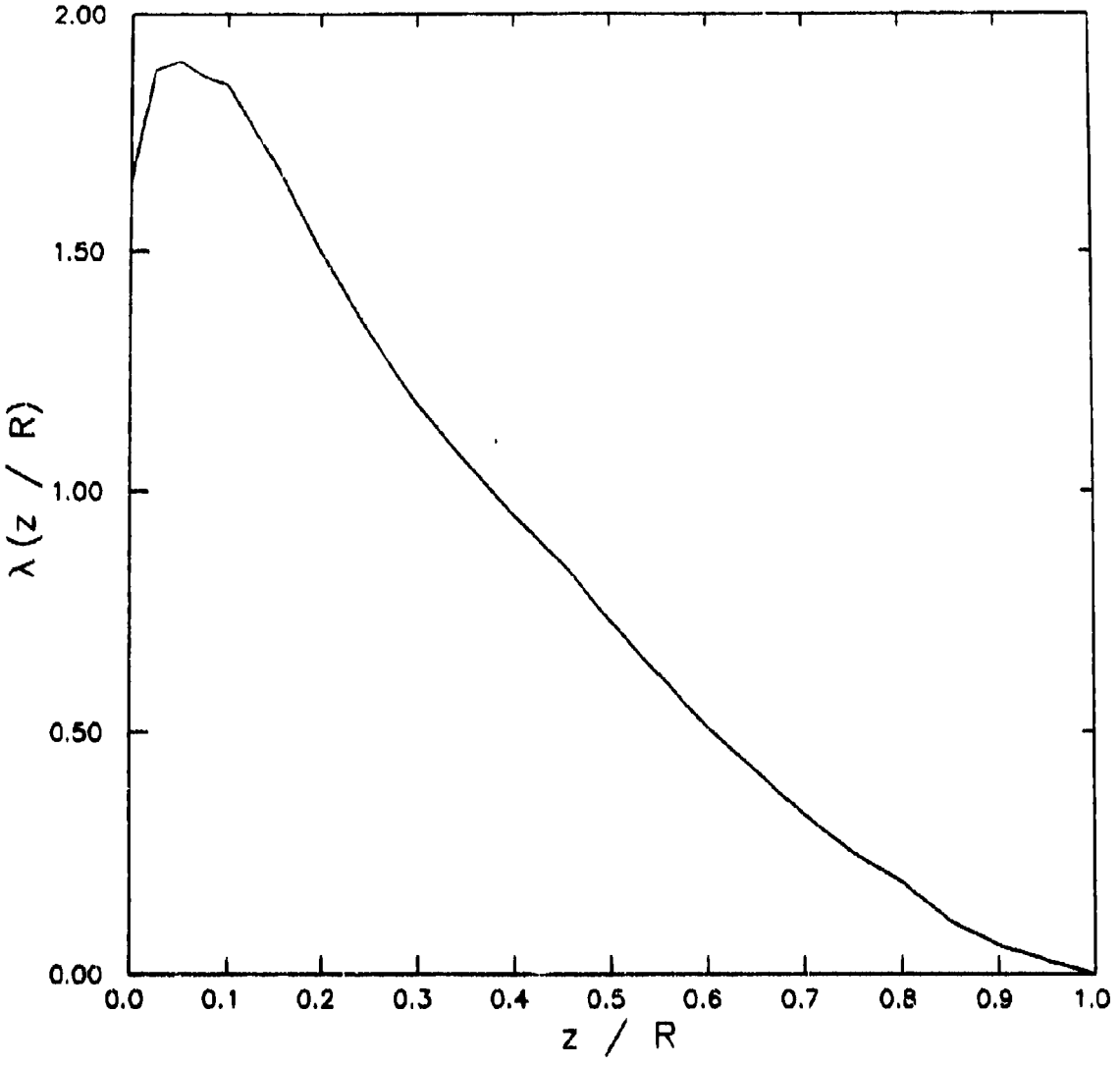

Figure 5. Energy-Dissipation Function Used in AARC.

material.[63] Using Eqs. (2-3) and (2-13), the ion-pair production rate (ion pairs/cm^3 sec) may be written

63. Dalgarno, A. (1960) Range and energy loss, in Atomic and Molecular Processes, D.R. Bates, Editor. Academic Press, New York, pp. 622-42.

$$q(z) = \frac{\rho(z)}{\Delta E_{ion}} \int_0^\infty dE_0(R) \, \frac{dF}{dE_0(R)} \, \frac{E_0}{R} \, \lambda\left(\frac{Z}{R}\right) \quad . \tag{2-14}$$

The relation between this expression and that of Rees is discussed in Appendix A. Letting

$$\frac{dF(E_0)}{dE_0} \, dE_0 = \frac{dG(R)}{dR} \, dR \quad , \tag{2-15}$$

so that dG/dR is the electron spectral flux density in range units (electrons/gm sec), our final expression for the ion-pair production rate is

$$q(z) = \frac{\rho(z)}{\Delta E_{ion}} \int_0^\infty dR \, \frac{dG}{dR} \, \frac{E_0(R)}{R} \, \lambda\left(\frac{Z}{R}\right) \quad . \tag{2-16}$$

2.2.3 ELECTRON FLUX AT THE TOP OF THE ATMOSPHERE

In general, precipitating auroral electron spectra have been found to be well represented by a sum of three terms: a Gaussian, a Maxwellian, and a power law.[64] However, often simpler expressions are quite suitable for representing auroral electron fluxes. Within AARC, two different simpler spectral forms[1] are used for the electron spectral number flux impinging on the atmosphere, a Maxwellian flux dF_M/dE_0 and a Gaussian flux dF_G/dE_0. The Maxwellian flux is characteristic of

64. Fontheim, E.G., Stasiewicz, K., Chandler, M.O., Ong, R.S.B., Gombosi, E., and Hoffman, R.A. (1982) Statistical study of precipitating electrons, J. Geophys. Res. 187: 3469-80.

continuous or diffuse auroras[18] and depends on two parameters, the total energy flux Φ_M (keV/cm^2 sec), where

$$\Phi_M = \int_0^\infty dE_0 \; E_0 \; \frac{dF}{dE_0} \; , \tag{2-17}$$

and a characteristic energy, or hardness, α (keV) corresponding to the peak value E_{peak} of dF_M/dE. The flux can be written

$$\frac{dF_M}{dE_0} = \frac{\Phi_M}{2\alpha^3} \; E_0 \; e^{-E_0/\alpha} \; , \tag{2-18}$$

and the mean energy can be written in terms of α as $\langle E_0 \rangle = 2\alpha$. The energy variance is not a separate parameter and has the form $\langle \Delta E_0^2 \rangle = \langle E_0^2 \rangle - \langle E_0 \rangle^2 = 2\alpha^2$.

On the other hand, the Gaussian flux represents well the more sharply peaked spectra seen in discrete arcs[18] and depends on three parameters, the total energy flux Φ_G, the mean energy $\langle E_0 \rangle$, and the variance $\langle \Delta E_0^2 \rangle$. The Gaussian flux can be written

$$\frac{dF_G}{dE_0} = \frac{\Phi_G}{f} \; E_0 \; \exp\left[-\left(\frac{E_0 - E_c}{\Delta} \right)^2 \right] \; , \tag{2-19}$$

where

$$\begin{aligned} f &= \int_0^\infty dE_0 \; E_0 \; \exp\left[-\left(\frac{E_0 - E_c}{\Delta} \right)^2 \right] \\ &= \frac{\pi^{1/2}}{2} \; E_c^3 \left\{ \eta \left[1 + \frac{\eta^2}{2} \right] \left[1 + \mathrm{erf}\left(\frac{1}{\eta} \right) \right] \right. \\ &\qquad \left. + \frac{\eta^2}{\pi^{1/2}} \exp\left[-\frac{1}{\eta^2} \right] \right\} \; , \end{aligned} \tag{2-20}$$

$\eta = \Delta/E_c$, and erf(x) is the error function. To lowest order in η, the mean energy and variance are given simply by $\langle E_0 \rangle = E_c$ and $\langle \Delta E_0^2 \rangle = \Delta^2$; the corresponding expression to any order in η can easily be derived.

Three energy-deposition profiles have been calculated in advance and stored as part of AARC for the convenience of the user who does not wish to specify the parameters of the electron distribution at the top of the atmosphere. These three profiles correspond to "typical" IBC II, III, and III$^+$ auroras with Maxwellian electron spectra. The values of the total energy flux Φ_M and characteristic energy α used in calculating these profiles are listed in Table 1.

Table 1. Electron Spectral Parameters for Standard Auroral Profiles Included in AARC

IBC CLASS	α (keV)	Φ_M (keV/cm^2 sec)
II	2.9	8.052×10^9
III	5.0	6.242×10^{10}
III$^+$	10.0	2.497×10^{11}

2.3 Secondary Electron Production

2.3.1. INTRODUCTION.

In the previous section various methods were discussed that calculate the vertical profile of electron deposition valid for keV electrons in the aurora. Empirical relations show that in air about 0.035 keV is required for each ion pair formed from primary electrons of energy above a few hundred eV. Energy degradation occurs as the primaries (the undisturbed spectrum of electrons before encountering the atmosphere) are slowed by collisions with the ambient atmosphere. For the high-energy primaries most of the energy is lost in the production of ion pairs. The energy lost goes into the ionization energy, ion excitation energy, and the energy of the ejected secondary electron. Kinematic considerations limit the kinetic energy imparted to the ion. As the primary continues to slow down, it produces many secondaries, most of them with too little energy to produce ionization. For this reason, the production of the first generation of secondaries dominates. A typical 3-keV primary will produce about 86 secondaries during degradation. The production of the j^{th} state of atmospheric species i can be calculated as,

$$\eta_{ij}(z) = \sum_k n_k \int_{E_{th}}^{E_{max}} \Phi(E, z)\, \sigma_{ijk}(E)\, dE \qquad (2\text{-}21)$$

where $\Phi(E, z)$ is the flux of electrons of energy E at altitude z, σ_{ijk} is the cross section for production of species i in state j from species k (k doesn't have to be the same as i; for example, production

of $N(^2D)$ from N_2).

As Eq. (2-21) indicates, the excitation rates produced by the secondary electron flux can be calculated once both accurate cross sections and an efficient method of calculating the flux of secondaries are given. The cross sections in many cases (for N_2 and O_2 especially) can be measured in the laboratory with varying degrees of accuracy. Cross sections for electron impact on atomic oxygen cannot be measured as easily, and often are obtained from theory. Fortunately, accurate theory is easier to apply to atoms than molecules. It should be kept in mind that the accuracy of the cross sections[65] ultimately affects the possible accuracy of the results, regardless of how well (and with how much effort) $\Phi(E, z)$ is calculated.

Rigorously, the calculation of the flux $\Phi(E, z)$ should be obtained from the distribution function $f(E, z)$ for electrons of all energies as a function of altitude z. The distribution function $f(E, z)$ is the solution to the Boltzmann equation. The solution of the Boltzmann equation is notoriously difficult and involves many uncertain collision terms (differential cross sections and electron loss cross sections) and many approximations relating to them. The total electron distribution function in the aurora has never been calculated by this method, although the distribution function for photoelectrons has been obtained in a lengthy calculation[66]. This calculation did show, however, that many of the more approximate calculations seem to be

65. Wadzinski, H.T. and Jasperse, J.R. (1982) Low Energy Electron and Photon Cross Sections for O, N_2, and O_2, and Related Data, AFGL-TR-82-0008, AD A118921.

surprisingly accurate at altitudes below about 135 km, the region where infrared active species are more prevalent.

Simpler transport schemes that also calculate the deposition profile[54] obtain the flux of hot electrons. They make a two fluid approximation: they calculate the hot component of the electron gas consisting of primaries, degraded primaries, and all orders of secondaries down to a low energy cut-off. The deposition causes ionization and chemical reactions which establish a population of ambient electrons. The temperature of the ambient electrons can be calculated assuming they are heated by collisions with the hot component (which is a large cooling term for the low energy portion of the hot component) and cooled by collision with neutrals, especially rotational excitation and fine structure excitation of O. In this approximation the hot electrons lose energy to neutrals and the ambient electrons, but are not allowed to gain energy from the ambient electrons (or from superelastic collisions with excited state species). This approximation becomes increasingly inaccurate at low energies where the flux of the thermal tail of the ambient electrons becomes comparable to the flux of secondaries. This cut-off energy generally occurs below one eV, depending upon n_e and T_e.

Most previous applications of the transport equation method used a cutoff at a few eV. This choice was reasonable since most easily observed optical emissions have thresholds greater than a few eV. It

66. Jasperse, J. R. (1976) Boltzmann-Fokker-Planck model for the electron distribution function in the earth's ionosphere, Planetary Space Sci. 24: 33.

was also fortunate since the cross sections for vibrational excitation of O_2 and rotational excitation of N_2 and O_2 are somewhat uncertain. The uncertain cross sections below one or two eV and the increasingly inaccurate calculation of $\Phi(E, z)$ might seem to be large obstacles to calculating accurate auroral excitation of infrared processes that have excitation energies of less than one eV. However, infrared-active species are minor or trace constituents, and their excited states are predominantly produced by chemiluminescent or energy transfer processes that are initiated by impact of electrons of energy greater than 2 eV with the major constituents. The details of these mechanisms will be discussed in Sections 2.4 and 2.5.

Jasperse and Strickland's calculations have shown that the production of secondary electrons of energy below about 40 eV is local, if one is considering distances of the order of a kilometer. Jasperse has shown[67] that for photoelectrons, the Boltzmann equation solution does not significantly differ from the simple solution obtained by the continuous-slowing-down (CSD) technique above a few eV cutoff. This somewhat surprising result convinced us to use the CSD technique since it is much easier to calculate.

2.3.2 CONTINUOUS-SLOWING-DOWN METHOD

In the CSD technique the electron flux is simply calculated by setting the production of secondaries equal to the loss. The loss is calculated using the loss function, which is proportional to energy

67. Jasperse, J.R., (1977) Electron distribution function and ion concentrations in the Earth's lower ionosphere from Boltzmann-Fokker-Planck theory, Planet. Space Sci., 28:743.

loss per unit distance. The continuous-energy-loss approximation assumes that the energy loss per unit distance is a continuous function, dE/dx. This assumption is not rigorous since electrons lose energy in discrete amounts as they interact with the neutral gas. When the energy loss becomes a sizable fraction of the electron's energy, which is more likely at low energies, the continuous-energy-loss approximation is more suspect. The loss function L(E) is related to the stopping power per unit mass

$$L(E) = -\frac{1}{N}\frac{dE}{dx} , \tag{2-22}$$

where N is the density of the stopping atmosphere. The loss function is comprised of two distinct parts. One comes from the excitation of discrete states

$$L_d(E) = -\frac{1}{N}\left(\frac{dE}{dx}\right)_d = \sum_j \sum_i f_j \, E_{ij} \, \sigma_{ij}(E) , \tag{2-23}$$

where the sum is over species j (fraction f_j) and states i, and E_{ij} is the energy lost (excitation energy of state i) in the collision with an electron of energy E. A contribution from continuum states is also important,

$$L_c(E) = -\frac{1}{N}\left(\frac{dE}{dx}\right)_c$$

$$= \sum_{i,j} f_j \int_{E_{th}}^{(E_p - I_{ij})/2} E' \, \sigma_{ij}(E, W) \, dE' . \tag{2-24}$$

In this equation, E' is the energy lost, which includes the energy of

ionization in addition to excitation of discrete states of the ion produced and kinetic energy of any molecular fragments (dissociative ionization), the primary energy is E_p, I_{ij} is the ionization potential producing the i^{th} state of the ion from the neutral parent j, $\sigma_{ij}(E, W)$ is the cross section at electron energy E with $W = I_{ij} + E_s$, and E_{th} is the threshold energy for producing state ij. At low energies (a few eV, dependent upon the fractional ionization) a third loss term becomes very important. This term arises from energy loss by Coulomb collisions with the ambient electron gas. We use the same formula used by Peterson et al.,[47] which was taken from Swartz et al.,[68]

$$L(E)_{elect} = \frac{3.37 \times 10^4}{E^{0.84} N_e^{0.03}} \left[\frac{E_s - E_e}{E_s - 0.53E_e} \right]^{2.36} , \qquad (2\text{-}25)$$

where E_e [eV] $= 8.618 \times 10^{-5} T_e$ is the average energy of ambient electrons with temperature T_e, E_s is the energy of the secondary electron, and N_e is the electron density.

The energy dependence of the secondaries produced in the ionization of N_2 and O_2 has been measured in the laboratory by Opal and coworkers[69]. It is remarkably independent of the primary energy E_p for energies $E_p > 500$eV. The differential cross section, σ, for production of secondaries of energy E_s from primaries of energy E_p fits the

68. Swartz, W.E., Nisbet, J.S., and Green, A.E.S. (1971) J. Geophys. Res. 76:8425.

69. Opal, C.B., Peterson, W.K., and Beaty, E.C. (1971) Measurements of secondary-electron spectra produced by electron impact ionization of a number of simple gases, J. Chem. Phys. 55:4100-4106.

expression

$$\sigma(E_p, E_s) = f(E_s)\,\sigma(E_p) ,$$

$$f(E_s) = \frac{C}{1 + (E_s/E_i)^{2.1}} , \qquad (2\text{-}26)$$

where E_i is a parameter on the order of the ionization threshold energy (for N_2, $E_i = 14.0$ while $E_{th} = 15.6$ eV; for O_2, $E_i = 18.0$ while $E_{th} = 12.1$ eV), and $f(E_s)$ is the shape function (eV^{-1}). Although the shape of the secondary spectrum was a weak function of E_p, the best values of E_i varied by 10 - 20 percent for various E_p. We have used the values for $E_p = 1000$ eV. The error in this approximation is larger than the error from replacing the value of the exponent in Eq. (2-26). 2.1, with 2.0. This expression is then integrable. Integration of the differential cross section in Eq. (2-26) over all energies of secondaries must yield the total ionization cross section $\sigma(E_p)$,

$$\int_0^{(E_p-I)/2} \sigma(E_p, E_s)\,ds = \sigma(E_p) . \qquad (2\text{-}27)$$

Thus one obtains

$$C = \left[\int_0^{(E_p-I)/2} \frac{1}{1 + (E_s/E_i)^2}\, dE_s \right]^{-1}$$

$$= E_i \arctan\left(\frac{E_p - I}{2 E_i} \right) , \qquad (2\text{-}28)$$

for the constant in Eq. (2-26). The upper limit of the integral is $(E_p-I)/2$ since the secondary electron is defined to be the lower-energy electron produced in the ionization. (The higher-energy electron is the degraded primary.) The differential production rate of secondaries can then be written as a sum of terms arising from the ioniza-

tion of N_2, O_2, and O. Letting $\eta(M^+)$ represent the production rate of M^+, we have

$$\eta(E_s) = f_{N_2}(E_s)\left[\eta(N_2^+) + \eta(N^+)\right] + f_{O_2}(E_s)\left[1.5\ \eta(O_2^+)\right] + f_O(E_s)\left[\eta(O^+) - 0.5\ \eta(O_2^+)\right] \quad (cm^{-3}\ s^{-1}\ eV^{-1}) \ . \tag{2-29}$$

Again, we mention that we choose $E_p = 1000$ eV. The shape function is quite insensitive to the choice of E_p, but we use the value that corresponds to the chosen E_i.

There are no measurements of the energy dependence of the secondary-electron production for O that could yield a fit similar to Eq. (2-28). We follow Rees et al[70] using the assumption of small momentum transfer in ionizing collisions. The use of the Bethe-Born approximation gives

$$f_O(E_s) = \frac{N(E_p)}{\sigma(E_p)}\ \sigma_V(E_s,\ E_p) \cdot \frac{1}{W}\ \exp\left[-\frac{W}{31.5} - 339\ \exp\left(-\frac{W}{2.49}\right)\right] \times ln\left[\frac{E_p^{0.5} + (E_p - W)^{0.5}}{E_p^{0.5} - (E_p - W)^{0.5}}\right] \quad (eV^{-1}) \ , \tag{2-30}$$

where $N(E_p)$ is a normalization factor equal to 2.71 for 1-keV primaries. The secondary-electron flux can then be obtained from

70. Rees, M.H., Stewart, A.I., and Walker, J.C.G. (1969) Secondary electrons in aurora, Planet. Space Sci. 17:1997-2008.

$$\Phi(E_s) = - \frac{\int_{E_s}^{(E_p-I)/2} \eta(E)dE}{(dE/dx)_{elect} + (dE/dx)_d + (dE/dx)_c} \quad (cm^{-2}\ s^{-1}\ eV^{-1}) \quad , \tag{2-31}$$

where the electron-electron energy loss term[68] was introduced in Eqs. (2-22) to (2-25).

This flux is truly the secondary flux, since it contains only the first generation of secondaries. Examination of the shape functions indicates that most secondaries produced do not have enough energy to produce further ionization. About 30 percent of the secondaries produced have energy above 0.035 keV (primaries 1 keV or greater), which on average could produce another ionization. Detailed energy degradation calculations indicate that at energies below 100 eV the number of ionizations occurring per 0.035 keV deposited decreases due to competition from non-ionizing excitations (which have cross sections that fall off faster at high energies than ionization). Thus only about 15 percent of the secondaries can produce further ionization. This error is smaller than the probable errors in the cross sections used in the calculation.

The energy dependence of the secondary electron flux in the CSD approximation (Eq. (2-31)) is dominated by the structure in the loss function. The numerator in Eq. (2-31) is a smooth function, while the denominator is dominated by the structure in the excitation cross section. At energies below a few eV the electron-electron term becomes dominant. The low energy cutoff is determined when the flux of the

ambient electron thermal tail, $\Phi_{th}(E_o)$ equals the flux of secondaries $\Phi_s(E_o)$

$$\Phi_{th}(E_o) = \frac{n_e}{kT_e} \exp\left(-\frac{E_o}{kT_e} \right) v_{th}$$
$$= \frac{n_e}{T_e} 6.878 \times 10^{11} E^{0.5} \exp\left(-1.16 \times 10^4 \frac{E}{T_e} \right) , \qquad (2\text{-}32)$$

where k is Boltzmann's constant and v_{th} is the thermal electron velocity corresponding to energy E_o.

The calculation of excitation rates of the i^{th} state of the j^{th} species is easily obtained as an integral of the specified cross section over the flux

$$\eta_{ij}(z) = \int_{E_{th}}^{(E_p-I)/2} \sigma_{ij}(E_s)\, \Phi(E_s, z)\, dE_s . \qquad (2\text{-}33)$$

In practice the excitation rate is calculated at a discrete set of points corresponding to those at which the flux is calculated. This discretization arises from our choice of using numerical values for the energy loss cross sections. Although this procedure is computationally less efficient than that of Petersen et al[47] which uses simple and analytically integrable fits to the cross sections, it causes less error. The smooth parameterized cross sections cannot represent structured cross sections such as the vibrational excitation of N_2.

All excitations can be calculated from secondaries and primaries if the cross sections are known. For allowed processes of ionization, dissociation, and dissociative ionization that have large cross sec-

tions that fall off slowly above E ≈ 50 eV and have similar shape, a simplification is possible.[71] The cross sections of dissociation, ionization and dissociative ionization are proportional to ionization rate which has been previously determined by the energy deposition program. The production rate is proportional also to the fractional population of the parent collision partner and the relative strength of the cross section well above threshold. For example,

$$\eta(N_2^+) = 0.92\ [N_2] \times \frac{q_e(z)}{1.15\ [N_2] + 1.5\ [O_2] + 0.56\ [O] + 0.43\ [He] + 0.8\ [H]}\ , \qquad (2\text{-}34)$$

where the square brackets indicate densities of the constituents, and q_e is the ionization rate. Since we are primarily interested in altitudes below 200 km in our calculations we neglect the terms involving the densities of He and H.

The production terms for O_2^+, O^+, and N^+ are given by terms similar to that of Eq. (2-34)

$$\eta(O_2^+) = \frac{q_e\ [O_2]}{1.15\ [N_2] + 1.5\ [O_2] + 0.56\ [O]} \qquad (2\text{-}35a)$$

$$\eta(O^+) = \frac{0.56\ q_e\ [O]}{1.15\ [N_2] + 1.5\ [O_2] + 0.56\ [O]} + 0.5\ \eta(O_2^+) \qquad (2\text{-}35b)$$

71. Rees, M.H. and Jones, R.A. (1973) Time dependent studies of aurora -II. Spectroscopic morphology, Planet. Space Sci. 21:1213-1235.

$$\eta(N^+) = 0.25\ \eta(N_2^+) \ . \qquad (2\text{-}35c)$$

These formulas assume that N^+ is produced only from dissociative ionization of N_2, a good approximation since $[N_2] >> [N]$. However, since $[O_2] \approx [O]$ the production of O^+ has significant contributions from ionization of O as well as dissociative ionization of O_2 [last term in Eq. (2-35b)].

2.4 Photochemistry

2.4.1. INTRODUCTION

The auroral electron deposition initiates a series of chemical reactions that can eventually lead to enhanced infrared emission. Since the infrared emitters in the thermosphere (altitudes above 90 km) are trace species (mixing ratios less than $3x10^{-4}$), they are unlikely to absorb a large fraction of the energy directly deposited by the primary and secondary electrons. We have calculated the direct excitation of $CO_2(001)$ and have shown that it contributes only a small fraction of the auroral energy that is transferred (always less than .1 quanta excited per ion pair produced). Table 2 shows the excitation rate of $CO_2(001)$ for an IBC III aurora. This number is somewhat uncertain since the threshold is at 0.3 eV and, as previously mentioned, the calculation of the secondary electron flux is inaccurate at this low energy. It should be noted that as the dosing increases, the excitation of CO_2 per ion pair decreases due to increased loss of

low energy secondaries to the increasing number of ambient electrons that exist in steady-state with the dosing.

Table 2. Secondary Electron Vibrational Excitation for IBC III Aurora (Φ_H = 100 ergs/cm^2 sec, ϵ = 5 keV).

Alt (km)	N_2(v) quanta/ ion-pair	N_2 mole fraction	CO_2 ν_3 photons/ ion-pair	CO_2 mixing ratio (ppm)
90	11.5	0.78	0.30	320
100	9.7	0.78	0.07	290
110	8.5	0.78	8.0×10^{-3}	100
120	7.6	0.73	1.2×10^{-3}	35
130	7.0	0.69	5.0×10^{-4}	28
140	6.5	0.64	3.2×10^{-4}	25

Since the atmosphere is mostly N_2, O_2, and O, these molecules are ionized or excited (N_2 and O_2 dissociated) by primary and secondary electrons. If allowed transitions are excited, they can lose the excitation energy by radiation (unless it is optically thick such as OI 1304 Å). Metastables are often quenched, giving up the energy by energy transfer or chemical reaction. N_2, O_2, and O excited states radiate many characteristic spectral features in the visible and UV. Many auroral modeling studies have done a reasonable job simulating these optical emissions.[15,72,73,74] These species do have some electronic IR transitions that originate from high-lying states.

72. Vallance-Jones, A. and Gattinger, R.L. (1975) Quantitative

Exothermic chemical reactions are a much more efficient method of excitation of minor species. The deposition of auroral electrons produces ions, dissociation products, and metastable species that initiate a series of fast exothermic chemical reactions that have the ability to produce extensive vibrational excitation of the products. The aurora produces NO and NO^+ in copious quantities, in exothermic reactions that can populate high vibrational levels. NO^+ is the terminal ion in the E-region and thus every ionization produced tends to end up as NO^+ unless recombination occurs first. Thus the NO^+ production rate can be a sizeable fraction of the ionization rate.

Large nighttime enhancements in the NO(Δv=1, Δv=2) and $CO_2(\nu_3)$ have been observed in many AFGL field programs[2,7,9,75]. NO^+ has been tentatively identified as a prompt emitter in the 4.3 μm region[76,77].

spectroscopy of the aurora. III. The spectrum of medium intensity aurora between 3100 Å and 4700 Å, Can. J. Phys. 53:1806-1813.

73. Vallance-Jones, A. and Gattinger, R.L. (1976) Quantitative spectroscopy of the aurora. IV. The spectrum of medium intensity aurora between 8800 Å and 11400 Å, Can. J. Phys. 54:2128-2133.

74. Strickland, D.J. (1981) Electron transport, chemistry and optical emissions in the auroral E-layer, AFGL-TR-81-0042, AD/A102345

75. Kumer, J.B. (1975) Summary analysis of 4.3 μm data, in Atmospheres of Earth and the Planets, B.M. McCormac, Editor. D. Reidel Publishing Co., Dordrecht, p 347-358.

76. Kumer, J.B. (1979) Multidimensional time dependent structure and mechanisms for non-LTE CO_2 infrared emissions and 4.3μm aurora, AFGL-TR-79-0224, ADA084940, p 78-86.

77. Winick, J.R., Picard, R.H., Sharma, R.D., Joseph, R.A., and Wintersteiner, P.P. (1987) Radiative transfer effects on aurora enhanced 4.3 μm emission, Adv. Space Res. 7:(No. 10).

AARC uses a simple chemical model to first determine the chemical reactions that produce NO and NO^+ and $N_2(v)$ which can transfer vibrational quanta to CO_2 ν_3. In the following sections we will describe the chemical model and the associated calculations that determine the emission of infrared photons from NO and NO^+. In Sec. 2.5.2 we will describe the time dependent calculation of $CO_2(001)$.

We have developed a photochemical equilibrium model that calculates the densities of the ten species $N(^2D)$, $N(^4S)$, $N_2(^3\Sigma)$, N_2^+, O_2^+, O^+, NO^+, N^+, $O_2^+(a^4\Pi)$ and e^- driven by the precipitating flux. Since we are concerned with altitudes above 90 km under disturbed conditions where the ionization rate is enhanced, we can neglect both the formation of positive cluster ions and negative ions. This model has been implimented in a FORTRAN program, AUROR.PCE.CHEM on the Apollo computer system at AFGL Infrared Technology Division. The densities of the nine species excluding the electrons are easily obtained in a steady-state approximation.

The continuity equation for each species has the form

$$\frac{dn_i}{dt} = 0 = P_i(\underset{\sim}{n}) - n_i L_i(\underset{\sim}{n}) + P_{0i} \quad (i = 1,\ldots,9), \tag{2-36}$$

where $\underset{\sim}{n} = (n_1, \ldots, n_{10})$ is the set of densities of the ten modeled species, P_i is the production rate from other species in the set, L_i is the loss frequency, and P_{0i} is an inhomogeneous production term which represents production of species i from species that are not modeled (for example, N_2^+ produced by ionization of N_2). The production term P_i is generally of the form

$$P_i(\underline{n}) = \sum_q k(q)\ n_{q1}\ n_{q2}. \qquad (2\text{-}37)$$

Here the index q runs over the reactions in Table 3 in which the i^{th} species is produced and appears on the right side, k(q) is the corresponding rate coefficient from Table 4, and n_{q1} and n_{q2} are the first and second species appearing on the left side of the q^{th} reaction. For some of these reactions, both n_{q1} and n_{q2} are densities of modeled species from the set $\underline{n}$, while for others one of the species is an unmodeled atmospheric constituent such as N_2 or NO. The loss freqency of species i is

$$L_i(\underline{n}) = \sum_q k(q)\ n_{q2}. \qquad (2\text{-}38)$$

Here k(q) is the rate coefficient for a reaction from Table 3 in which species i is chemically destroyed and appears on the left-hand side, n_{q2} is the collision partner of n_i and can be either a modeled or an unmodeled species density, and the sum is over all destruction reactions. The loss rate (the second term on the right-hand side of Eq. (2-36)) is obtained by multiplying the loss frequency by the species density n_i. For three-body reactions there will be an extra density term in the corresponding production or loss expression in Eq. (2-37) or (2-38). Three-body reactions usually involve a major constituent (N_2, O_2 or O which are specified in our model atmosphere input) as the third body.

Table 3a. Photochemical Reactions

R1A	$N_2(A) + O \rightarrow N_2 + O(^1S)$
R1B	$N_2(A) + O \rightarrow NO + N(^2D)$
R2	$N_2(A) + O_2 \rightarrow N_2 + O_2$
R3	$N(^4S) + O_2 \rightarrow NO(v) + O$
R4	$N(^2D) + O_2 \rightarrow NO(v) + b_9 \cdot O(^1D)$
R5	$N(^2D) + O \rightarrow N(^4S) + O$
R6	$N(^2D) + NO \rightarrow N_2(v) + O(^1D, ^3P)$
R7	$N(^4S) + NO \rightarrow b_{11} \cdot N_2(v=1) + O(^1D, ^3P)$
R8	$N(^2D) + e^- \rightarrow N(^4S) + e^-$
R9	$N(^2D) + O_2^+ \rightarrow N^+ + O_2$
R10	$NO + h\nu \rightarrow N(^4S) + O$
R11	$NO + h\nu \rightarrow NO^+ + e^-$
R12	$N_2^+ + O_2 \rightarrow N_2 + O_2^+$
R13A	$N_2^+ + O \rightarrow NO^+ + b_1 \cdot N(^2D) + (1-b_1) \cdot N(^4S)$
R13B	$N_2^+ + O \rightarrow O^+ + N_2$
R14	$N_2^+ + e^{-*} \rightarrow b_2 \cdot N(^2D) + (2-b_2) \cdot N(^4S) + e^-$
R15	$N_2^+ + NO \rightarrow NO^+ + N_2$
R16	$O_2^+ + N_2 \rightarrow NO^+ + NO$
R17	$O_2^+ + NO \rightarrow NO^+ + O_2$
R18	$O_2^+ + N(^2D) \rightarrow N^+ + O_2$
R19	$O_2^+ + e^- \rightarrow (2-b_{10}) \cdot O + b_{10} \cdot O(^1D)$
R20	$O_2^+ + N(^4S) \rightarrow NO^+ + O$
R21	$O^+ + N_2 \rightarrow NO^+ + N(^4S)$
R22	$O^+ + O_2 \rightarrow O_2^+ + O$
R23	$O^+ + NO \rightarrow NO^+ + O$
R24	$O^+(^2D) + N_2 \rightarrow NO^+ + N(^4S)$
R25	$O^+(^2D) + N_2 \rightarrow N_2^+ + O$
R26	$O^+(^2D) + e^- \rightarrow O^+(^4S) + e^-$
R27	$O^+(2P) + e^- \rightarrow O^+(^4S) + e^-$
R28	$O^+(2P) + N_2 \rightarrow N_2^+ + O$
R29	$O^+(2P) + N_2 \rightarrow NO^+ + N(^4S)$
R30	$O_2^+(a\ ^4\Pi) + N_2 \rightarrow N_2^+ + O_2$
R31	$O_2^+(a\ ^4\Pi) + O \rightarrow O_2^+ + O(^3P, ^1D)$
R32	$O_2^+(a\ ^4\Pi) + e^- \rightarrow O + O$
R33	$N^+ + O_2 \rightarrow NO^+ + b_{13} \cdot O(^1D)$
R34	$N^+ + O_2 \rightarrow O_2^+ + b_6 \cdot N(^2D) + (1-b_6) \cdot N(^4S)$
R35	$NO^+ + e^- \rightarrow O + b_3 \cdot N(^2D) + (1-b_3) \cdot N(^4S)$
AN2A	$N_2(A) \rightarrow N_2 + h\nu$(Vegard-Kaplan Bands)
R36	$O(^1D) + N_2 \rightarrow 2b_1 \cdot N_2(v=1) + O$
R37	$O(^1D) + O_2 \rightarrow f \cdot O_2(b) + (1-f) \cdot O_2(X) + O$
A01D	$O(^1D) \rightarrow O + h\nu(630\ nm)$

Table 3b. Important Branching Ratios

b_1 =1.0	R13A	$N_2^+ + O \rightarrow NO^+ + b_1 \cdot N(^2D) + (1-b_1) \cdot N(^4S)$
b_2 =1.0	R14	$N_2^+ + e^- \rightarrow b_2 \cdot N(^2D) + (2-b_2) \cdot N(^4S) + e^-$
b_3 =0.76	R35	$NO^+ + e^- \rightarrow b_3 \cdot N(^2D) + (1-b_3) \cdot N(^4S)$
b_4 =1.0	DISS N2	$e^{-*} + N_2 \rightarrow b_4 \cdot N(^2D) + (2-b_4) \cdot N(^4S) + e^-$
b_5 =0.5	DISS ION PNP	$e^{-*} + N_2 \rightarrow N^+ + b_5 \cdot N(^2D) + (1-b_5) \cdot N(^4S) + e^-$
b_6 =0.7	R34	$N^+ + O_2 \rightarrow O_2^+ + b_6 \cdot N(^2D) + (1-b_6) \cdot N(^4S)$
b_7 =1.21	PDN2	$e^{-*} + N_2 \rightarrow N + N + e^-$ (Rate = $b_7 \cdot q_e$)
b_8 =0.3	PN2A	$e^{-*} + N_2 \rightarrow N_2(A) + e^-$ (Rate = $b_8 \cdot q_e$)
b_9 =0.9	R4	$N(^2D) + O_2 \rightarrow NO + b_9 \cdot O(^1D) + (1-b_9) \cdot O$
b_{10}=0.95	R19	$O_2^+ + e^- \rightarrow (2-b_{10}) \cdot O + b_{10} \cdot O(^1D)$
b_{11}=2.82	R7, R6	$N + NO \rightarrow b_{11} \cdot N_2(v=1) + O$
b_{12}=2.20	R36	$O(^1D) + N_2 \rightarrow b_{12} \cdot N_2(v=1) + O$
b_{13}=0.8	R33	$N^+ + O_2 \rightarrow NO^+(v) + b_{13} \cdot O(^1D)$

The set of nine equations can be solved very efficiently if the equations are linear. The equations are linear if $L_i(n_j)$ does not depend upon n_i and P_i is only linearly dependent upon any of the nine species. Since we are solving mostly for ions and radicals, most of the reactions are linear except for recombination of the positive ions with the electrons. The requirement of electrical neutrality supplies a further constraint,

$$[n_e] = \sum_I [M_i^+] \quad ; \tag{2-39}$$

the electron density (total negative charge) equals the sum of the positive ions, since multiply charged ions are insignificant. The steady-state electron density is obtained from its steady-state conti-

Table 4. Reaction Rate Constants[a]

Reaction No.	A	B	C
R1A	5.0×10^{-12}	0.0	0.0
R1B	5.0×10^{-12}	0.0	0.0
R2	3.0×10^{-12}	0.0	0.0
R3	4.4×10^{-12}	0.0	-3220.
R4	7.4×10^{-12}	0.5	0.0
R5	4.0×10^{-12}	0.0[a]	-250.
R6	7.0×10^{-11}	0.0	0.0
R7	3.4×10^{-11}	0.0	0.0
R8	1.0×10^{-9}	0.5[b]	0.0
R9	2.5×10^{-10}	0.0	0.0
R10[c]			
R11[c]			
R12	5×10^{-11}	-0.8	0.0
R13A	1.4×10^{-10}	-0.44	0.0
R13B	9.8×10^{-12}	-0.44	0.0
R14	1.8×10^{-7}	[d]	0.0
R15	3.3×10^{-10}	0.0	0.0
R16	5.0×10^{-16}	0.0	0.0
R17	4.4×10^{-10}	0.0	0.0
R18	2.5×10^{-10}	0.0	0.0
R19	1.1×10^{-5}	[e]	0.0
R20	1.8×10^{-10}	0.0	0.0
R21	5×10^{-13}	0.0	0.0
R22	2.0×10^{-11}	-0.4	0.0
R23	8.0×10^{-13}	0.0	0.0
R24	5.0×10^{-13}	0.0	0.0
R25	1.0×10^{-9}	0.0	0.0
R26	7.8×10^{-8}	-0.5[b]	0.0
R27	0.0		
R28	1.0×10^{-10}	0.0	0.0
R29	5.0×10^{-13}	0.0	0.0
R30	2.5×10^{-10}	0.0	0.0
R31	1.0×10^{-10}	0.0	0.0
R32	1.0×10^{-7}	0.0	0.0
R33	3.0×10^{-10}	0.0	0.0
R34	3.0×10^{-10}	0.0	0.0
R35	4.2×10^{-7}	-0.85[b]	0.0
R36	1.8×10^{-11}	0.0	107.
R37	3.2×10^{-11}	0.0	67.

(a) Here $k = A(T/300)^B e^{C/T}$; units are $cm^3 sec^{-1}$ (bimolecular reactions).
(a) A slower rate, $k_3 = 4\times10^{-13}$, was also used in sensitivity studies.
(b) Temperature dependence uses electron temperature T_e.
(c) Reactions R10, R11 are photodissociation and photoionization rates that are zero for the nighttime auroral model.
(d) Temperature factor is T_v/T_e, where T_v is the vibrational temperature of N_2^+.
(e) Temperature factor is $T_e^{-0.7}$.

nuity equation, which becomes a quadratic equation upon substitution of Eq. (2-39),

$$q(z) = n_e \sum_I \alpha_i \, [M_i^+]$$

$$= n_e^2 \sum_I \alpha_i \frac{[M_i^+] \, n_e}{\sum_j [M_j^+]} = n_e^2 \sum_I \alpha_i \, f_i$$

$$= \alpha_{eff} \, n_e^2 \, . \qquad (2\text{-}40)$$

Here, $q(z)$ is the electron production rate from Eq. (2-16), and α_i is the recombination rate of electrons with positive ion M_i^+. Initially q_e is known, but not the f_i which determine the effective recombination rate α_{eff}. However, the α_i are not widely varying, and, in the region below between 90 and 150 km, NO^+ and O_2^+ are the predominant ions, so that an initial choice of α_{eff} of 3×10^{-7} cm^3 sec^{-1} gives a good first guess of n_e. The first iteration then gives values of the $[M_i^+]$ and thus f_i and a revised value of α_{eff} and n_e. This iterative procedure converges rapidly to the point at which consecutive values of n_e change by less than 0.1% within 5 to 15 iterations.

The linearized set of equations is readily put into matrix form

$$Ax = b \qquad (2\text{-}41)$$

with $b = P_0(i)$, $A(i, j) = P_i$ $(i \neq j)$, and $A(i, i) = -L_i$. The equations are then solved with a standard linear equation package (LINEQSV from the NCAR Scientific Subroutine Package).

This simple photochemical equilibrium solution neglects the time

dependence in the continuity equation and any transport terms. The chemical time constants of the nine species (see Table 5) under auroral conditions is less than the vertical transport time with the possible exception of $N(^4S)$ (which has a shorter lifetime than at low latitudes due to the greatly enhanced NO density), and thus our neglect of transport in this one-dimensional solution is reasonable. Above 150 km where O^+ becomes a significant ion species and its photochemical lifetime increases, ion transport becomes important. It should be noted that transport, especially horizontal winds, can significantly move aurorally produced long-lived species such as $N(^4S)$ and NO. Even qualitative modeling of horizontal winds over the tens of kilometers scale of auroral arcs is beyond the scope of this work and probably beyond the present state of the science.[78,79,80] For this reason we do not try to model the ambient NO density, but allow it to be an adjustable parameter. In reality its density is determined by pre-dosing and by present and past transport. We do, however calculate the NO production rate since it leads to prompt infrared radiation. There may be some error involved in the $N(^4S)$ density

78. Fuller Rowell, T.J. and Rees, D. (1981) A three-dimensional time-dependent simulation of the global dynamical response of the thermosphere to a geomagnetic substorm, J. Atmos. Terr. Phys. 43:701.

79. Fuller-Rowell, T.J. (1984) A two-dimensional,high-resolution, nested grid model of the thermosphere. 1. Neutral response to an electric field "spike", J. Geophys. Res. 89, 2971-2990.

80. Fuller-Rowell, T.J. (1985) A two-dimensional,high-resolution, nested grid model of the thermosphere. 2. Response of the thermosphere to narrow and broad electrodynamic features, J. Geophys. Res. 90, 6567-6586.

Table 5. Chemical Lifetimes of Metastables and Ions.

Species	Major Source	Major Loss	Reciprocal Lifetime τ^{-1}	τ (s)[@]
$N(^2D)$	N_2+e^{-*} N^++O_2 NO^++e^- N_2+O	$N(^2D)+O_2$	$k_4[O_2]$	0.1# 3.8x 45.0&
$N(^4S)$	N_2+e^{-*}	$N(^4S)+NO$ $N(^4S)+O_2$	$k_7[NO]+k_8[O_2]$	59.0# 89.0x 697.&
$N_2(A\ ^3T)$	N_2+e^{-*}	$N_2(A\ ^3T)+h\chi$ $N_2(A^3T)+O$	$(k_{1A}+k_{1B})[O]+A_{N2A}$	0.2# 0.7x 1.5&
N_2^+	N_2+e^-	$N_2^++O_2$ N_2^++O	$k_{12}[O_2]+(k_{13A}+k_{13B})[O]$	0.004# 0.07x 0.50&
O_2^+	$N_2^++O_2$ $O_2^++e^-$	O_2^++NO $O_2^++e^-$	$k_{15}[NO]+k_{19}[e^-]$	2.1# 3.9x 13.7&
O^+	O_2+e^{-*} $O+e^{-*}$	O^++O_2 O^++NO O^++N_2	$k_{21}[N_2]+k_{22}[O_2]+k_{23}[NO]$	0.02# 1.0x 17.7&
NO^+	N_2^++O N^++O_2 O_2^++NO	NO^++e^-	$k_{35}[e^-]$	1.5# 3.4x 9.0&
N^+	N_2+e^{-*}	N^++O_2	$(k_{33}+k_{34})[O_2]$	< 0.001# 0.04x 0.6&
$O_2^+(a\ ^4\Pi)$	O_2+e^{-*}	$O_2^+(a\ ^4\Pi)+N_2$ $O_2^+(a^4\Pi)+O$	$k_{30}[N_2]+k_{31}[O]$	< 0.001# 0.01x 0.1&
e^-	$\epsilon^{-*}+N_2, O_2, O$	$e^-+O_2^+$ e^-+NO^+	$k_{19}[O_2^+]+k_{35}[NO^+]$	<u>IBC III</u> 2.2# 3.9x 16.0& <u>IBC II</u> 16.0# 9.2x 26.7&

@ Lifetime in seconds for standard IBC III aurora with high NO profile.
# 100 km altitude.
x 120 km altitude.
& 150 km altitude.

since we calculate it using photochemical equilibrium and reaction with NO is its major loss process. However, $N(^4S)$ is not the major source of NO(v) under aurorally disturbed conditions (see next section) and thus error in its computation will not have a serious impact on the IR emission. Choice of the NO profile will, however, have a major impact on the NO airglow radiance.

Our use of the photochemical equilibrium approximation means that long-lived species that are affected by time-varying sources and transport will not be calculated accurately. Production of NO is greatly enhanced during auroral precipitation. However, the NO density cannot be accurately calculated with our simple model since the dominant chemical loss is

$$k_7 \, [N(^4S)] \, [NO]$$

$$\tau = 1 \, / \, (k_7 \, [N(^4S)]) \geq 1 \text{ hr.}$$

(During daytime, NO dissociation (R10) produces $N(^4S)$ and O, the $N(^4S)$ then further removing more NO). The inclusion of NO in the chemical model will then be inaccurate, since its density depends strongly upon the pre-dosing history and transport. The chemical calculation is further complicated by the fact that the loss of both N and NO would be nonlinear. After the auroral precipitation decreases or stops, N and NO cannibalize each other and the smaller of the two (usually N) is dramatically decreased. As the densities decrease the lifetime becomes longer and can become many hours (days in the polar night).

For this reason we give the user the choice of two NO profiles which remain constant during the calculation. In future releases, the treatment of NO can be improved by allowing the user to supply the NO profile, allowing different profiles within the arc and outside it, and allowing a time-dependent calculation within the arc. A truly accurate calculation would need to include horizontal transport over scales of tens to thousands of kilometers which is beyond the present state of the science, especially for an interactive model.

Solving Eq. (2-41) iteratively at each altitude on a 2 km grid between 90 and 160 km yields the nine constituent densities that determine the rates of chemiluminescent reactions producing NO(v), $NO^+(v)$ and the chemical sources that produce $N_2(v)$. In the next sections we will discuss in more detail the calculation of the volume emission rates of NO(v) and $NO^+(v)$ before we discuss the more complex calculation of the CO_2 ν_3 emission rate and radiative transfer.

2.4.2 NO $\Delta v=1$ AND $\Delta v=2$ SEQUENCES.

The photochemical equilibrium (PCE) calculation described above yields the steady-state densities of $N(^2D)$ and $N(^4S)$ as a function of altitude. These two species are precursors of NO(v) in the two reactions

$$N(^2D) + O_2 \rightarrow NO(v) + O, \qquad \text{R4}$$

$$k_4(v) = f_4(v)(7.4 \times 10^{-12})(T/300)^{0.5} \quad cm^3\ sec^{-1} ,$$

and

$$N(^4S) + O_2 \rightarrow NO(v) + O, \qquad R3$$

$$k_3(v) = f_3(v)(1\times10^{-12}) \exp(-3220/T) \text{ cm}^3 \text{ sec}^{-1},$$

where f(v) is the fractional rate populating state v of the NO product. The reaction numbers are taken from Tables 3a and 4. The f(v) have been obtained from experiments at AFGL.[27,29,81,82] Figure 6 shows the values of f(v) for reaction R4 from COCHISE[27] and LABCEDE[29]. The reaction of $N(^2D) + O_2$ is the predominant source of NO. $N(^4S)$ is important only at high temperatures because the large activation energy for reaction R3 makes the rate orders of magnitude smaller. For example at 200 K, k_4 is 6.04×10^{-12} while k_3 is 1.1×10^{-19}. Even at 400K the ratio of the $N(^2D)$ rate to the $N(^4S)$ rate is still greater than 2.5×10^4. Furthermore, reaction R4 can populate higher vibrational levels. Reaction of O_2 with $N(^4S)$ is an insignificant source of NO(v) compared to reaction with $N(^2D)$ (see Figure 7). The $N(^4S)$ component can become a more significant portion of NO(v) at higher altitudes, and because of the long lifetime of $N(^4S)$, it is still present after the $N(^2D)$ source has decayed away (after dosing has decreased). It should be remembered that the $N(^4S)$ term is likely to be less accurate due to the inappropriate use of the steady-state

81. Winkler, I.C., Stachnik, R.A., Steinfeld, J.I., and Miller, S.M. (1986) Determination of NO(v=0-7) product distribution from the $N(^4S) + O_2$ reaction using two-photon ionization, J. Chem. Phys. 85:890-899.

82. Rahbee, A., and Gibson, J.J. (1981) Rate constants for formation of NO in vibrational levels $\nu = 2$ through 7 from the reaction $N(^4S) + O_2$ --> $NO^* + O$, J. Chem Phys. 74:5143-8.

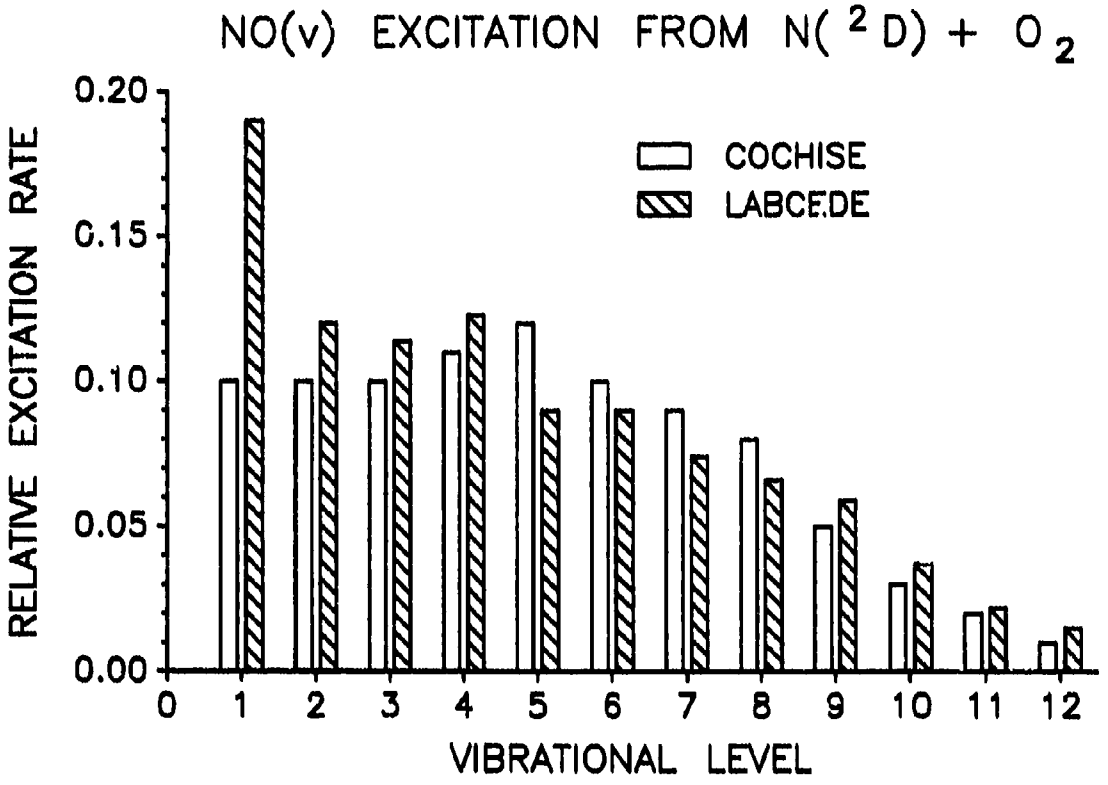

Figure 6. The Relative Excitation Rate, f(v), of Specific NO(v) Levels Populated via $N(^2D) + O_2$ Reaction Determined from Laboratory Experiments at AFGL. The triangles (Δ) are COCHISE results that assume $f(v=0) \approx 0.1$. The * are LABCEDE results that assume $f(v=0) = 0.0$.

approximation to calculate $N(^4S)$.

The COCHISE[27] experiments have measured vibrational excitation of NO out to v=12 (see Figure 6) resulting from reaction R4. The fractional rate constants f(v) are sometimes referred to as the nascent distribution, although they are only derived from measuring emission from a nascent or unrelaxed distribution of vibrational states pro-

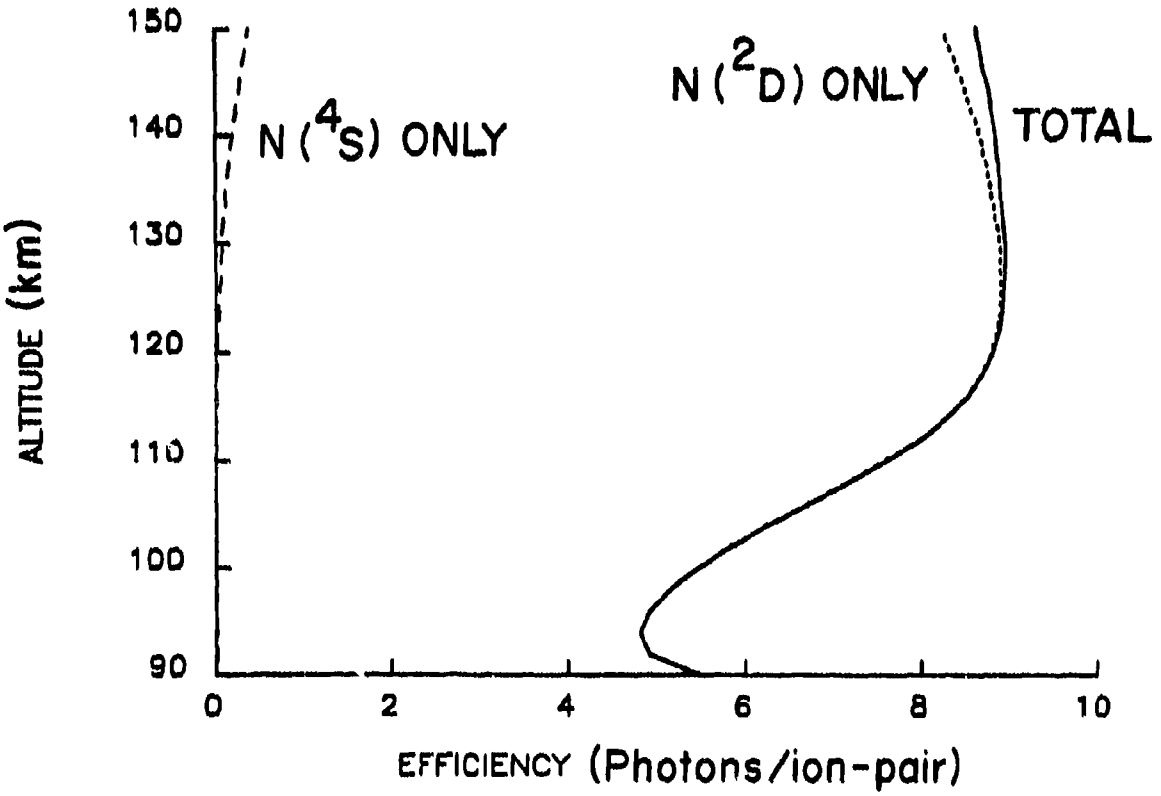

Figure 7. Efficiency of NO(Δv=1) Supplied in ALLDAT for AARC. The contribution (----) from N(^{4}S) + O_2 is small at 150 km and becomes negligible below 120km.

duced by reaction R4. Figure 6 shows that the two measurements of f(v) are in fair agreement with the possible exception of v=1 where there are large uncertainties. COCHISE measurements also measured high f(1) but argued that f(v) for v=1 through 7 were essentially equal[27]. Neither of these experiments could measure formation of NO(v=0). If NO(v=0) is largely populated by R4, then the corresponding f(v>1) would be decreased. Consequently, we estimate that there is an uncertainty in the production rate of NO(v) [$k_4 f(v)$] that is likely to be 20-30%.

In the atmosphere the volume emission rate is produced from a population that is relaxed by radiative cascade and collisional processes. The band Einstein coefficients[83-85] for v = 1 - 12 are in the range 10 - 60 sec^{-1}. This means that the radiative lifetime is always less than 0.1 sec^{-1}. This short lifetime allows us to calculate the relaxed vibrational distribution assuming a steady state is established (we assume that the dosing rate remains constant over such short times). Setting the loss rate of each of the twelve levels equal to the production rate results in a set of twelve linear equations

83. Billingsley II, F.P. (1975) Calculated Vibrational-Rotational Intensities and Line Positions for Ground State Nitric Oxide, AFGRL-TR-75-0586, AD A019790.

84. Billingsley II, F.P. (1976) Calculated vibration-rotation intensities for NO($X^2\Pi$), J. Mol. Spectrosc. 61:53.

85. Gillis, J.R. and A. Goldman (1982) Nitric oxide IR line parameters for the upper atmosphere, Appl. Opt. 21:1161-1162.

$$\sum_{k=i+1}^{N} [NO(v = k,\ z)] \left(A_{ki} + \sum_j k_{kij}\ [Q_j(z)] \right)$$

$$+ f(v = i)\ k_4\ [N(^2D;\ z)]\ [O_2(z)]$$

$$- \sum_{l=0}^{i-1} [NO(v = i;\ z)] \left(A_{il} + \sum_j k_{ilj}\ [Q_j] \right), \qquad (2\text{-}42)$$

where A_{il} is the Einstein coefficient for spontaneous emission from the i^{th} vibrational level to the l^{th} and k_{ilj} is the quenching rate from the i^{th} level to the l^{th} level by quencher Q_j at level z. The top two lines of the equation are the production of the i^{th} level and the third line is the loss. Radiative cascade and quenching are both production and loss processes for all intermediate levels. For each of the 12 excited vibrational levels that can be populated (and radiate) there is one equation. This coupled set of linear equations can be put into matrix form

$$Bx = c \qquad (2\text{-}43)$$

where c is a vector of the inhomogeneous production rate terms arising from the second line of Eq. (2-42), and B is the matrix of production and loss terms by radiation and quenching. The loss terms all appear on the diagonal.

The straightforward use of Eq (2-42) is hampered by the lack of knowledge of the quenching rates and radiative lifetimes. The radiative lifetimes are more certain than the quenching rates. The radiative loss is dominated by the fundamental (Δv=1) and overtone (Δv=2)

transitions. We initially used the Einstein coefficients calculated by Billingsley,[83] and later rescaled these values upward by 21% for the $\Delta v=1$ transitions to be consistent with the AFGL line tape[36] based on the measurements of Gillis and Goldman.[85] For the overtone transition probabilities, Gillis and Goldman derive only $v'= 2$, 3, 4, and 5, and the ratios of the first two to Billingsley's are 1.83 and 0.84. However, the ratios for $v' = 4$ and $v' = 5$ are close to 1.21, so that the rest of Billingsley's $\Delta v=2$ values are multiplied by the same 1.21 used for the fundamental. Table 6 shows the values used in AURORVIBNO.

The quenching rates are much less certain, being much harder to measure and nearly impossible to calculate theoretically. Laboratory measurements indicate that O and O_2 are the only atmospheric species that could be significant quenchers of NO(v) above 90km. The experimental values are for atomic oxygen[86,87] $k_{1,0} = 6.5 \times 10^{-11}$ cm^3 sec^{-1}, and for molecular oxygen[88,89,90] $k_{1,0} = 3 \times 10^{-14}$ cm^3 sec^{-1}. Above

86. Fernando, R.P., and Smith, I.W.M. (1979) Vibrational relaxation of NO by atomic oxygen, Chem. Phys. Lett. 66:218.

87. Glanzer, K., and Troe, J. (1975) Vibrational relaxation of NO in collisions with atomic oxygen and chlorine, J. Chem. Phys. 63:4352.

88. Murphy, R.E., Lee, E.T.P., and Hart, A.M. (1975) Quenching of vibrationally excited nitric oxide by molecular oxygen and nitrogen, J. Chem. Phys. 63:2919-2925.

89. Fernando, R.P., and Smith, I.W.M. (1981) Relaxation of NO(v=1) by radical species, J. Chem. Soc. Farad. Trans. II 77:459.

90. B.D. Green, Caledonia, G.E., Murphy, R.E., and Robert, F.X. (1982) The vibrational relaxation of NO(v=1-7) by O_2, J. Chem. Phys. 76:2441-2448.

Table 6. Band Parameters for NO Δv=1 and Δv=2 Transitions

v'	Band origin, Δv=1 (cm^{-1})	$A_{v',v'-1}1$ (sec^{-1}) (This work)	$A_{v',v'-1}1$ (sec^{-1}) (Billingsley)	Band origin, Δv=2 (cm^{-1})	$A_{v',v'-1}2$ (sec^{-1}) (This work)	$A_{v',v'-1}2$ (sec^{-1}) (Billingsley)
1	1875.95	13.16	10.78	----	----	----
2	1847.60	24.92	20.43	3723.75	0.46	0.84
3	1819.76	35.52	29.11	3687.56	1.51	1.27
4	1791.78	44.51	36.49	3611.54	3.78	3.10
5	1763.86	52.37	42.93	3555.63	5.98	4.90
6	1735.88	59.22	48.54	3499.74	8.89	7.29
7	1708.00	65.32	53.54	3443.89	11.75	9.63
8	1680.10	70.13	57.48	3388.11	15.25	12.50
9	1652.06	73.87	60.45	3332.16	19.13	15.68
10	1624.07	76.58	62.77	3276.12	23.35	19.14
11	1596.02	78.26	64.15	3220.08	27.99	22.94
12	1567.73	78.82	64.64	3163.75	33.12	27.15

90 km the O/O_2 ratio increases and quenching by O becomes correspondingly more important. Thus the uncertainty in the atomic oxygen profile will impact the accuracy of model calculations of NO(v) radiance. A possibly greater uncertainty arises from the unknown dependence of $k^q_{i,l}$ upon the upper vibrational level i and possibly the lower level l. Due to the lack of measurements of the vibrational-level dependence, we have chosen reasonable limiting cases. For quenching by O the two cases are

$$\text{I.} \quad k_{i,l} = \delta_{l,i-1}\, k_{i,0} \tag{2-44a}$$

$$\text{II.} \quad k_{i,l} = \frac{(i-l)\, k_{i,0}}{\sum_{k=0}^{i-1}(i-k)} = \frac{2\,(i-l)}{i\,(i+1)} \quad . \tag{2-44b}$$

Case I is a reasonable lower limit for the total quenching. It assumes only quenching to the next lowest level (single-quantum-quenching) with all rate constants equal to that for the first level (SQQ1). Case II follows from the suggestion of Quack and Troe[91] that the total quenching from any level i is the same (measured for v'=1), but that multiquantum quenching should be preferred. It yields much less radiation since the preferred quenching to v''=0 prevents subsequent radiative cascade after the initial quenching.

The 12x12 set of linear equations is then solved by standard techniques yielding the steady-state populations $n_{v'}(z_i)$ at altitude grid point z_i. The volume emission rate is $n_{v'}(z_i)A_{v'v''}$. Since these emissions are prompt and accurately described by the steady-state solution, we can characterize the volume emission rate by an efficiency. We define an efficiency ϵ in terms of photons emitted per ion-pair produced by the precipitating electrons. These units are most convenient since the calculation of a spectrum depends directly on the photons emitted. This efficiency can be converted to an energy

91. Quack, M., and Troe, J. (1975) Complex formation in reactive and inelastic scattering: statistical adiabatic channel model of unimolecular processes. III, Ber. Bunsenges. Phys. Chem. 79: 170.

efficiency by noting that the photon energy is $hc\nu$, where h is Planck's constant, c is the speed of light, and ν is the frequency in cm^{-1}. Since 35 eV is used per ion-pair produced,

$$\text{Energy-eff.} = \frac{(6.626 \times 10^{-27}\text{erg sec})\ (3 \times 10^{10}\text{cm/sec})}{(35\ \text{eV/ion-pair})\ (1.6 \times 10^{-12}\text{erg/eV})}\ \nu\ \epsilon$$

$$= 3.55 \times 10^{-6}\ \nu\ \epsilon\ . \qquad (2\text{-}45)$$

The efficiency is calculated and stored as a function of altitude for each upper-state vibrational level for the fundamental $\epsilon_1(v', z_i)$ and the overtone $\epsilon_2(v', z_i)$. The total efficiency for the fundamental, $\epsilon_1(z_i)$ and overtone $\epsilon_2(z_i)$ are obtained by summing the individual efficiencies over all upper levels. If the concept of an efficiency is valid (prompt emission, independent of dosing level, which we will show is true later in this section) then for a given dosing profile, the volume emission rate in each band at each level can be easily reconstructed without performing additional photochemical calculations. From the volume emission rate of these optically thin emissions the line-of-sight radiance is easily calculated by summing up the contributions along the path.

The photochemical calculation of the nitric oxide radiance depends upon many parameters. We have already mentioned the most important ones, the quenching rates and the atomic oxygen profile. Since there are uncertainties in these parameters, we have performed a limited sensitivity analysis. The neutral-ion aurorally driven photochemical code AUROR.PCE.CHEM is run with different values of the selected pa-

rameters, followed by AURORVIBNO. The key output of AUROR.PCE.CHEM that effects NO(v) is the efficiency of $N(^2D)$ per ion pair. $N(^2D)$ is sensitive to branching ratios of dissociation, dissociative ionization, dissociative recombination and ion-molecule reaction. We have used the generally accepted values for these branching ratios[23] in the production of $N(^2D)$,

$$e^* + N_2 \text{ ---> } b_4\ N(^2D) + (2-b_4)\ N(^4S) \qquad b_4 = 1.0 \qquad \text{PDN2}$$

$$e^* + N_2 \text{ ---> } N^+ + b_5\ N(^2D) + (1-b_5)\ N(^4S) \qquad b_5 = 0.50 \qquad \text{PNP}$$

$$NO^+ + e \text{ ---> } b_3\ N(^2D) + (1-b_3)\ N(^4S) + O \qquad b_3 = 0.76 \qquad \text{R35}$$

$$N_2^+ + e \text{ ---> } b_2\ N(^2D) + (2-b_2)\ N(^4S) \qquad b_2 = 1.0 \qquad \text{R14}$$

$$N_2^+ + O \text{ ---> } NO^+ + b_1\ N(^2D) + (1-b_1)\ N(^4S) \qquad b_1 = 0.90\ . \qquad \text{R13A}$$

The most important of these reactions are PDN2, R13A, and R35, since N_2^+ is not a dominant ion, and dissociative ionization is less likely than dissociation of N_2. The branching ratio b_4 is usually assumed to be about 1.0 (about half $N(^2D)$), probably between 0.9 - 1.1. Near $b_4 = 1$, the amount of NO that can be formed is very sensitive to the value of b_4, since $N(^4S)$ tends to destroy NO (R7), while $N(^2D)$ will produce it. The branching ratio b_3 has been measured in the laboratory[92], and b_1 is usually assumed to be between 0.8 and 1.0. The loss

processes for N_2 are

$$N(^2D) + O_2 \text{ ---> } NO(v) + O(^1D, {}^3P) \qquad R4$$

$$k_4 = 7.4 \times 10^{-12}(T/300)^{0.5} cm^3 \text{ sec}^{-1}$$

$$N(^2D) + O \text{ ---> } N(^4S) + O \qquad R5$$

$$k_5 = [4.0 \times 10^{-13} - 4.0 \times 10^{-12} \exp(-250/T)] cm^3 \text{ sec}^{-1}$$

$$N(^2D) + NO \text{ ---> } N_2(v) + O(^1D, {}^3P) \qquad R7$$

$$k_7 = 3.3 \times 10^{-11} cm^3 \text{ sec}^{-1}$$

$$N(^2D) + e \text{ ---> } N(^4S) + e \qquad R8$$

$$k_8 = 1.0 \times 10^{-9} cm^3 \text{ sec}^{-1}$$

$$N(^2D) + O_2^+ \text{ ---> } O_2 + N^+ \qquad R9$$

$$k_9 = 2.5 \times 10^{-10} cm^3 \text{ sec}^{-1}$$

$$N(^2D) \text{ ---> } N(^4S) + h\nu \qquad R10$$

$$A(N(^2D)) = 1.1 \times 10^{-5} \text{ sec}^{-1}.$$

At low altitudes R4, which produces NO(v), is the major loss process of $N(^2D)$. Above 120 - 130 km, as the ratio of $[O]/[O_2]$ becomes greater than one, R5 becomes a significant loss of $N(^2D)$. The quenching of $N(^2D)$ by R5 causes a slight decrease in the number of $N(^2D)$

92. Kley, D., Lawrence, G.M., and Stone, E.J. (1977) The yield of $N(^2D)$ atoms in the dissociative recombination of NO+, J. Chem. Phys. 66:4157.

that react with O_2 per ion-pair, thus causing a slow decrease in the efficiency with increasing altitude above about 120-130km. At 120 km the fraction of positive ions that are NO^+ (NO^+/M^+) is maximum, which causes a maximum in the $N(^2D)$ produced by R35. The fraction of NO^+/M^+ is also the cause of the very weak dosing dependence of the $N(^2D)$ efficiency. As the dosing rate goes up with a corresponding increase in plasma density, the recombination rate increases. Slowly, recombination of O_2^+ starts to compete with charge transfer to NO^+, thus lowering the NO^+/M^+ ratio. This decrease in NO^+ again leads to less $N(^2D)$ via R35. This effect is one of the causes of the decrease in the $N(^2D)$ production, and thus NO(v) efficiency, for high dosing rates, as is seen in Figure 8. In this figure we have plotted three different levels of dosing, 5, 50, and 500 ergs cm^{-2} sec^{-1}. We have kept the Maxwellian characteristic energy constant at 10 keV, which is unrealistic, but causes the ratio of the energy deposition at all altitudes to be constant. This would not be true for our standard profiles in which the total deposition increases by about two orders of magnitude going from IBC II to IBC III$^+$. However, since the shapes of the standard profiles vary, the dosing at 96 km for IBC III$^+$ is more than 1000 times that of an IBC II using the standard Maxwellian deposition profile. (The more peaked Gaussian would yield an even greater value.)

The altitude dependence of the NO(v) efficiency is directly dependent on the altitude dependence of the $N(^2D)$ efficiency except around 90-100 km where the peak in the [O] profile supplies enough O to quench some of the NO(v). Above 100 km R13A becomes the increas-

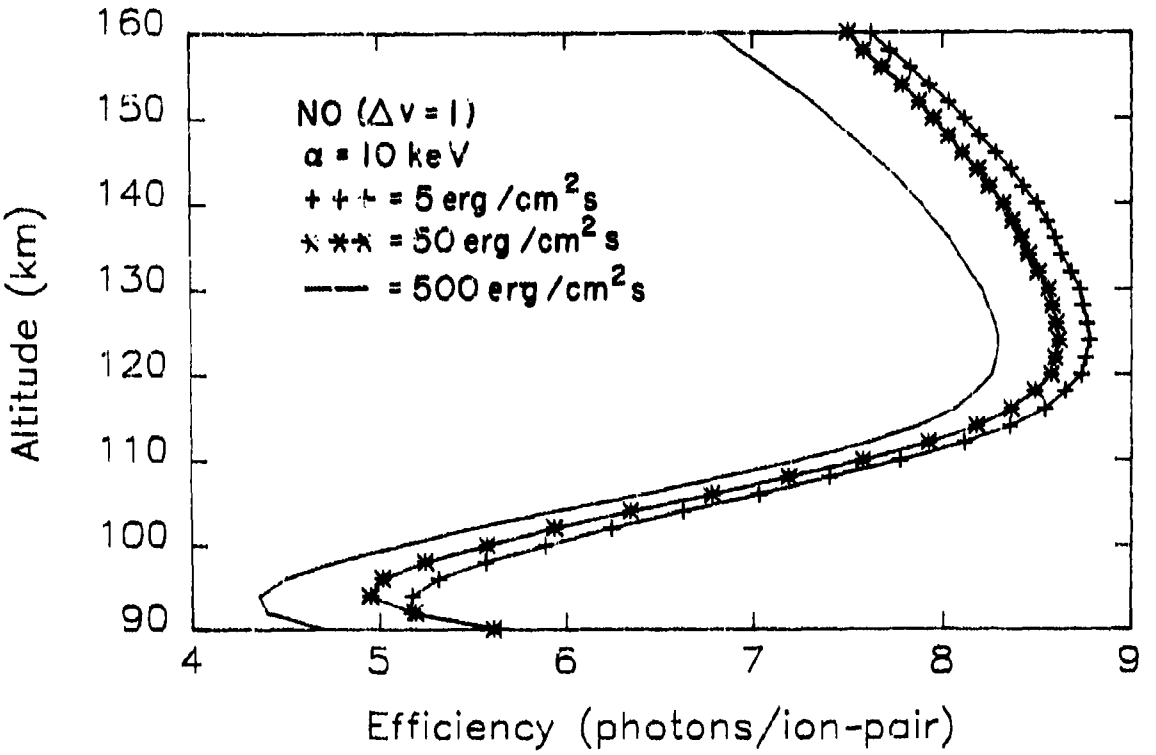

Figure 8. Sensitivity of NO(Δv=1) Efficiency is Shown as a Function of the Dosing Rate. All calculations use a Maxwellian spectrum with α=10keV. The efficiency is fairly independent of dosing until $\Phi \geq 250$ ergs/cm²/s. In AARC α=10 keV, Φ=100 ergs/cm²/s is used to calculate the efficiencies supplied in ALLDAT. At high dosing rate efficiencies decrease due to electron quenching and decrease in $[NO^+]/[O_2^+]$, thus decreasing the $N(^2D)$ production from recombination of NO^+.

ingly important source of NO^+ since the $[O]/[O_2]$ ratio is increasing. This not only supplies $N(^2D)$ when NO^+ recombines, but supplies nearly one $N(^2D)$ for each NO^+ produced by R13A. At higher altitude as the O_2 continues to decrease faster than O, R5 begins to compete as a loss mechanism for $N(^2D)$, and the efficiency slowly decreases.

The dominant sensitivity of the $\epsilon_1(z_i)$ and $\epsilon_2(z_i)$ and also the largest uncertainty in the calculation is the quenching rate of NO(v). Figure 9a shows plots of total NO $\Delta v=1$ and Figure 9b shows NO $\Delta v=2$ efficiency as a function of altitude for two choices of quenching mechanisms. Since the quenching is dominated by atomic oxygen [k_O/k_{O2} = 2000], the total efficiency decreases as [O] increases. However, above 100 km the lifetime of NO(v) is short and is determined mainly by the radiative lifetime (less than 0.1 sec). This means that for NO(v=1) to be significantly quenched, [O] must be greater than 1.6×10^{11} ($k_O = 6.5 \times 10^{-11}$). Above 110 km quenching becomes a small loss for v=1. For higher vibrational levels the radiative lifetime becomes even smaller (Table 6). The effect of quenching on these levels depends upon how k_O depends upon v'. The effect of the two choices previously mentioned [Single Quantum Quenching at rate k_1 (SQQ1), Multi-Quantum Quenching (MQQ)] upon $\epsilon_1(z_i)$ and $\epsilon_2(z_i)$ are shown in Figures 9a and 9b, respectively, for the standard [O] profile. This effect is quite dramatic in the altitude range below about 110-115 km where quenching is significant. The effect of changing the [O] profile is also shown in Figure 9a. Recall also that the dependence upon dosing was shown in Figure 8. These figures indicate that,

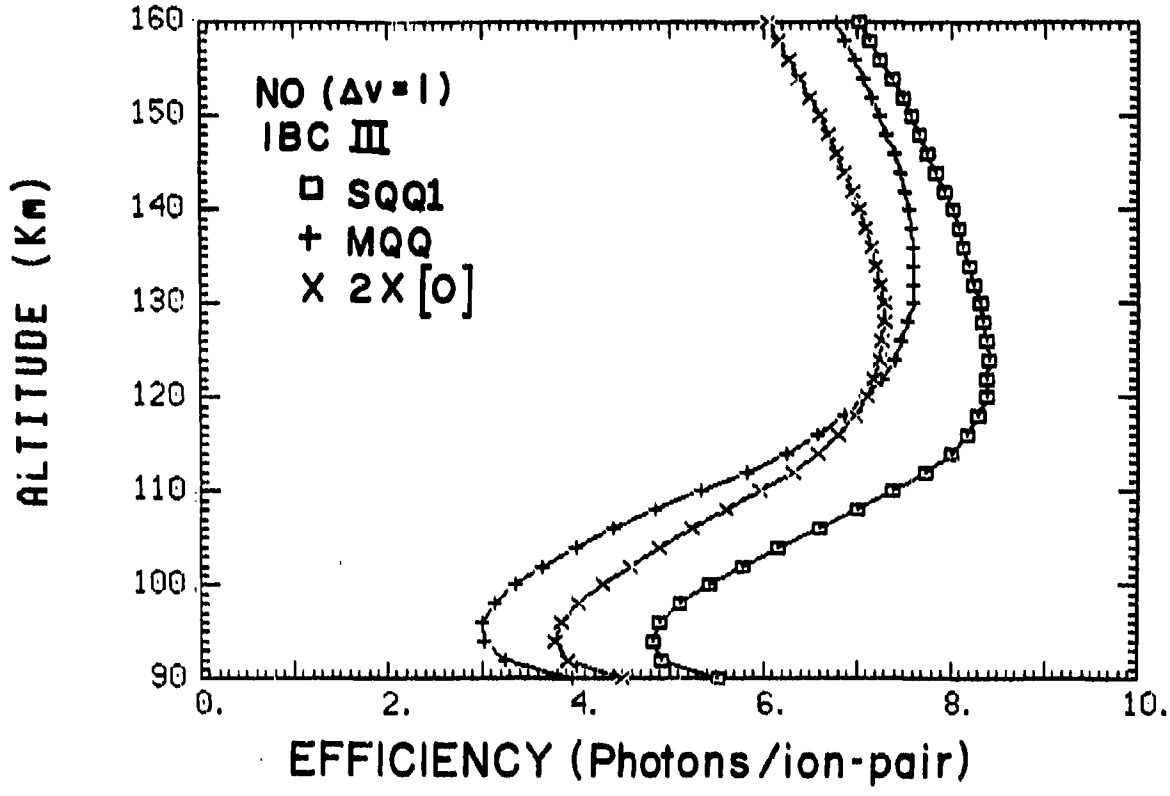

Figure 9a. Sensitivity of NO(Δv=1) Efficiency to Quenching Mechanism and Quencher Density. Squares (□) represent standard model which uses single quantum quenching (SQQ1) as discussed in text. The (+) represent multiquantum quenching (MQQ), which decreases the efficiency noticeably below 130 km. The (x) represent the standard case, except that the atomic-oxygen density is twice that of the USSA76 profile.

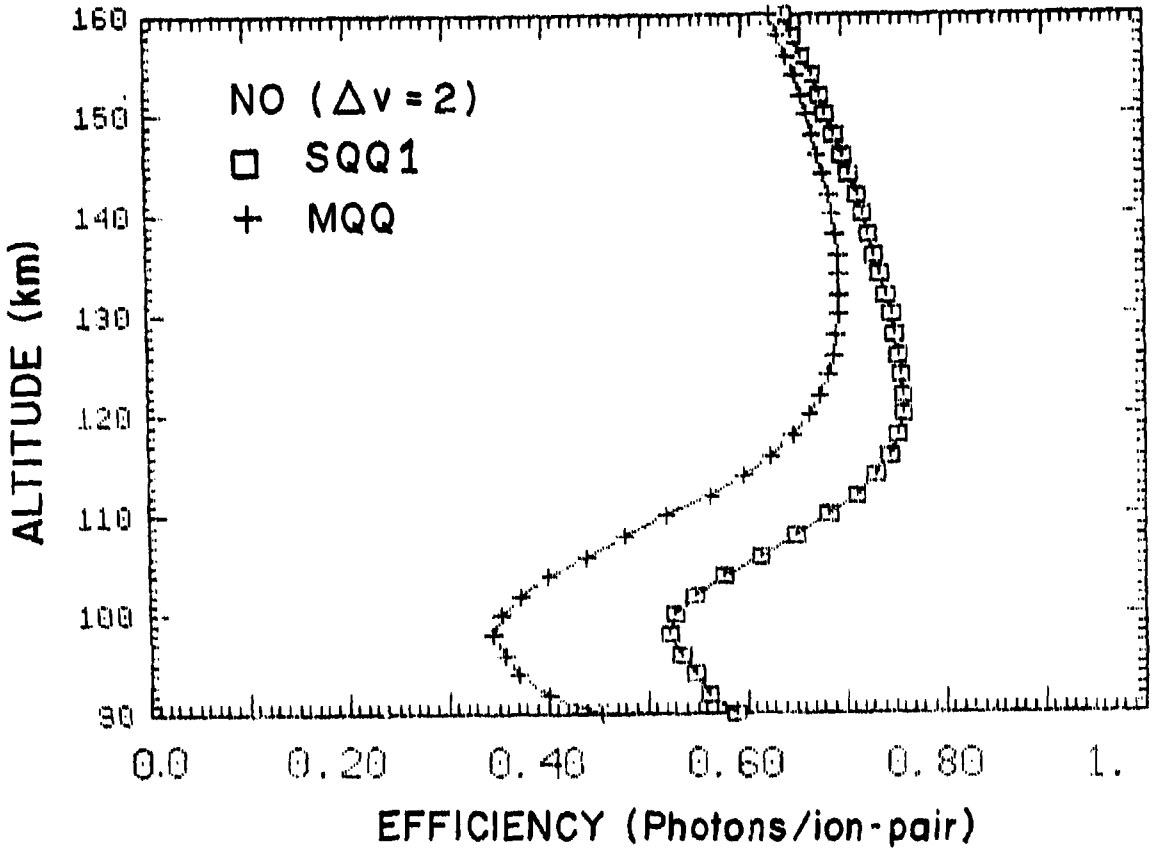

Figure 9b. Sensitivity of NO(Δv=2) Efficiency to Quenching Mechanism Similar to Figure 9a.

although the exact efficiency is somewhat uncertain due to uncertainties in [O], $k_0(v)$, and $k_4 f(v)$, the use of the concept of efficiency is valid. Over the range of likely auroral dosing, the change in NO(v) photons emitted per ion-pair formed is much smaller than the uncertainties in the kinetic parameters. In the standard version of AARC, the total system efficiencies, $\epsilon_1(v', z_1)$ and $\epsilon_2(v', z_1)$ obtained using the COCHISE values of f(v) in Figure 6, the SQQ1 quenching rates, and the standard [O] profile are stored in a file ALLDAT. These sets of parameters yield efficiencies that are near the likely upper limit, assuming that no other major processes are left out. These high efficiencies seem to give good agreement with the zenith radiance observed in an IBC II aurora by the AFGL/USU Field-Widened Interferometer[22] in April, 1983.

2.4.3 NO^+ VIBRATIONAL KINETICS

$NO^+(v)$ vibrational kinetics is handled in a similar manner to NO(v). A FORTRAN routine, AURORVIBNOP as part of AUROR.PCE.CHEM calculates the efficiency of $NO^+(v)$ photons per ion-pair from the steady-state concentration of $NO^+(v)$. The $NO^+(v)$ concentrations are calculated using chemical excitation and relaxation via collisions and radiation. NO^+ is the terminal E-region ion and it is produced by a number of fast exothermic ion-molecule reactions. All of the following reactions are exothermic enough to produce vibrational excitation:

$N_2^+ + O \text{ ---> } NO^+(v) + N(^4S)$, ΔE=3.08 eV, v_{max}=10 R13A(a)

$N_2^+ + O \text{ ---> } NO^+(v) + N(^2D)$, ΔE=0.69 eV, v_{max}= 2 R13A(b)

$$k_{13A}(\text{total}) = 1.4 \times 10^{-10}(T/300)^{-0.44} \text{ cm}^3 \text{ sec}^{-1}$$

$N^+ + O_2 \text{ ---> } NO^+(v) + O(^1S)$, ΔE=2.43 eV, v_{max}= 8 R33(a)

$N^+ + O_2 \text{ ---> } NO^+(v) + O(^1D)$, ΔE=4.66 eV, v_{max}=18 R33(b)

$N^+ + O_2 \text{ ---> } NO^+(v) + O(^3P)$, ΔE=6.63 eV, v_{max}=28 R33(c)

$$k_{33}(\text{total}) = 3.0 \times 10^{-10} \text{ cm}^3 \text{ sec}^{-1}$$

$N^+ + O_2 \text{ ---> } N + O_2^+$ R34

$$k_{34} = 3.0 \times 10^{-10} \text{ cm}^3 \text{ sec}^{-1}$$

$O_2^+ + NO \text{ ---> } NO^+(v) + O_2(X)$, ΔE=2.83 eV, v_{max}= 9 R17(a)

$O_2^+ + NO \text{ ---> } NO^+(v) + O_2(a)$, ΔE=1.85 eV, v_{max}= 6 R17(b)

$O_2^+ + NO \text{ ---> } NO^+(v) + O_2(b)$, ΔE=1.20 eV, v_{max}= 4 R17(c)

$$k_{17}(\text{total}) = 4.4\ 6{\cdot}10^{10} \text{ cm}^3 \text{ sec}^{-1}.$$

Reaction R33 is the only reaction for which the vibrational distribution of the products has been measured in the laboratory. Smith et al[28] have measured the infrared $NO^+(v)$ spectra produced from $N^+ + O_2$ and have deduced the fractional rate that populates v=1 through 14 (see Figure 10). These values are obtained by fitting synthetic band shapes to the fairly low resolution CVF spectrum of the chemiluminescence in a flowing afterglow. The Einstein coefficients of the levels v'=1 through 14 are needed to obtain the populations from the photon

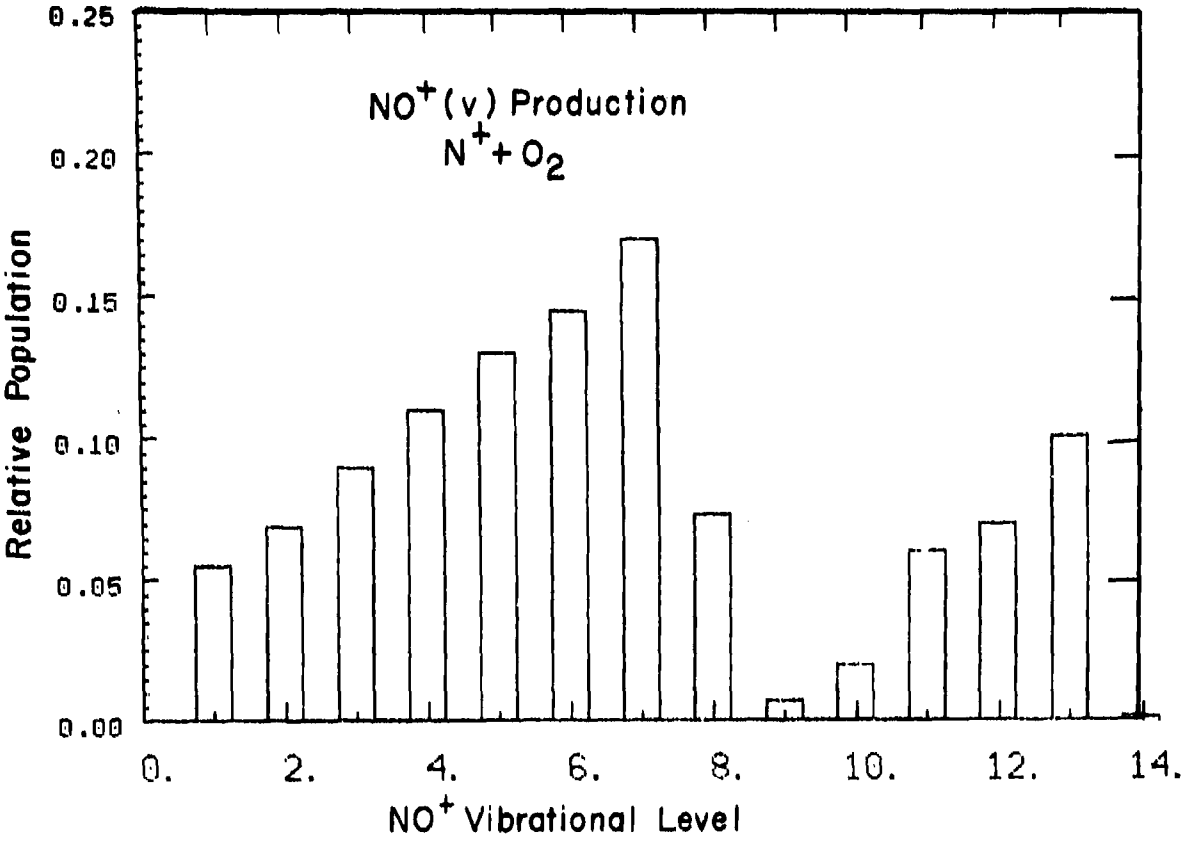

Figure 10. Relative Production Rate of NO^+ in Various Vibrational Levels from $N^+ + O_2$ Reaction.

emission rates. Smith et al[28] used the calculated values of Werner and Rosmus[93] (Table 7). These values seem reasonable, but there are no good experimental values with which to compare. The Δv=1 and Δv=2 Einstein coefficients are very similar to those for NO. The level v=0 can not be observed since it does not radiate, but if the fractional population of v=0 fits smoothly on the curve, it does not significantly affect the other rates.

Table 7. Band Parameters for $NO^+(v)$ Transitions

v'	Band origin, Δv=1 (cm^{-1})	$A_{v',v'-1}$@ (s^{-1})	Band origin, Δv=2 (cm^{-1})	$A_{v',v'-2}$@ (s^{-1})
1	2344.17	10.9	-------	----
2	2311.51	20.2	4655.67	0.697
3	2278.77	28.4	4590.27	1.93
4	2245.93	35.5	4524.69	3.61
5	2213.00	41.5	4458.92	5.74
6	2179.97	46.6	4392.96	8.24
7	2146.85	50.9	4326.82	11.1
8	2113.64	54.3	4260.48	14.2
9	2080.34	57.0	4193.97	17.7
10	2046.94	58.9	4127.26	21.3
11	2013.44	60.2	4060.36	25.1
12	1976.86	60.8	3993.29	29.0
13	1946.18	60.7	3926.02	33.2
14	1912.40	59.9	3858.56	37.4

@See reference 92.

93. Werner, H.-J., and Rosmus, P. (1982) *Ab Initio* calculations of radiative transition probabilities in the $^1\Sigma^+$ ground state of NO^+ ion, J. Molec. Spect. 96:362.

Process R13 becomes the major source of NO^+ at higher altitudes where $[O]>[O_2]$. Modeling of NO chemistry has indicated that $k_a/k_b > 0.9$. Thus the dominance of the $N(^2D)$ channel means that v=2 is the highest level that can be populated. Since this is so large a source of NO^+, we have included this reaction in some calculations as an additional source of $NO^+(v)$ with the assumption $f_I(v=0)=0.25$, $f_I(v=1)=0.50$, and $f_I(v=2)=0.25$. This source not only almost doubles the total $\Delta v=1$ efficiency (Figure 11), but it also changes the shape of the resulting spectrum since it predominantly populates the v=1 level, which radiates in the 4.3-μm region along with the $CO_2(001)$ (Figure 12). Since this source has not been documented by laboratory or atmospheric measurements, it is not presently included in the working version of AARC.

Process R17 is the third major source of NO^+ in the D and lower E-region. This pathway is most important for high [NO] and lower dosing rates when the O_2^+ lifetime for R17 is shorter than for recombination R19. The large exothermicity again makes the production of $NO^+(v)$ possible. However, we neglect this reaction as a source of $NO^+(v)$ because no evidence of vibrational excitation has been observed, and we believe that the vibrational excitation of the product is less likely for a charge transfer reaction where no new bond is formed.

We use the same fractional production rates (Figure 10) as the source terms in a set of steady-state equations for the v=1 through v=14 levels analogous to the set of 12 equations [Eq. (2-43)] used for the NO(v). We also use the Einstein coefficients for the fundamental

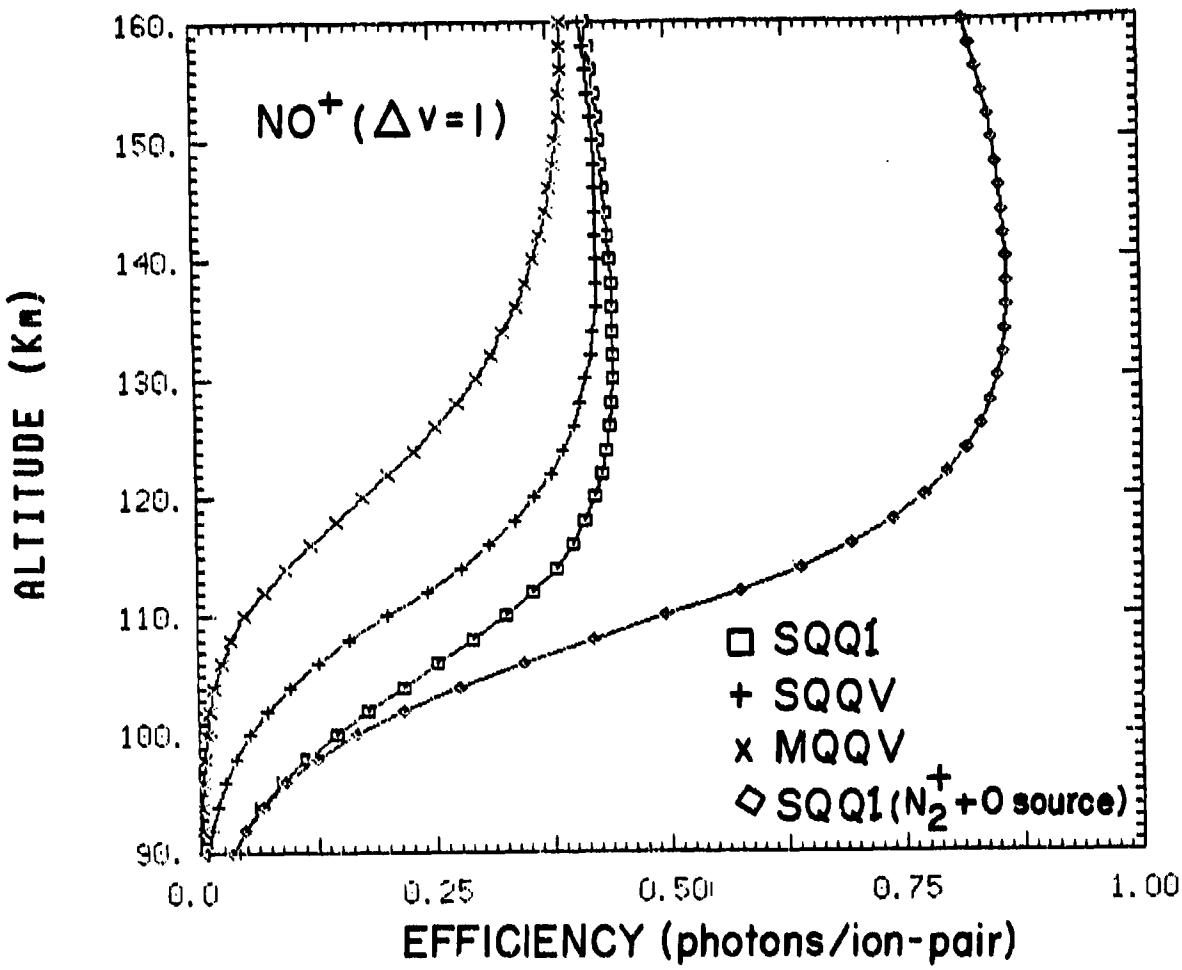

Figure 11. Sensitivity of $NO^+(\Delta v=1)$ Efficiency to Quenching Mechanism and Chemiluminescent Source. Squares (□) are single-quantum quenching (SQQ1) which is the AARC standard case; (+) are JQQV (see text), and (x) are multiquantum quenching MQQV (see text). The diamonds are for the standard case with the addition of $N_2^+ + O$ source of $NO^+(v)$ (see text).

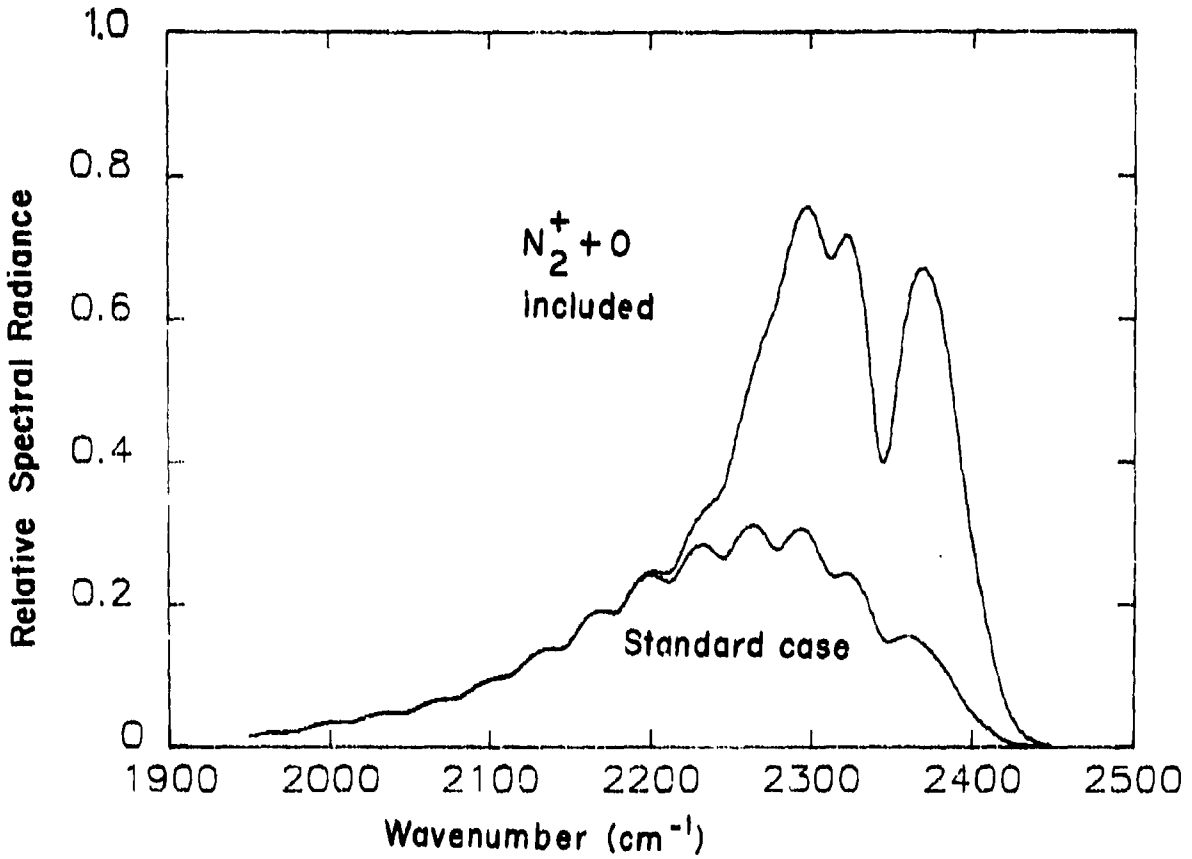

Figure 12. Low Resolution Spectra of NO^+ for the Standard Case and the Case That Includes $N_2^+ + O$ Reaction as Discussed in Text.

and overtone sequences from Werner and Rosmus. The other loss process for $NO^+(v)$ is vibrational quenching. The quenching of $NO^+(v=1)$ by N_2 is very fast[94,95], $k_{N2(1,0)} = 7 \times 10^{-12}$ cm^3 sec^{-1}, and, since N_2 is the major atmospheric component, quenching is important for v=1 up to about 110 km. Again, the quenching rates of the levels with v>1 have not been measured. Therefore, we make a few representative choices for the quenching rate:

I. Single-quantum quenching at rate $k_{1,0}$ (SQQ1) -

$$k_{v',v''} = \delta_{v'',v'-1}\, k_{1,0}$$

II. Single-quantum quenching at rate $v'k_{1,0}$ (SQQV) -

$$k_{v',v''} = \delta_{v'',v'-1}\, v'k_{1,0}$$

III. Multi-quantum quenching at rate $v'k_{1,0}$ (MQQV) -

$$k_{v',v''} = \delta_{v'',0}\, v'k_{1,0} \quad .$$

Choice I is a reasonable choice that is also a likely lower limit, assuming that quenching rates do not decrease with v', which might be the case if the resonant energy exchange were important and the proc-

94. Dobler, W., Federer, W., Howorka, F., Lindinger, W., Durup-Ferguson, M., and Ferguson, E. (1983) Vibrational relaxation of $NO^+(v)$ ions in neutral collisions, J. Chem. Phys. 79:1543-1544.

95. Ferguson, E.E., Adams, N.G., Smith, D., and Alge, E. (1984) Rate coefficients at 300K for the vibrational energy transfer reactions from $N_2(v=1)$ to O_2^+ and $NO^+(v=0)$, J. Chem. Phys. 80: 6095-6098.

ess became less resonant for higher v'. Choice II follows the common harmonic-oscillator scaling law for quenching, but becomes very fast for higher v (nearly quenching on every collision). Choice III is likely an upper limit, but the large multi-quantum loss is not likely.

The fast quenching rate of $NO^+(v=1)$ by N_2 and the near resonant vibrational levels of these two molecules suggest that it might be a resonant V-V process. If it is resonant, the reverse process would proceed at the same rate

$$N_2(v=1) + NO^+(v=0) \text{ ---> } N_2(v=0) + NO^+(v=1). \qquad \text{R20}$$

This would mean that large auroral enhancements of $N_2(v)$ could supply a long-lived (non-prompt) source of $NO^+(v)$ even though $[NO^+] < 1 \times 10^6$. However, recent experiments[83] have shown that reaction R20 proceeds at a rate much less than $NO^+(v)$ quenching, indicating that quenching proceeds through a cluster ion type complex, not by resonant vibrational transfer. Thus only the prompt mechanism using R33 is included in the calculation of NO^+ IR emission.

The $NO^+(\Delta v=1)$ efficiency obtained using only R33 depends strongly on the quenching mechanism. Figure 11 shows the $\Delta v=1$ efficiencies as a function of altitude. All of the profiles show evidence of the strong quenching at the lower altitudes, the quenching effect being evident at higher altitudes for SQQV and MQQV. Above 130 km quenching is unimportant and the efficiency falls off a little due to the decreasing mixing ratio of N_2. This behavior occurs since the N^+ pro-

duction is predominantly from N_2 [PNP proportional to N_2 and q_e, Eq. (2-35c)] and reaction with O_2 is the predominant loss mechanism for N^+. The SQQV and MQQV curves have the same shape as the SQQ1 curve but are considerably smaller in the region below 110 km where quenching is large. When process I is included, the efficiency is almost doubled as is shown in Figure 11. The shape of the curves when I is included are very similar to those using just process II. Preliminary analysis of the ELIAS data[77] and Kumer's analysis of the 1978 Auroral Dynamics experiment[76] indicate that the efficiency curve of SQQV agrees best with the data if only process II is used. However, the experimental errors are large so that SQQ1 with or without inclusion of I is just about as likely to be the correct mechanism. The resolution of the $NO^+(v)$ problem will take laboratory measurements of vibrational excitation in processes I and III and the quenching of higher states, and/or high resolution measurements of the 2100-2400 cm^{-1} spectral region during a strong aurora. In the FWI experiment the dosing was only about 7 erg/cm^2 with peak in the highly quenched 104 km region; thus the predicted $NO^+(v)$ radiation was in the noise and in fact was not observed.[22]

$NO^+(v)$ produced by reaction R33 leads to very prompt infrared emission. N^+, the precursor of $NO^+(v)$, is overwhelmingly produced by the nearly instantaneous dissociative ionization of N_2. The lifetime of the N^+ ion is determined by R33 and R34, with its conversion into $NO^+(v)$ within a lifetime

$$\tau_{N+} \sim 1/(k_{33}[O_2]) \quad = \quad 3.33 \times 10^9 \text{s cm}^{-3}/[O_2]. \qquad (2\text{-}47)$$

Since O_2 is a major constituent, $NO^+(v)$ is produced in less than 1 sec after dosing, even at 150 km. At altitudes near 100 km, the radiative lifetime of the $NO^+(v)$ states is longer than the characteristic time τ_{N+}. Thus our use of a steady-state approximation is totally justified for $NO^+(v)$. Time-resolved experiments with a coincident measure of the dosing rate should be able to distinguish this source in the 4.3-μm region from the $CO_2(001)$ even without high spectral resolution. The fact that R33 produces vibrational levels of NO^+ up to v=14 also means that a whole series of hot bands in the $\Delta v=1$ sequence will extend the radiation out to the 5 μm region. Table 7 shows the band origins for NO^+ $\Delta v=1$. Figure 13a shows a low-resolution (10 cm^{-1}) limb spectrum of NO^+ for an IBC III aurora at a tangent height of 110 km. At this resolution the overlapping R and P branches of the various hot bands give a scalloped appearance. Figure 13b shows the same limb spectra at 1 cm^{-1} resolution which clearly distinguishes the individual rotational lines. However, the overlapping bands produce some near-coincident lines that appear as one line if they are less than 1 cm^{-1} apart, giving a spectrum that is hard to interpret if it is noisy or contaminated with other emitters.

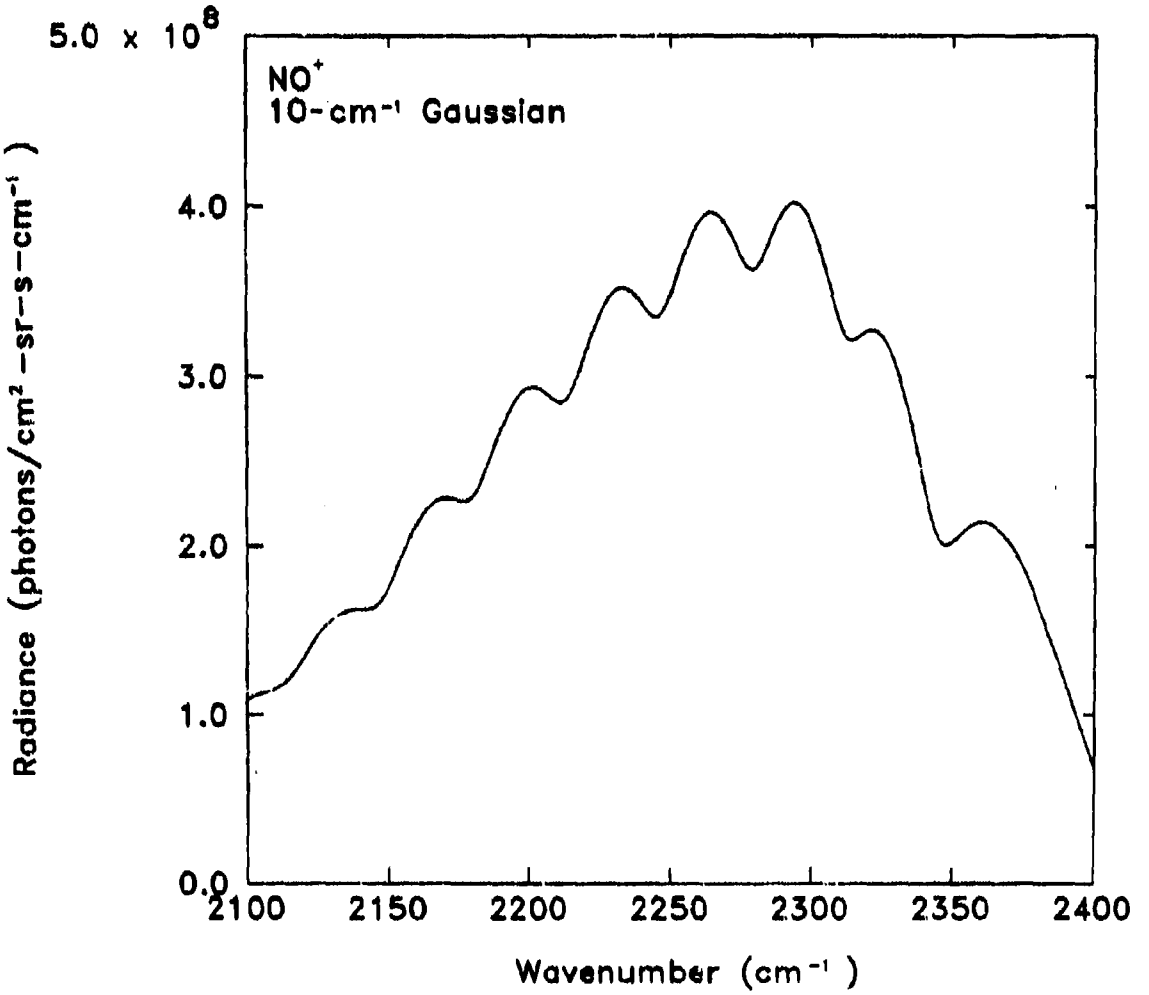

Figure 13a. Low Resolution ($10cm^{-1}$ Gaussian Window) Spectrum of NO^{+}.

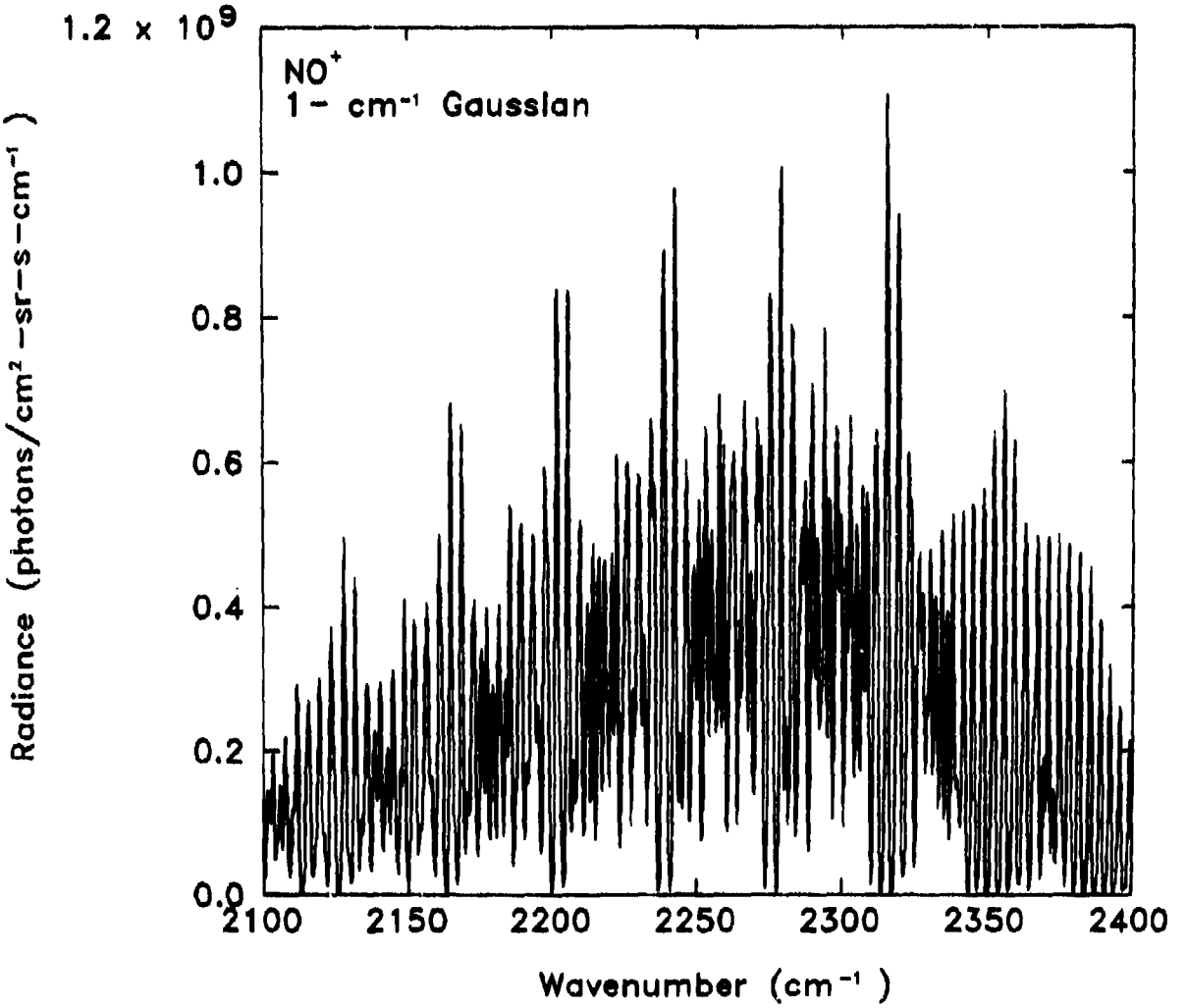

Figure 13b. High Resolution (1 cm^{-1} Gaussian Window) Spectrum of NO^+. Overlapping of bands originating from the many different v' complicates the identification of NO^+ by the overall shape.

2.5 Collisional Energy Transfer Processes

2.5.1. NO(v=1) AIRGLOW

Above 100 km during quiescent conditions, the NO(v=1) → NO(v=0) fundamental at 5.3 μm is one of the strongest IR emitters and a major cooling source of the lower thermosphere.[25,96,97] The major excitation (and quenching) mechanism is collisions with atomic oxygen,

$$NO(v=1) + O \rightleftarrows NO(v=0) + O \qquad R21$$

$$k_f = 6.0 \times 10^{-11} cm^3\ sec^{-1}$$

$$k_r = 6.0 \times 10^{-11} \exp(-1875c_2/T)\ cm^3\ sec^{-1},$$

where c_2 is the second radiation constant, 1.439 K/cm^{-1}. Earthshine is a smaller, but significant, source of excitation especially for small [O] and/or low temperature. We use an earthshine rate from Caledonia and Kennealy[25] which was calculated using LOWTRAN. The range of values stated corresponded to arctic winter and mid-latitude summer conditions, and the earthshine radiance seemed to correspond to the blackbody radiance of the earth's surface. If overlap of water lines in the troposphere is important, the earthshine pumping will come from a much colder region of the atmosphere, resulting in a lower excitation rate. Work is progressing (ARC) on an accurate line-by-line non-local-thermodynamic-equilibrium (NLTE) calculation of NO vibrational temperature in the quiescent atmosphere. We believe that

96. Stair, A.T., Sharma, R.D., Nadile, R.M., Baker, D.J., and Grieder, W.F. (1985) Observations of limb radiance with cryogenic spectral infrared rocket experiment, J. Geophys. Res. 90:9763-9775.

97. Kockart, G. (1980) Nitric oxide cooling in the terrestrial atmosphere, Geophys. Res. Lett. 7:137.

the present earthshine rate is a reasonable upper limit. Above 120 km, where the overwhelming amount of NO airglow originates, the earthshine is an insignificant source. Using the atomic-oxygen collision mechanism, an earthshine source, and radiative loss, we obtain the continuity equation for NO(v=1),

$$d[NO(v=1)]/dt = S_E[NO] + k_r[O][NO(v=0)] - k_f[O][NO(v=1)] - A_{5,3}[NO(v=1)] \quad , \tag{2-48}$$

where S_E is the earthshine pumping rate and $A_{5,3}$ is the Einstein coefficient for the (1-0) transition. If we solve for [NO(v=1)] assuming a steady state, we obtain the simple formula

$$[NO(v=1)] = \frac{S_E[NO] + k_R[O][NO(v=0)]}{A_{5,3} + k_f[O]} \tag{2-49}$$

or, in terms of the volume emission rate,

$$A_{5,3}[NO(v=1)] = \frac{[NO(v=0)](S_E + k_r[O])}{1 + k_f[O]/A_{5,3}} \quad . \tag{2-50}$$

This is a simple expression that is easily solved if [O], [NO], and the previously mentioned S_E are known. Both [O] and [NO] as mentioned earlier cannot be calculated accurately in a one-dimensional model, especially a time-independent model of the auroral atmosphere. Since [NO] is so dependent upon the dosing history and transport, its self-consistent calculation is beyond the scope of this model. However, we do supply the user a choice of a high [NO] that may be appropriate to the region of an active auroral arc[96], and a moderate[25] [NO] profile that may be representative of the auroral region outside the arc, which is higher than most mid-latitude or zonally averaged and time-

averaged high-latitude profiles.[99] The uncertainty in the [O] and [NO] is larger than that of S_E.

A further uncertainty is introduced into the NO(v=1) volume emission rate by the temperature dependence of k_r. The large activation energy corresponds to the energy of the NO vibrational transition, 1875 cm^{-1}. For this reason, the volume emission rate peaks in the 130-140 km region, well above the region of maximum [O] and [NO]. In this region the earthshine is insignificant and $A_{5.3} > k_r[NO]$; thus

$$A_{5.3}[NO(v=1)] \approx k_r[O][NO] = 6.0 \times 10^{-11}\exp(-1875c_2/T)[NO][O] ,$$

with the emission rate directly proportional to [O] and [NO] and an exponential dependence upon temperature. Although [O] and [NO] can easily be uncertain to greater than a factor of 2, it should be noted that a 10% increase in temperature for T in the 300 K range can also double the volume emission rate as shown in Figure 14.

2.5.2 CO_2(001) 4.3-μm AURORAL EMISSION

Large enhancements in the 4.3-μm emission during aurora have been known since the ICECAP experiments[3,7] of the early 1970's. Figure 15 shows a number of zenith radiance profiles measured during the ICECAP program. The enhancements in the 75-95 km region are orders of magnitude. These zenith-viewing measurements have been extensively ana-

98. Gérard, J.-C., and Barth, C.A. (1977) High-latitude nitric oxide in the lower thermosphere, J. Geophys. Res. 82:674-680.

99. Cravens, T.E., Gérard, J.-C., LeCompte, M., Stewart, A.I., and Rusch, D.W. (1985) The global distribution of nitric oxide in the thermosphere as determined by the atmospheric Explorer D satellite, J. Geophys. Res. 90:9862-9870.

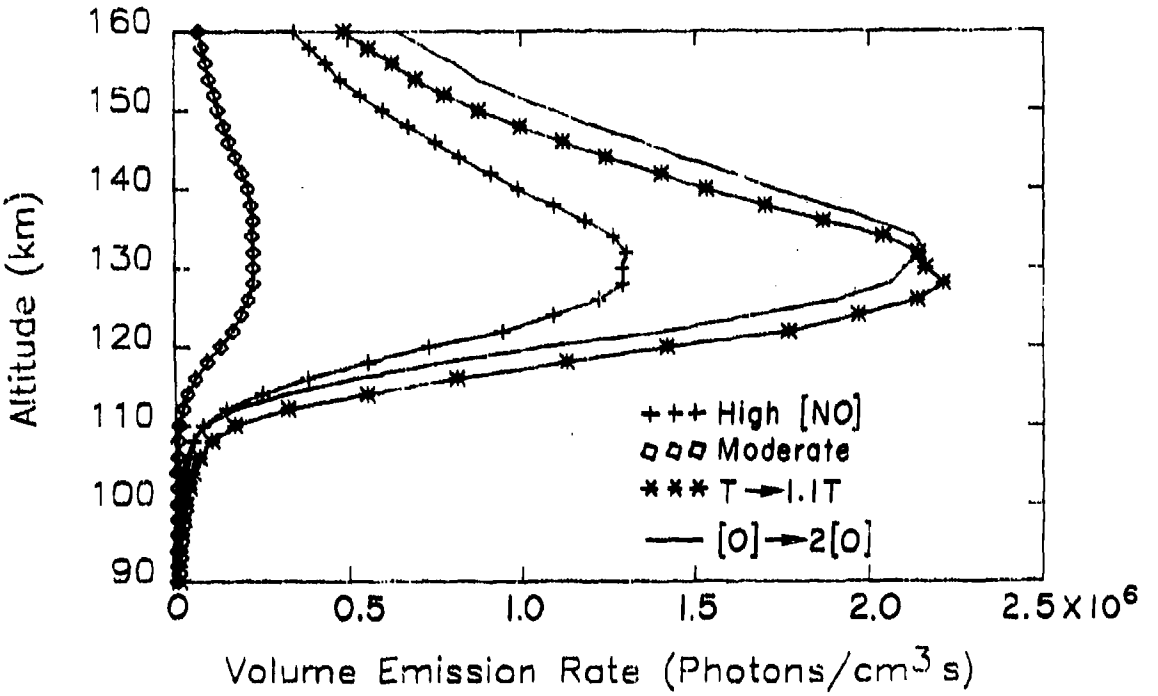

Figure 14. Sensitivity of NO Airglow to Model Parameters as Discussed in the Text. Standard model (+) uses the high NO profile and (◊) represents use of the moderate NO profile (see Fig. 4); (**) for case T'=1.1 T shows the large sensitivity to temperature; (-) indicates the increase due to doubling of atomic oxygen profile.

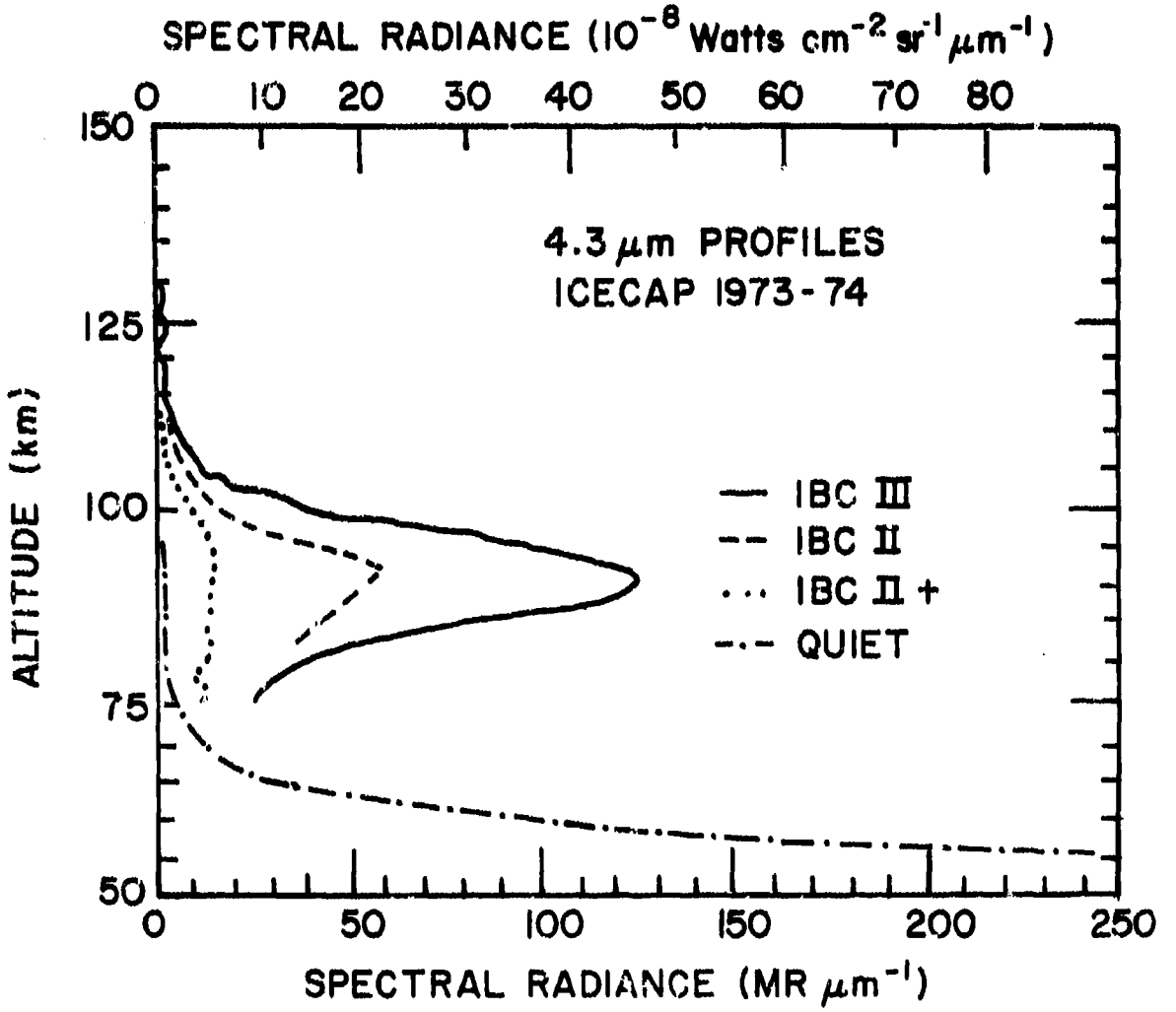

Figure 15. Spectral Radiance of the 4.3μm Signature in Aurora Measured During ICECAP Experiments. (——) is IBC III aurora; (----) is IBC II, and (••••) is IBC II^{+}. Note that radiance for IBC II is greater than for the more strongly dosed IBC II^{+} (see text).

lyzed and modeled by Kumer.[24,100] The predominant mechanism was determined to be the near-resonant transfer of vibrational quanta between $N_2(v=1)$ and $CO_2(001)$,

$$N_2(v=0) + CO_2(001) \rightleftarrows CO_2(000) + N_2(v=1), \qquad \text{R22}$$

$$\Delta E = 18 \text{ cm}^{-1},$$

$$k_{22} = 1.71 \times 10^{-6}\exp(-175.3/T^{1/3}) + 6.07 \times 10^{-14}\exp(15.27/T^{1/3})$$

$$\approx 8 \times 10^{-13} \text{ cm}^3 \text{ sec}^{-1} \text{ at } 200 \text{ K}.$$

Since N_2 is a major constituent of the atmosphere, it absorbs much of the energy of the precipitating electrons. $N_2(v)$ is populated by collisions with secondary electrons in the 2-5 eV range and by the chemical reactions[101]

$$N(^4S) + NO \rightarrow N_2(v) + O \qquad \text{R7}$$

$$k_7 = 7.0 \times 10^{-11} \text{ cm}^3 \text{ sec}^{-1}$$

$$O(^1D) + N_2 \rightarrow N_2(v) + O \qquad \text{R36}$$

$$k_{36} = 1.8 \times 10^{-11}\exp(107/T) \text{ cm}^3 \text{ sec}^{-1},$$

where 2.82 N_2 vibrational quanta (B_{11}) are produced per reaction R7 and 2.2 vibrational quanta (B_{12}) are produced by R6. The sources of $O(^1D)$ in the aurora are still a question of debate,[103,104,104] espe-

100. Kumer, J.B., and James, T.C. (1974) $CO_2(001)$ and N_2 vibrational temperatures in the $50 < z < 130$ km altitude range, J. Geophys. Res. 79:638.

101. Slanger, T.G., and Black, G. (1974) Electronic to vibrational energy transfer efficiency in the $O(^1D)$-N_2 and $O(^1D)$-CO systems, J. Chem. Phys. 60:468.

cially the branching ratios of $O(^1D)$ as products in reactions R4, R7, R19, and R33. The $O(^1D)$ chemical source does not appear to contribute more than about 25% of the total $N_2(v)$; thus even an error of about 50% would lead to only about 12% error in total $N_2(v)$. The major sources of $N_2(v)$ production per ion pair are shown in Figure 16. The efficiency $\epsilon[N_2(v)]$ depends weakly on the dosing rate and the [NO] chemistry (through R4 and R6 especially). The dosing dependence is most apparent in the secondary-electron contribution. At higher dosing levels and correspondingly higher plasma densities the few eV electrons start to lose a larger proportion of their energy to heating the ambient electrons at the expense of exciting $N_2(v)$. We have used the IBC III value for our standard auroral model since it is representative of bright auroras where enhancements are large.

The proper treatment of the CO_2 ν_3 radiation is more complex than the NO and NO^+ prompt radiation. The relatively slow $N_2(v)$-$CO_2(001)$ transfer leads to delayed emission. Furthermore, the $CO_2(001)$ radiation is optically thick below 100 km for radiation to space. Thus photons are reabsorbed and can be converted by collision with N_2 back

102. Link, R. (1983) A rocket observation of the 6300 Å/5200 Å intensity ratio in the dayside aurora: Implicastions for the production of $O(^1D)$ via the reaction of $N(^2D) + O_2 \rightarrow NO + O(^1D)$, Geophys. Res. Lett. 10:225-228.

103. Rusch, D.W., Gérard, J.-C., and Sharp, W.E. (1978) The reaction of $N(^2D)$ with O_2 as a source of $O(^1D)$ atoms in aurorae, Geophys. Res. Lett. 5:1043.

104. Langford, A.O., Bierbaum, V.M., and Leone, S.R. (1985) Auroral implications of recent measurements of $O(^1S)$ and $O(^1D)$ formation in the reaction of N^+ with O_2, Planet. Space Sci 33:1225-1228.

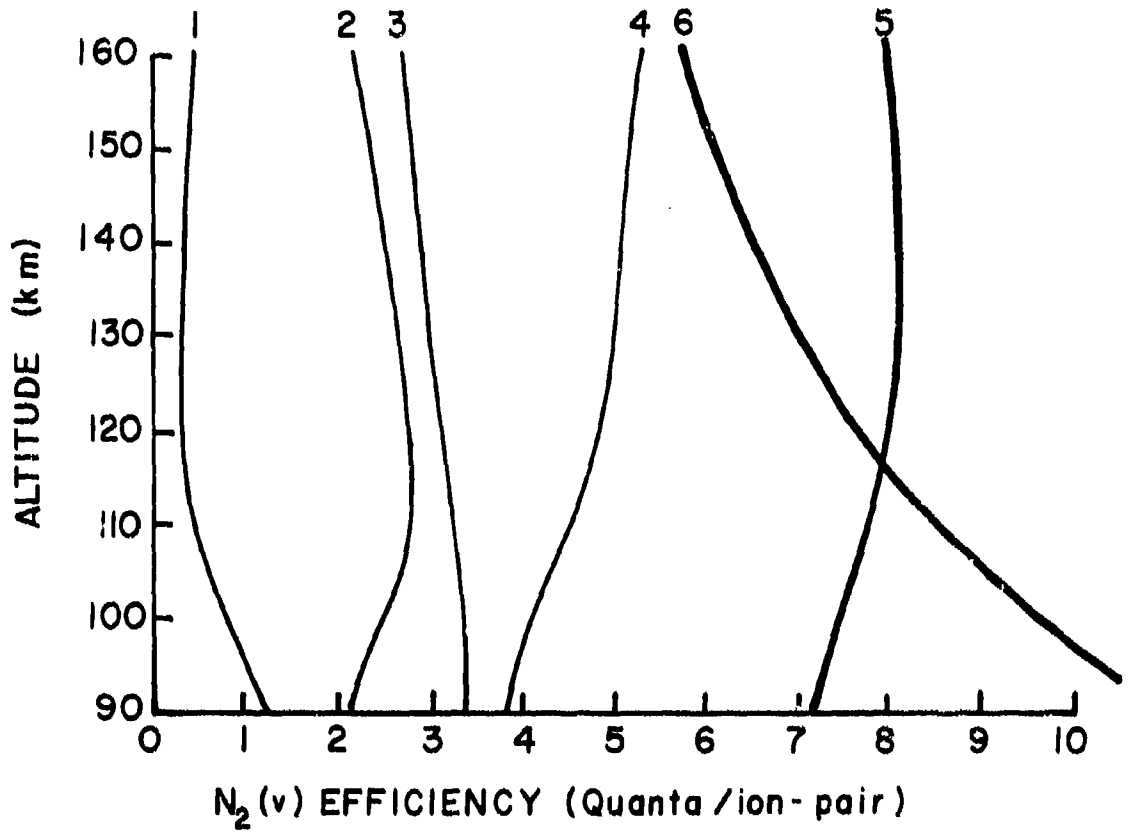

Figure 16. Contribution to $N_2(v)$ Efficiency (quanta/ion-pair) from Various Sources for IBC III Dosing. Curve 1 is $O(^1D) + N_2$ due to $O(^1D)$ from O_2^+ recombination; (2) $O(^1D) + N_2$ with $O(^1D)$ from the $N(^2D) + O_2$ reaction; (3) total contribution from $O(^1D) + N_2$; (4) contribution from N + NO; (5) total chemically produced $N_2(v)$; (6) secondary electron production of $N_2(v)$.

into $N_2(v)$. Since radiation from $CO_2(001)$ is trapped, the effective lifetime of a vibrational quantum is much longer than $1/A_{4.28}$. For this reason, as shown by Kumer.[24], weak bands (and also some hot bands and isotopic bands) are important. The problem is also time-dependent due to the relatively long vibrational transfer time for the reverse of R22. Above 90 km the transfer time lengthens from abou[illegible] minutes to more than 20 minutes above 100 km. Above about 110 km there is important atomic oxygen deactivation of $N_2(v)$ via[105]

$$N_2(v=1) + O \rightarrow N_2(v=0) + O, \qquad \text{R23}$$

$$k_{23} = 1.07 \times 10^{-10}\exp(-69.9/T^{1/3}) \text{ cm}^3 \text{ sec}^{-1}.$$

Thus $N_2(v)$ becomes uncoupled from $CO_2(001)$. However, at any altitude above 90 km, the vertical optical depth is sufficiently low, so that the rate determining step for the loss of vibrational quanta is $N_2(v) \rightarrow CO_2(001)$. Figure 17 shows the $N_2(v)$-$CO_2(001)$ time constant as a function of altitude. The CO_2 4.3-μm radiance is delayed from the dosing that excites the $N_2(v)$. There is no way to define an efficiency that is independent of time. The $N_2(v)$ and $CO_2(001)$ densities must be solved as a set of time-dependent equations with the added complication of the optical thickness in the CO_2 ν_3 band.

Kumer[24,100] has had success in modeling zenith 4.3 μm radiance using a number of simplifying approximations. He has used a band model

105. Taylor, R.L. (1974) Energy transfer processes in the stratosphere, Can. J. Chem. 52:1436-1451.

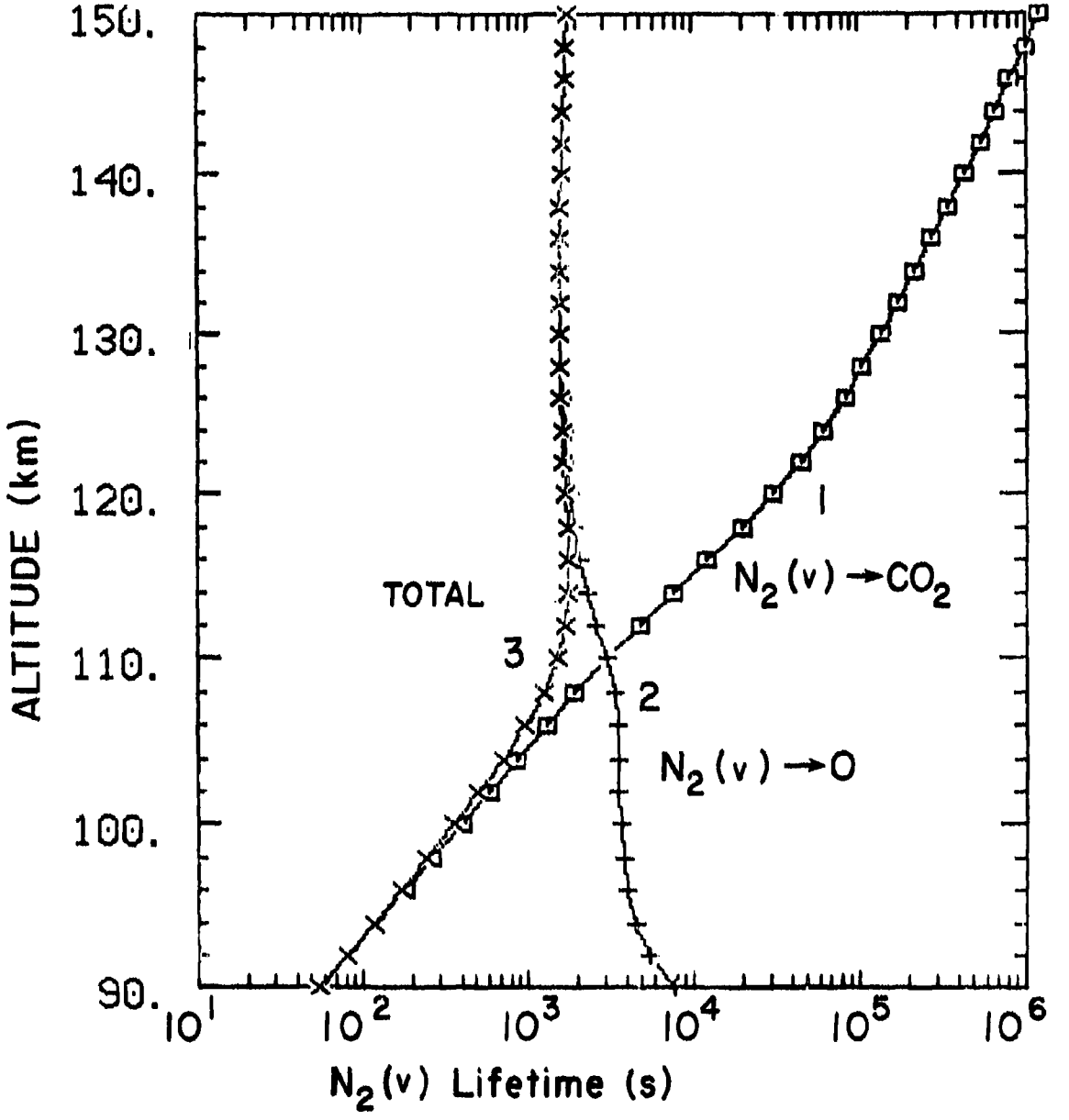

Figure 17. $N_2(v)$ Lifetime as a Function of Altitude: (1) due to CO_2 V-V transfer, (2) due to atomic-oxygen collision, (3) total.

that is further approximated by assuming a constant temperature (and thus lineshape). Above 90 km where only the strong CO_2 626 (001-000) band is significantly self-absorbed (about 20% of the photons escape), Kumer finds that he can largely uncouple the weak bands by using what he calls the Qw approximation. Kumer sets up the coupled equations for the CO_2 bands with density $[n_j]$ which we present in our slightly modified notation as

$$\frac{d[n_j]}{dt} = k_{22}\left(f_j[CO_2][N_2^*] - [n_j][N_2] \right) - (A_L + A_{4.26}E_j + k_{2M}[M])[n_j]$$
$$+ A_{4.26}\int \sigma w_j dN_j' H_{bp}(\sigma w_j |N_j - N_j'|)([n_j(N_j')] - [n_j(N_j)]) \quad , \qquad (2\text{-}51)$$

where A_L is the Einstein coefficient for transitions from (001) to (020) and (100) (which are so small they can be neglected as loss terms above 90 km but contribute to LWIR radiation at 9.4 and 10.4 μm) and $k_{2M} = 1.0 \times 10^{-15} + 5.2 \times 10^{-11}\exp(-76.8/T^{1/3})$ is the rate constant for the quenching of $CO_2(001)$ by air (exclusive of vibrational transfer). Here N_j is the column density of the lower state of the j^{th} isotopic or hot band of CO_2,

$$N_j = \delta z' \, f_j(z') \, [CO_2] \quad , \qquad (2\text{-}52)$$

and f_j is the corresponding fractional abundance; E_j is the escape function for the ν_3 transition obtained from the band functions

$$E_j = E_{bp}(w_j \sigma N_j) + E_{bp}(w_j \sigma |N_{jL} - N_j|), \qquad (2\text{-}53)$$

where $N_{jL} = N_j(z_L)$ and z_L is the lower boundary and σ is the band-"averaged" cross section[100]

$$\sigma = \left[\frac{\pi e^2}{m_e c}\right]\left[\frac{f}{\pi^{1/2}\nu_D}\right] . \qquad (2\text{-}54)$$

Here e is the charge of the electron, m_e is its mass, f is the oscillator strength (related to the band strength[106]), and ν_D is the Doppler width[107]. The weighting factor w_j takes into account the number of lines in the weak band compared to the number of lines from the 626 isotope. (For example, w_j is 1/2 for isotopic bands 627 and 628, which have twice as many lines since both odd and even J are allowed.) The integral term represents the excitation of the j^{th} CO_2 ν_3 band by radiation emitted from all other levels. The band functions H_{bp} and E_{bp} are as defined by Kumer.[98]

A companion equation is obtained for the vibrationally excited N_2 (N_2^*=$N_2(v=1)$) where we have assumed all N_2 vibration relaxes to v=1 ($N_2(v=n) \rightarrow nN_2(v=1)$) before it is quenched,

$$\frac{d}{dt}[N_2^*] = k_{22}'\sum_j\left([n_j][N_2] - f_j[N_2^*][CO_2]\right)$$
$$- (k_{10}[O] + k_{e11}[O_2])[N_2^*] + \epsilon(N_2(v))q_e + P_0 . \qquad (2\text{-}55)$$

Here k_{e11} is the effective quenching rate of $N_2(v=1)$ by O_2. At altitudes above 90 km this term is negligible. This is because

106. Penner, S.S. (1959) Chapter 2 of Quantitative Molecular Spectroscopy and Gas Emissivities. Addison-Wesley, Reading, Massachusetts, p. 21.

107. Reference 106, Chapter 3, p. 31.

$$N_2(v=1) + O_2 \rightarrow O_2(v=1) + N_2(v=0) \qquad \text{R11}$$

$$k_{11} = 1.74 \times 10^{-10}\exp(-124/T^{1/3}) \text{ cm}^3 \text{ sec}^{-1},$$

so that at 200 K $k_{11} = 1.08 \times 10^{-19}$, and the lifetime for $N_2(v=1)$ against k_{11} is longer than $1/(1.08 \times 10^{-19})(1.5 \times 10^{13})$ sec = 6.2×10^5 sec. The auroral production term is the efficiency $\epsilon(N_2(v))$ times the ion-pair production rate q_e. We have included a separate time-independent background production term, P_0, accounting for earthshine and collisions. The effective production rate, P_0, when combined with the radiative loss by CO_2 and quenching, yields the assumed steady-state vibrational temperature. Since we do not wish to carry out the full NLTE calculation of the background vibrational temperature in AARC, we supply the background CO_2 ν_3 temperature and from the steady-state equations calculate P_0. In this manner we simplify the calculation while still assuring that after the auroral production ceases our solutions will asymptotically approach the background (and initial) solution.

Our equations for the coupled $N_2(v)$ - CO_2 ν_3 system involve further approximations. Reactions R7 and R36 produce an average of 2.82 and 2.20 vibrational quanta in N_2 per reaction.[99] The actual distribution of this quanta among vibrational levels is unknown. The excitation of $N_2(v)$ by secondary electrons up to v=10 is calculated using known cross sections. However, there is no quantitative kinetic data concerning the relaxation of high v levels of $N_2(v)$ by N_2, O_2, O, and

CO_2. Thus we have made the approximation that all $N_2(v)$ relaxes to v=1 without quenching. This is probably an unrealistic assumption since $N_2(v)$ vibrational relaxation (V-V) with N_2 is slow. However, quenching by other molecules is also extremely slow. Our assumption will not be very inaccurate if quenching of higher v levels occurs at the same rate as v=1 assuming that all quenching involves only one quantum at a time. It is likely that the V-V transfer with CO_2 is slower for v>1 since it is less resonant by about 28 cm^{-1} for each higher v. Transfer of multiple quanta, for example $N_2(v=n) + CO_2(000) \rightarrow N_2(v=n-2) + CO_2(002)$, is unlikely, and there is no evidence of ν_3 bands in the spectra of aurora or laboratory simulations with $v_3' > 1$. There is a need for more laboratory work to determine the kinetic parameters that control the relaxation of $N_2(v)$, as well as an efficient method for remotely sensing the population of $N_2(v)$ in the upper atmosphere.

Even with the approximations noted above, the set of coupled equations for $[N_2^*]$ and $[n_j]$ are quite complex and the solution of these equations is too lengthly to be repeated at each time step when the equations are finite differenced in time. The time consuming step is the calculation of the integral term involving H_{bp} in Eq. (2-51), which represents excitation of CO_2 at altitude z by radiation emitted from all altitudes z'. The accurate and efficient solution of these coupled equations requires the construction of altitude layers optimized for the changes in optical depth, not the equally spaced Δ=2km used in the photochemical calculations.

Kumer assumes complete frequency redistribution in each line, which means that the relative emission rate for each rotational line depends only upon the local rotational temperature (assumed in equilibrium with the kinetic temperature) and does not depend upon the amount absorbed in each line. This approximation is good if the time constant for obtaining rotational equilibrium is shorter than the radiative lifetime. However, Kumer further simplifies the problem (as do many others such as Degges[108]) by assuming the the lineshape is independent of altitude, and that the Doppler width and the CO_2 (001) rotational temperature is fixed at 225 K or alternatively he uses a Lorentzian width appropriate to the pressure at 50 km. This assumption makes E_{bp} and H_{bp} functions of the column amount, N, only, although the line shape in reality depends upon the temperature (affecting the Doppler width) and the pressure (affecting the Lorentzian width) of the atmosphere along the column. Kumer then calculates a table of plane-parallel band functions as a function of $N\sigma$ that can be interpolated for the column amount appropriate to any layer. It would be reasonable to assume that solutions that are labeled Voigt should be more accurate since the Voigt lineshape is more appropriate than the Doppler profile. However, use of the 50 km Voigt lineshape throughout the atmosphere could result in a larger error since the 50-km Voigt profile greatly overestimates transfer in the pressure-broadened wings at higher altitudes. The assumption of constant tem-

108. Degges, T., and Smith, H.J.P. (1977) A High-Altitude Infrared Radiance Model, AFGL-TR-77-0271, AD A059242.

perature of 225 K is probably a better one since the USSA 1976 atmosphere varies from a low of 187 K at 86 km to 240 K at 110 km (where CO_2 is optically thin). The assumption of rotational equilibrium is inconsistent with fixing the CO_2 rotational temperature at a value different than the kinetic temperature.

Kumer does not routinely solve Eq. (2-51) for the time dependent auroral case. Time-independent coupled equations similar to these are solved for twelve species to obtain the ambient nighttime and daytime CO_2 vibrational temperatures[100] in the 50-130 km range. The 11 CO_2 bands include fluorescent bands that are only important during daytime, and isotopic bands of the (011-010) sequence that are negligible, especially at auroral altitudes. Thus in our calculations we include only four isotopes, namely 626, 636, 627, and 628 (627 is $^{12}C\ ^{16}O\ ^{17}O$), of the (001) → (000) transition and the 626 hot band (011) → (010). This hot band is most likely populated since the ν_2 mode ($\Delta E = 667\ cm^{-1}$, 960 K) is populated at 0.8% of the ground state for a vibrational temperature of 200 K. In our calculation we take a fixed ambient ν_2 vibrational temperature from Kumer's calculation. At this time there is no accepted mechanism for enhancing the CO_2 ν_2 temperature by auroral chemistry. The very low excitation threshold, however, makes calculation of secondary electron excitation very uncertain (as mentioned earlier). Also, the efficient collisional excitation by atomic oxygen[96] means that any auroral mechanism must be quite efficient to compete. Thus we do not expect the ν_2 temperature to be noticeably affected by the auroral deposition. However, the

accuracy of the ν_2 calculation will be directly reflected in the hot band radiance. An accurate calculation by ARC of the ν_2 temperature for the appropriate model atmosphere will be included in a future update.

As shown by Kumer,[24] even total neglect of the weak bands gives an effective lifetime for $N_2(v)$-CO_2 ν_3 vibrational quanta that is within 10-15% of the 12 state calculation at altitudes above 90 km. Thus the weak bands are not going to contribute more than about 15% of the zenith radiance at 90 km. The total lower state population of the weak bands is only about 2.5%, a factor of 6 less, indicating that optical thickness in the major isotope fundamental is important. For limb viewing lines-of-sight this optical thickness will be even more pronounced due to a factor of about 40-70 more CO_2 absorber in the path. The CO_2 optical depth is no longer moderate, but is very large, similar to the vertical path from about 70 km. We know that an accurate radiative transport calculation is necessary. We thus chose to use a line-by-line method adopted from the non-local-thermodynamic equilibrium code called NLTE which is well documented elsewhere.[26,34]

The module CO2 first integrates the continuity equations for the five CO_2 ν_3 species and $N_2(v=1)$ for a user-determined length of time. The user also chooses the time after dosing t_r at which the radiance is to be calculated. Since this time may not coincide with a time step of the integration in the subroutine SLOWCO2, the vibrational temperature for the five CO_2 bands at time t_r is obtained by interpolation. These vibrational temperatures are then input to the limb

radiance code.

NLTE was modified to accommodate the horizontal inhomogeneity of the auroral atmosphere. For the present case the auroral geometry is simplified, with just one arc allowed which must be coaligned with geographic or geomagnetic coordinates. The dosing is uniform within this domain and thus the calculated vibrational temperature from SLOWCO2 is used in this region, and the background vibrational temperatures for the rest of the LOS. Since SLOWCO2 calculates only the temperature for the ν_3 transitions, the temperature for the (011) state must be converted to the vibrational temperature with respect to the ground state before it is input into NLTE.

The large optical depth of the CO_2 626 isotope for radiation in the 4.26-μm band has significant implications for the limb spectral radiance. Although an IBC II aurora will lead to about a factor of 10 increase in the (001) density, for many LOS geometries it can lead to negligible increase in the limb radiance. For a 100-km-long aurorally dosed path at or on the far side of the 100-km-altitude tangent point, the total 4.26-μm band limb radiance observed at 300 km is not significantly greater than the background. Figure 18 shows a low-resolution spectrum of IBC II and IBC III aurora for tangent height near 100 km compared to the quiet background. If the arc is moved toward the observer so that the radiation passes through less atmosphere, the radiance observed increases. The proportion of prompt NO^+ radiation compared to the slow CO_2 emission in the 4.3 μm region can vary greatly with the geometry of the auroral arc along the LOS.[77] Interactive

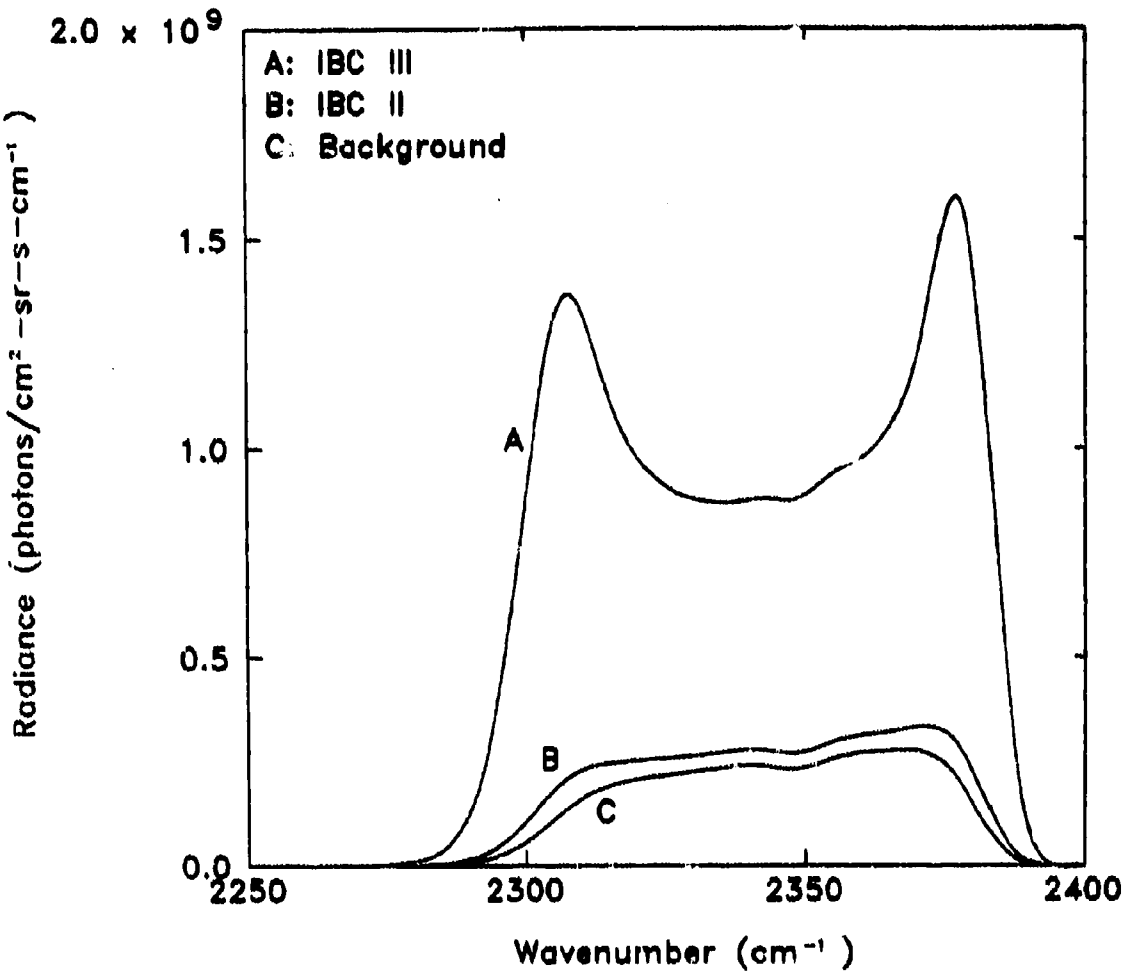

Figure 18. Synthetic Spectra for LOS Having a Tangent Height of 100 km. Auroral dosing occurs over 112 km of the LOS spanning the tangent point. Only CO_2 626 ν_3 band is shown.

use of AARC is a convenient way to explore this dependence upon auroral LOS geometry. It emphasizes the care that must be taken in analyzing auroral limb-viewing experiments. Without ground-based (or satellite-based) information defining the horizontal location of the dosing regions and predosing, it is difficult to interpret the relative importance of CO_2 and NO^+ emission, even with good spectral resolution.

2.6 Auroral Arc Specification

Auroral dosing occurs with the greatest frequency and strength within a range of geomagnetic latitudes known as the auroral oval.

The concept of the auroral oval was introduced by Feldstein[109] on the basis of IGY all-sky camera observations. These observations were sensitive to optical emissions from discrete aurorae with a minimum intensity of 0.5 to 1.0 kR[110] for the 5577 Å [OI] line or 1 to 2 kR for the 6300 Å [OI] line. Studies by Sandford[111] indicated the existence of diffuse aurora co-existing with the discrete aurora within the auroral zone. The diffuse, or mantle, aurora described by Sandford is associated with the continuous energetic particle dosing in the E region of the atmosphere described by Whalen et al.[112] In contrast to the discrete aurora, the diffuse aurora is continuous in longitude and slowly varying in time.

109. Feldstein, Y.I. (1964) Auroral morphology: I. Location of auroral zone, Tellus 16:252.

110. 1 kR = 1 kilo Rayleigh = 10^9 photons/cm^2-sec into 4π steradians.

111. Sandford, B.P. (1968) Variations of auroral emissions with time, magnetic activity and the solar cycle, J. Atmos. Terr. Phys. 30:1921.

To a first approximation, the equatorward and poleward boundaries of the auroral oval may be considered circles with centers offset slightly from the geomagnetic pole. The radii of these circles are functions of the Q index of geomagnetic activity, with the radius of the equatorward circle increasing[113] from 17° at Q = 0 to 24° at Q = 7. The poleward circle remains relatively constant at a radius of approximately 16°. The positions of the centers of the circles are also functions of Q. At Q = 0, the centers of both circles are offset approximately 3° from the geomagnetic pole in an antisunward direction. As magnetic activity increases, the center of the equatorward boundary shifts to an offset of 5° from the pole while the center of the poleward boundary shifts to an offset of less than one degree.

Whalen[114] has shown that the instantaneous energy flux due to the diffuse aurora is a simple function of latitude only in a coordinate system with its pole offset from the geomagnetic pole. In this offset-pole coordinate system the latitude Γ of a point on the earth of constant energy flux is given by

---

112. Whalen, J.A., Buchau, J., and Wagner, R.A. (1971) Airborne ionospheric and optical measurements of noontime aurora, J. Atmos. Terr. Phys. 33:661.

113. Starkov, G.V. and Feldstein, Y.I. (1967) Variations of auroral oval zone boundaries, Geomagn. Aeron. 7: 62.

114. Whalen, J.A. (1983) A quantitative description of the spatial distribution and dynamics of the energy flux in the continuous aurora, J. Geophys. Res. 88:7155.

$$\Gamma = \Lambda_{CG} + \theta_p \cos\frac{2\pi}{24}(UT - UT_{MN}) \quad , \tag{2-56}$$

where Λ_{CG} is the corrected geomagnetic (CG) latitude, θ_p is the CG co-latitude of the offset pole, found to be 4.2°, UT is universal time, and UT_{MN} is the universal time corresponding to CG local midnight. In this offset-pole coordinate system the energy flux, Φ, in erg cm^{-2} sec^{-1}, is described by a Gaussian in Γ,

$$\Phi = \Phi_{max} \exp\left[-\frac{1}{2}\left(\frac{\Gamma - \Gamma_{max}}{\sigma}\right)^2 \right] \quad , \tag{2-57}$$

where Φ_{max} is the maximum of the energy flux, Γ_{max} is the latitude of the maximum, and the Gaussian standard deviation σ is typically 1.4°, while Γ_{max} and Φ_{max} are typically 71° and 1 erg $cm^{-2}sec^{-1}$, respectively.

Although the diffuse aurora accounts for the greater part of auroral dosing to the earth,[106] it is not associated with any appreciable infrared enhancements. Large infrared enhancements tend to be associated with the occurrence of discrete auroral arcs.

The current version of AARC assumes a simple geometry for the dosed region, considered to be an idealized discrete arc. The boundaries of the arc are assumed to lie along contours on which a geographic or geomagnetic coordinate is constant; with the region inside the boundary dosed uniformly. Thus the northern and southern boundaries are specified by giving the geographic or (uncorrected) geomagnetic

latitude lines along which they are assumed to lie, and the eastern and western boundaries are specified by giving their geographic latitude or (uncorrected), geomagnetic local time. The geomagnetic option is included because there is ample evidence[115] that stable arcs within the auroral oval tend to be aligned along the oval, and hence approximately in a geomagnetic east-west direction.

Given the geographic latitude, λ, and longitude, ϕ, of a point P, the geomagnetic latitude, λ_m, may be calculated via the spherical law of cosines[116]

$$\sin(\lambda_m) = \sin(\lambda_p)\,\sin(\lambda) + \cos(\lambda_p)\,\cos(\lambda)\,\cos(\phi - \phi_p), \qquad (2\text{-}58)$$

where λ_p and ϕ_p are the geographic latitude and longitude of the north magnetic pole (Figure 19) taken to be 78.8° and 69.0°, respectively. The geomagnetic longitude, ϕ_m, is then given by the spherical law of sines

$$\sin(\phi_m) = \frac{\cos(\lambda)}{\cos(\lambda_m)}\,\sin(\phi - \phi_p)\ . \qquad (2\text{-}59)$$

Care must be exercised when taking the arcsine to find ϕ_m to ensure that an angle in the proper quadrant is obtained. In Eqs. (2-58) and (2-59) the angles ϕ, ϕ_p, and ϕ_m are assumed positive for longitudes east of the prime meridian. The geomagnetic local time, t_m, in hours

115. Akasofu, S.-I. (1968) Polar and Magnetospheric Substorms, D. Reidel, Dordrecht, Netherlands.

116. Reference 44, page 66.

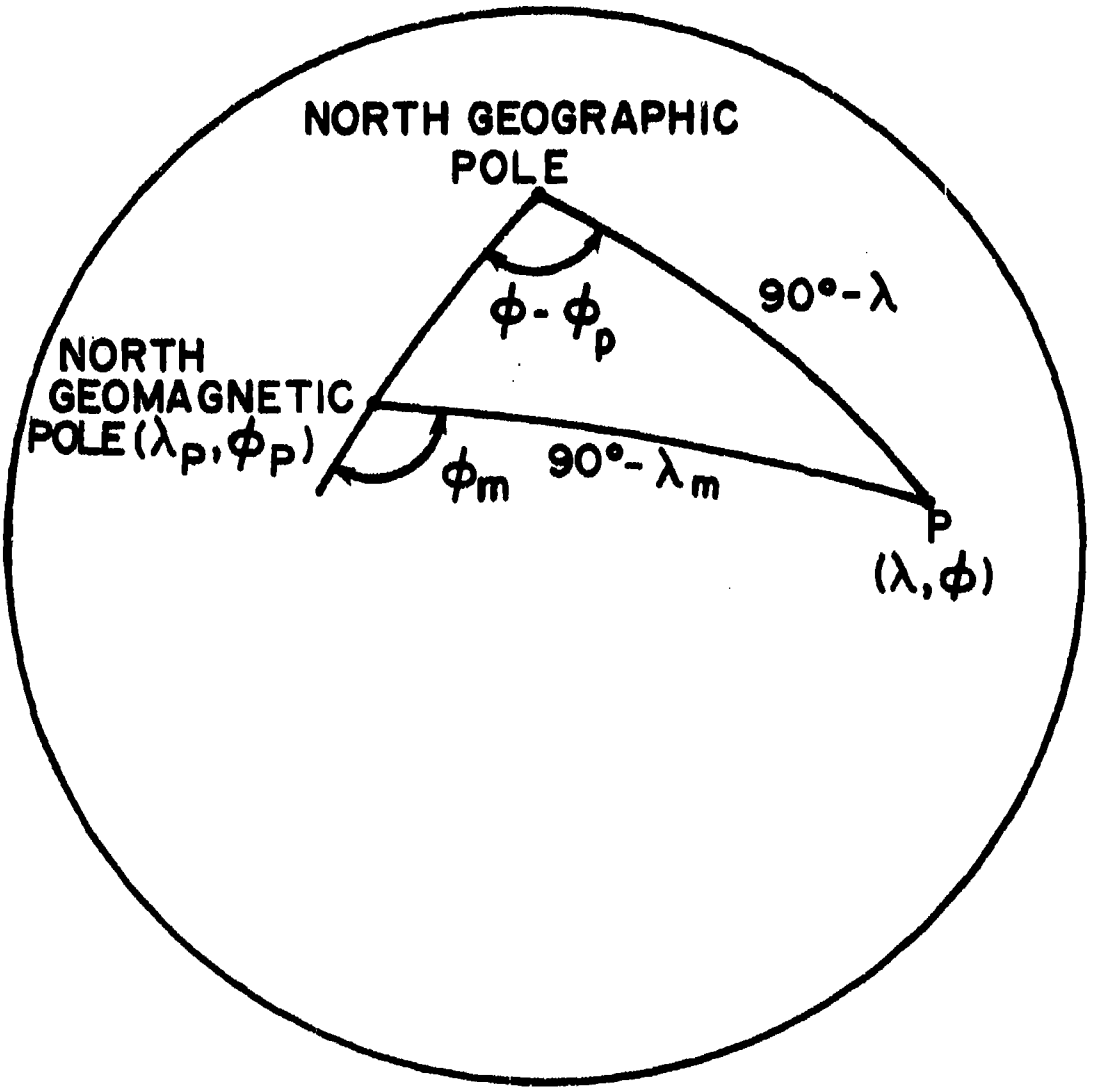

Figure 19. Calculation of the Geomagnetic Coordinates of a Point from the Geographic Coordinates. Here $P(\lambda, \phi)$ is the point of interest with geographic latitude and longitude λ and ϕ.

is then calculated by

$$t_m = \frac{\phi_m - \phi_{m,ss}}{15^\circ} + 12^h ,$$

where $\phi_{m,ss}$ is the geomagnetic longitude of the subsolar point.

2.7 Calculation of Line-of-Sight Radiance

Calculation of the infrared radiances over the line-of-sight (LOS) requires that the path through the atmosphere taken by the LOS be calculated and that the LOS be divided into a number of segments. After calculating the position and altitude of each segment, the emissions from each segment are calculated. The emissions from the segments are then summed, obtaining the radiance as seen by the observer.

The AARC calculation allows a limb-look geometry, where the observer is in space above the atmosphere and looking at space through the intervening atmosphere (Figure 20). The program will not allow situations where the LOS passes through altitudes lower than those for which data are provided (currently, 90 km) or where the LOS does not enter the atmosphere. The altitude of the top of the atmosphere, z_{max}, is specified by the user during the parameter input procedure and should be an altitude below which complete data are specified. Currently, complete data are specified for NO and NO^+ below 160 km, and for CO_2 below 140 km. The CO_2 radiance is very weak above 140 km, but caution should be exercised when using AARC for tangent heights above 140 km.

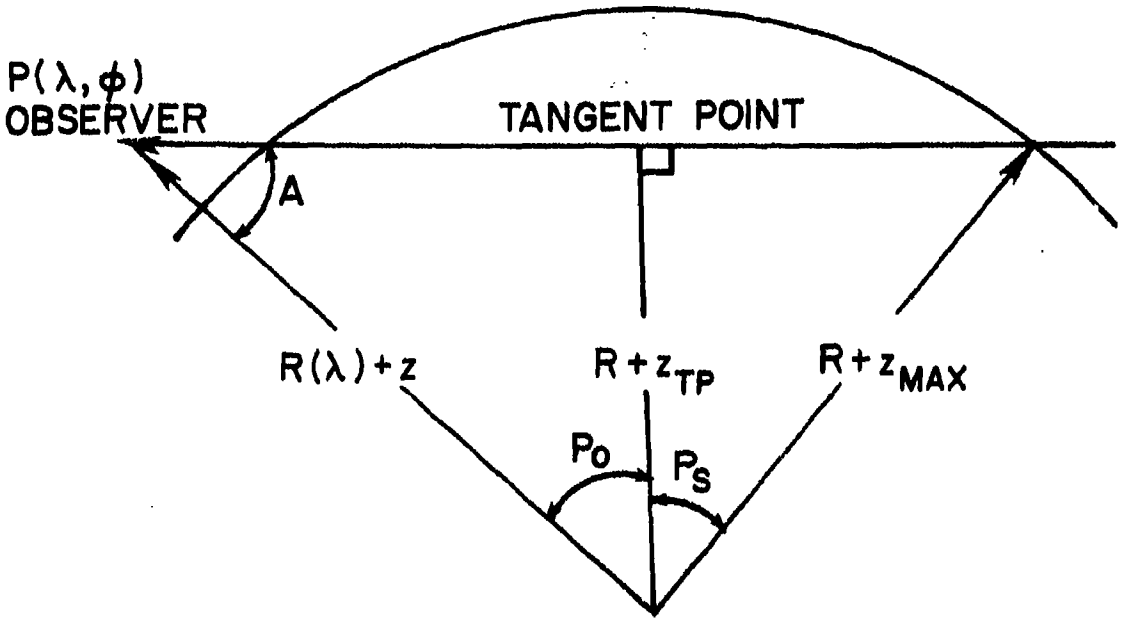

Figure 20. Limb-look Geometry.

The user specifies the LOS by giving the altitude, z, the latitude, λ, and the longitude, ϕ, of the observer. The user must also specify the nadir angle, A, and the azimuth angle, B, of the LOS. The angle A is indicated in Figure 20 while B is shown in Figure 21. The distance from the observer to earth center is calculated by adding the radius of the earth, $R(\lambda)$, at the latitude of the observer to the altitude. The radius is calculated via

$$R(\lambda) = R_E[1 - a_1\sin^2(\lambda) + a_2\sin^2(2\lambda)] , \qquad (2\text{-}60)$$

where R_E = 6378.116 km is the radius of the earth at the equator, and

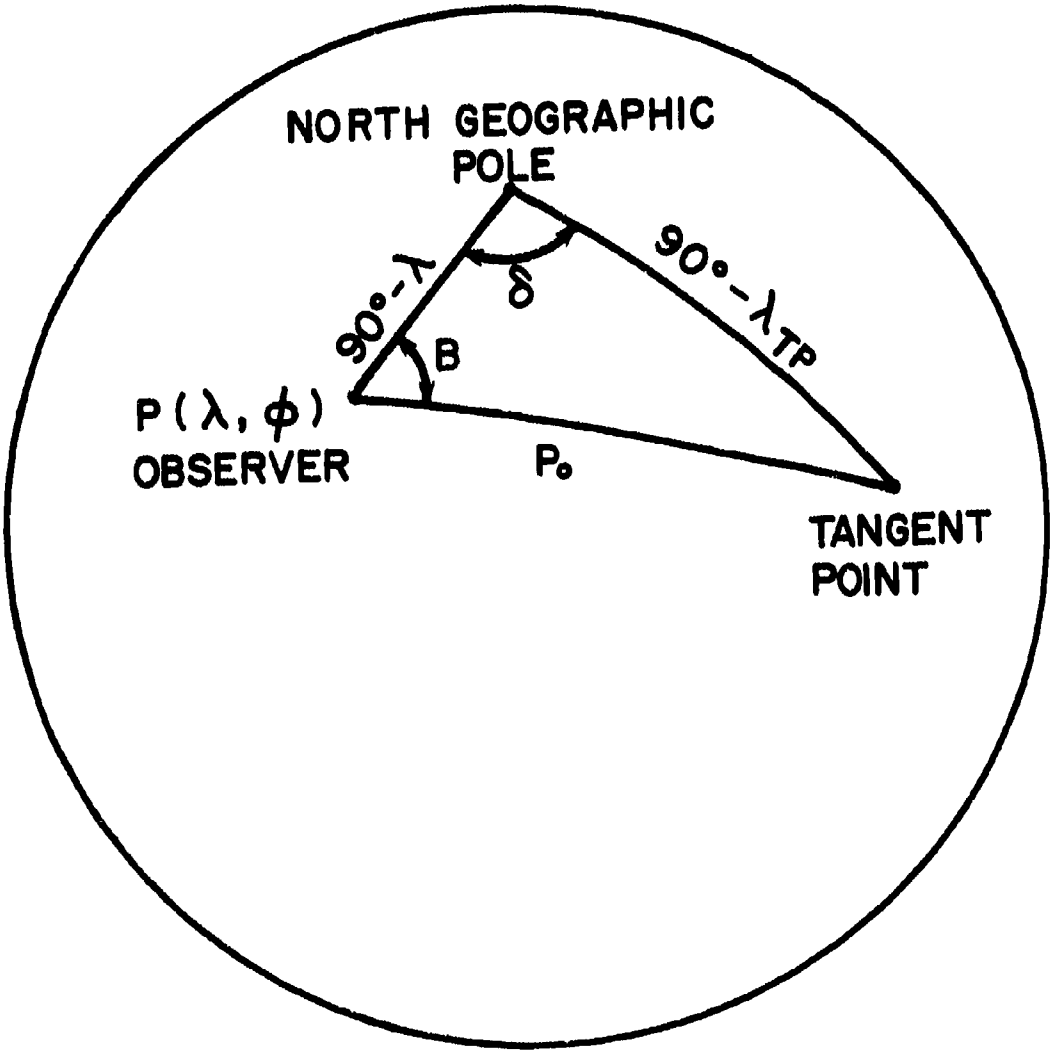

Figure 21. The Path of the LOS Along the Earth Showing the Procedure for Calculating the Coordinates of the Tangent Point.

the coefficients a_1 and a_2 are 0.003367 and 7.08×10^{-6}, respectively. Failure to use a good local value of earth radius can result in altitude errors of up to 20 km.

The characterization of the LOS begins with the determination of the position and altitude of the tangent point. This part of the calculation is carried out in the spherical-earth approximation, using the local value of the earth radius $R(\lambda_{TP})$ at the location of the tangent point from Eq. (2-60). The angular separation between the observer and the tangent point as measured at earth center is (Figure 20)

$$P_0 = 90^\circ - A. \tag{2-61}$$

As may be seen from an examination of Figure 21, the latitude of the tangent point, λ_{TP}, is given by

$$\sin(\lambda_{TP}) = \sin(\lambda)\cos(P_0) + \cos(\lambda)\sin(P_0)\cos(B). \tag{2-62}$$

The longitude of the tangent point is given by

$$\phi_{TP} = \phi + \delta, \tag{2-63}$$

where δ is given by

$$\cos(\delta) = \frac{\cos(P_0) - \sin(\lambda)\sin(\lambda_{TP})}{\cos(\lambda_{TP})\cos(\lambda)}. \tag{2-64}$$

The altitude of the tangent point, as calculated from Figure 20 and Eq. (2-60), is checked to ensure that the LOS traverses altitudes lying within the range for which the program has data available and

that it enters into the atmosphere below z_{max}.

Infrared emissions from NO and NO^+ are summed over that portion of the LOS lying between the two points with altitude z_{max}. This portion of the LOS intercepts an angle $2P_s$ at earth center, where P_s is given by

$$\cos(P_s) = \frac{R + z_{TP}}{R + z_{max}} , \tag{2-65}$$

where z_{TP} is the altitude of the tangent point.

The LOS is then partitioned into a number, 2n, of small segments (currently, 2n = 400), each spanning a constant angle D at earth center, where D is given by

$$D = \frac{P_s}{n} . \tag{2-66}$$

Knowing the angular separation between the observer and a segment allows the program to calculate the latitude, longitude, and altitude of that segment using the same procedure used for the tangent point. The linear distance from the observer to each segment and the length of each segment is also calculated.

The coordinates of each segment are compared to the coordinates of the auroral dosing region and the volume emission rates are calculated accordingly. These rates are multiplied by the segment lengths and then summed over the LOS. In addition, the routine calculates a weighted average of the kinetic temperature over the LOS for each band system. The weighting function is the local volume emission rate.

This resulting effective temperature is later used to distribute the band radiances over the spectral lines making up the bands.

2.8 Band and Spectral Radiances

2.8.1 SPECTRAL LINE FILES

The chief output of AARC consists two different kinds of line-of-sight (LOS) radiances, band radiances and spectral radiances. Both of these forms of output are available for all bands of all species included in AARC.

Insofar as is possible, the source of data on line positions and strengths is the HITRAN database, or AFGL line compilation[35-37]. This database is extensive and, in the 1982 version,[35,36] consists of two parts, the main compilation and the trace-gas compilation. In the 1986 version,[37] the two parts were merged, and the format of the listings was changed. Since the line tapes are biased toward radiators important in the neutral troposphere and stratosphere, where local-thermodynamic-equilibrium (LTE) conditions prevail, it is lacking in several bands and radiators of importance in the infrared emissions of the auroral thermosphere. These include (1) lines of positive ions such as NO^+ and (2) lines originating in highly excited vibrational states of neutral molecules populated by energetic-electron-induced chemical reactions. Therefore, AARC has extended and enlarged the HITRAN database where necessary.

The AARC code follows the 1982 version of the database and preserves its format in the AARC line files in all ways except one;

namely, the absorption line intensity parameter S [cm^{-1}/(molecule/cm^2)] at reference temperature T_s = 296 K appearing in the AFGL compilation is replaced by the Einstein A-coefficient A [sec^{-1}]. The A-coefficient is not proportional to the LTE population of the lower state for the transition, as the line intensity S is; moreover, unlike S, it is directly related to photon emission rates. Hence, considerable execution time is saved by calculating the Einstein coefficient once and for all and storing it permanently in the AARC line file. The A-coefficients are calculated from the line intensities by using the relation (see, for example, Sharma et al[26])

$$A_{ul} = 8\pi c\nu_0^2 \frac{g_l}{g_u}\left(\frac{S(l,\ u;\ T_s)}{P_l(T_s)}\right)\left[1 - \exp\left(\frac{c_2\nu_0}{T_s}\right)\right]^{-1}. \qquad (2\text{-}67)$$

In this equation A_{ul} is the Einstein A-coefficient for the transition from the upper state u = (v',J') to the lower state l = (v",J"), v and J being the vibrational and rotational quantum numbers; c is the speed of light; $g_l = 2(2J"+1)$ and $g_u = 2(2J'+1)$ are the degeneracies of the lower and upper states, respectively; C_2 = 1.4388 K/cm^{-1} is the second radiation constant; $\nu_0 = E_u - E_l$ is the transition energy in wavenumber, where E_l and E_u are the energies of the lower and upper states; P_l is the occupation probability for the lower state, given by

$$P_l(T_s) = \frac{g_l}{Q(T_s)} \exp\left(-\frac{c_2\ E_l}{T_s}\right), \qquad (2\text{-}68)$$

where Q is the overall partition function.

The new line file used by AARC, with A-coefficients replacing line

intensities, is also ordered differently than the HITRAN database; this is accomplished by sorting it into bands, according to the values of v' and v", then into sub-bands if any, and finally into branches. The AARC line file is also extended where necessary beyond the bands appearing in the AFGL line compilation by adding lines in the same format as the rest of the file. The details of how this is accomplished depend on the species and transition involved. Each of the band systems will now be discussed in turn.

2.8.1.1 NO($\Delta v = 1, 2$)

The NO fundamental and overtone ro-vibrational transitions are complicated by the fact that the ground electronic state of NO is a $^2\Pi$ state, with projection of electron orbital and spin angular momentum on the internuclear axis given by $\Lambda = 1$ and $\Sigma = 1/2$, respectively, and having an angular-momentum coupling scheme[117] intermediate between Hund's case (a) and Hund's case (b). The transition is thus a $^2\Pi - {}^2\Pi$ transition with a total of 24 branches obtained as follows: There are four sub-bands corresponding to the four possible transitions among the two fine-structure levels, split according to the total electron angular momentum along the internuclear axis, $\Omega = |\Lambda + \Sigma| = 1/2, 3/2$, by the spin-orbit interaction; in addition, there are three branches (P, Q, R) within each sub-band, and finally each branch is split further into two by Λ-doubling, resulting from the interaction between electronic motion and nuclear rotation.

117. Herzberg, G. (1950) Molecular Spectra and Molecular Structure I. Spectra of Diatomic Molecules. D. Van Nostrand Co., New York.

Designating the sub-bands by the initial and final values of electron angular momentum, Ω' and Ω'', they fall naturally into two groups, the 1/2-1/2 and 3/2-3/2 corresponding to intramultiplet transitions and the 1/2-3/2 and 3/2-1/2 corresponding to intermultiplet transitions. The intermultiplet lines violate the Hund's case (a) selection rule $\Delta\Omega = 0$ and are weaker than the corresponding intramultiplet lines by four orders of magnitude; hence, they are deleted from the line file. In addition, the splitting $\Delta\nu$ resulting from Λ-type doubling can safely be ignored since it vanishes as $J \to 0$ and never amounts to more than ≈ 0.1 cm^{-1}, even at high J values. This is accomplished by averaging the transition frequencies and lower-state energies of the two components of a Λ-type doublet occurring in the AFGL compilation while summing their line intensities; the result is a replacement of the doublet by an equivalent line at frequency $\langle\nu\rangle = (\nu_1 + \nu_2)/2$. As a result of these manipulations, the 24 branches appearing in the NO spectrum are reduced to 6, namely P, Q, and R branches for the 1/2-1/2 and 3/2-3/2 sub-bands.

The NO lines on the AFGL compilation do not extend to the highly excited vibrational states necessary to describe chemiluminescent auroral emissions; the highest lying lines in the compilation are (5, 4) for the fundamental series and (6, 4) for the first overtone series. The lines have been extended through (12, 11) and (12, 10) by using Billingsley's line positions[83] and by scaling the line A-coefficients as discussed in Section 2.4.2 for the band A-coefficients.

Some properties of the NO bands included in the AARC line file are

listed in Table 6. A sample of some of the NO lines from the AARC line file is included in Table 8.

2.8.1.2 NO^+ ($\Delta v = 1$)

Since the HITRAN data base contains no ionic lines, NO^+ ro-vibrational lines for the simple $^1\Sigma^+$ electronic ground state have been generated in the format of the compilation using empirical spectral parameters. The parameters used are listed in Table 9.

The production of NO^+ by ion-molecule reactions involving auroral ions results in a vibrationally hot distribution of $NO^+(v)$ excited states; consequently, bands up to (14, 13) have been included in the AARC line file. The overtone bands have not been included in the data base because their intensities are so much weaker than those of the fundamental bands; however, there is no reason why they could not be included should the situation warrant it. Some characteristics of the NO^+ bands are listed in Table 7, and a sample of the NO^+ spectral lines is included at the bottom of Table 8.

2.8.1.3 CO_2 ν_3

There are five CO_2 ν_3 bands appearing in the AARC line file; all of them have been selected from the AFGL line compilation. In addition to the main band $00^01 - 00^00$ (00011 - 00001 in the notation of the HITRAN compilation), we have included a hot band $01^11 - 01^10$ (or 01111 - 01101) involving excitation of the ν_2 mode, and three isotopic bands involving replacement of ^{16}O by ^{17}O or ^{18}O or replacement of ^{12}C by ^{13}C. In the notation of the HITRAN compilation the normal CO_2 isotope is designated 626 and the three minor isotopic bands included are

Table 8. Sample of the AARC NO and NO^+ Line File, LINE25.

1	2	3†	4	5	6	7	8	9	10	11	12
1736.6724	5.339E+00	.0430	2161.927	1	0	1/2-1/2	P	35.5	382	46	8
1741.1678	5.375E+00	.0430	2043.652	1	0	1/2-1/2	P	34.5	382	46	8
...				...						...	
2161.2798	4.327E+00		3100.664	1	0	NO+	P	39.0		46	
2166.6829	4.361E+00		2945.631	1	0	NO+	P	38.0		46	

1. The wavenumber of the transition in cm^{-1}.

2. The Einstein A-coefficient for the transition (sec^{-1}).

3. The pressure broadening coefficient, α, in cm^{-1} per atmosphere. The AARC calculation assumes that the linewidths are narrower than the resolution of the instrument. Therefore, these data are not used. The values of α are missing for NO^+ and for some NO lines.

4. The energy, E", of the lower level of the transition in cm^{-1}.

5. The vibrational quantum number, v', of the upper level of the transition.

6. The vibrational quantum number, v", of the lower level of the transition.

7. In the case of NO this field identifies the electronic transition involved. All NO lines used are intramultiplet lines. In the case of NO^+ this field is used to identify the species.

8. The branch of the transition.

9. The angular momentum quantum number, J", of the lower level.

10. AFGL identification code[35]. Not applicable to NO^+.

11. Isotope code[35].

12. The AFGL molecule code[36] for NO. Not applicable to NO^+.

†The values in Field 3 begin with a decimal point. There is no separation in the computer listing between Fields 2 and 3.

Table 9. Empirical Constants for NO^+ Line Positions

Parameter	Value (cm^{-1})	Reference
ω_e	2376.721	Billingsley (1973)[118]
$\omega_e x_e$	16.2553	"
$\omega_e y_e$	-0.01560	"
$\omega_e z_e$	0.0	"
B_e	1.997	Huber and Herzberg (1979)[119]
α_e	0.01879	"
D_e	5.64×10^{-6}	"

the 00011 - 00001 bands of the 627, 628, and 636 isotopes. Since the fractional abundances of the C and O isotopes are all ≤ 1%, the abundances of CO_2 isotopes with two isotopic atoms, such as 637 or 828, are ≤ 10^{-4}, and the latter can safely be neglected. Some properties of the five CO_2 bands included in AARC are listed in Table 10, and a sample of the AARC line file's CO_2 lines is tabulated in Table 11.

2.8.2 BAND RADIANCES

The band radiances for CO_2 are obtained by summing the line radiances calculated by the NLTEA line-by-line radiative transfer code, described above in Section 2.5.2. In the case of the other (optically

118. Billingsley II, F.P. (1973) Calculation of the absolute infrared intensities for the 0-1, 0-2, and 1-2 vibrational-rotational transitions in the ground state of NO^+, Chem. Phys. Lett. 23:160-166.

119. Huber, K.P. and Herzberg, G. (1979) Molecular Spectra and Molecular Structure IV. Constants of Diatomic Molecules, Van Nostrand Rienhold Co., New York.

Table 10. Band Parameters for CO_2 Transitions.

Isotope	v'	v''	Highest Wavenumber (cm^{-1})	Lowest Wavenumber (cm^{-1})	Band Origin (cm^{-1})
626	00011	00001	2220.011	2396.840	2349.143
636	00011	00001	2182.035	2330.934	2283.488
627	00011	00001	2249.605	2383.371	2340.014
628	00011	00001	2236.712	2375.427	2332.113
626	01111	01101	2227.570	2383.807	2336.633

thin) radiators, the band radiance is calculated first using band A-coefficients computed as described in the next paragraph; then the band radiance is distributed over the lines in the band assuming rotational equilibrium at a rotational temperature equal to the kinetic temperature ($T_{rot} = T_{kin} = T$).

The band A-coefficients are calculated from the A-coefficients of the individual lines composing the band by summing over final (lower) states and averaging over initial (upper) states. It is assumed that the vibrational population is distributed over the rotational levels according to the Boltzmann distribution. Thus the rotational-equilibrium band A-coefficient is given by

$$A_{v'v''}(T) = \sum_{J',J''} A_{ul} P_{u|v'}(T), \qquad (2\text{-}69)$$

where $P_{u|v'}$ is the conditional probability of occupying the state $u = (v', J')$, given that the molecule is in the v' vibrational state. The

Table 11. Sample of the CO_2 Line File, LCO2.

1	2	3†	4	5	6	7	8	9	10	11
2182.0352	7.529E-27	.0490	3622.346	00011	00001	P	96	482	636	2
2184.6850	1.517E-26	.0500	3474.203	00011	00001	P	94	482	636	2
2187.3124	3.008E-26	.0500	3329.124	00011	00001	P	92	482	636	2
2188.5125	3.830E-27	.0540	2440.727	00011	00001	P	81	482	638	2
2189.6854	5.052E-27	.0540	2380.833	00011	00001	P	80	482	638	2
2189.9175	5.876E-26	.0510	3187.113	00011	00001	P	90	482	636	2

1. The wavenumber of the transition in cm^{-1}.
2. Line intensity, S, per absorbing molecule at 296K, (cm^{-1} / molecule-cm^{-2}).
3. The pressure broadening coefficient in cm^{-1} per atmosphere.
4. The energy, E", of the lower level of the transition in cm^{-1}.
5. The designation[35] of the upper level of the transition.
6. The designation[35] of the lower level of the transition.
7. The branch of the transition.
8. The angular momentum quantum number, J", of the lower level.
9. AFGL identification code[35].
10. Isotope code[35].
11. AFGL molecule code[35]. The number 2 is the code for CO_2.

†The values in Field 3 begin with a decimal point. There is no separation in the computer listing between Fields 2 and 3.

conditional probability can be expressed in terms of the rotational partition function $Q_{v'}(T)$ by

$$P_{u|v'}(T) = \frac{g_u}{Q_{v'}(T)} \exp\left[- \frac{C_2}{T}(E_{v',J'} - E_{v',0}) \right] , \qquad (2\text{-}70)$$

where

$$Q_{v'}(T) = \sum_{J'} g_u \exp\left[- \frac{C_2}{T}(E_{v',J'} - E_{v',0}) \right] . \qquad (2\text{-}71)$$

Note that $P_{u|v'}$ is defined so that it sums to unity,

$$\sum_u P_{u|v'}(T) = 1 . \qquad (2\text{-}72)$$

The values of $A_{v',v''}$ and $Q_{v'}$ calculated for T = 273 K using Eqs. (2-69) and (2-71) for both NO and NO^+ are listed in Tables 6 and 7.

The band radiances (photons cm^{-2} sec^{-1} sr^{-1}) for NO and NO^+ are computed from the band A-coefficients by multiplying the A-coefficient by the local value of the upper-state density divided by 4π and integrating along the LOS, as described in Section 2.7. The effective emission temperature of the band $T_{eff}(v',v'')$ is also calculated by summing the local temperatures along the LOS, weighted by the fraction of the total band radiance arising from the local volume element. (See Section 2.7.)

2.8.3 LINE RADIANCES - OPTICALLY THIN CASE

Once the band radiances for the optically thin radiators are obtained, the line radiances (photons cm^{-2} sec^{-1} sr^{-1}) follow from the approximation that the total radiation in the band (v',v") can be dis-

tributed over the contributing lines as if their upper states were in rotational equilibrium at temperature $T_{eff}(v'',v')$. Denoting the total band radiance by $s_B(v',v'')$ and the constituent line radiances by $s_{J'}(v',v'')$. we can then write

$$s(J',\ v';\ J'',\ v'') = s_B(v',\ v'')\ \frac{A_{ul}\ P_{u|v'}}{\sum_{J',J''} A_{ul}\ P_{u|v'}}\ , \qquad (2\text{-}73)$$

from which Eq. (2-72) gives the obvious result

$$s_B(v',\ v'') = \sum_{J',J''} s_{J'}(J',\ v';\ J'',\ v'')\ . \qquad (2\text{-}74)$$

All of the line radiances so calculated are written to a file of radiances and corresponding line positions for use in generating spectra.

2.8.4 SPECTRAL RADIANCES

The spectrum $I(\nu)$ (photons cm^{-2} sec^{-1} sr^{-1} cm) resulting from the line-radiance file generated by Eq. (2-73) is a spectrum of weighted unit impulses, or Dirac delta functions, having zero width (a "stick" spectrum),

$$I(\nu) = \sum_i s_i\ \delta(\nu - \nu_i)\ . \qquad (2\text{-}75)$$

Here i is a label for a spectral line, and $(\nu_i,\ s_i)$ are the set of frequencies ν_{ul} and radiances $s(J',\ v'\ ;\ J'',\ v'')$ read from the AARC line-radiance file. Since we wish to restrict AARC to a minimum resolution $\approx 0.1\ cm^{-1}$, and the infrared emission lines from the lower thermosphere have widths $< 10^{-2}\ cm^{-1}$, for all practical purposes the atmospheric lines can be considered to be delta functions.

The thermospheric earthlimb spectrum of Eq. (2-75) is broadened by the spectrometer used to observe the earthlimb spectral radiance, so that the observed spectrum $I'(\nu)$ (photons cm^{-2} sec^{-1} sr^{-1} cm) is the convolution of the true spectrum $I(\nu)$ with the spectrometer's instrumental lineshape or spectral spread function $G(\nu)$, that is,

$$I'(\nu) = G(\nu) * I(\nu) = \int_{-\infty}^{+\infty} d\nu' \; G(\nu - \nu') \; I(\nu') \; . \qquad (2\text{-}76)$$

Upon substituting Eq. (2-75) into this expression, one sees that $I'(\nu)$ is a sum of the line radiances s_i weighted by the instrumental lineshape at distance $\nu - \nu_i$ from line center,

$$I'(\nu) = \sum_i s_i \; G(\nu - \nu_i) \; . \qquad (2\text{-}77)$$

We can require, without changing the problem in any essential way, that the instrument conserve the total energy flux. Provided the width Δ of the response function $G(\nu)$ is much less than the optical transition energies ν_i, this is equivalent to the requirement that the photon number flux s_T be conserved. Using Eqs. (2-76) and (2-77), this requirement can be stated

$$s_T = \int_0^\infty d\nu \; I(\nu) = \int_0^\infty d\nu \; I'(\nu) = \sum_i s_i = \sum_{\nu', \nu''} s_B(\nu', \nu'') \; . \qquad (2\text{-}78)$$

Equation (2-78) requires, in turn, that the lineshape function be normalized,

$$\int_0^\infty d\nu\ G(\nu - \nu_0) = 1 \ , \qquad (2\text{-}79a)$$

which can also be written

$$\int_{-\infty}^{\infty} d(\delta\nu)\ G(\delta\nu) = 1 \ , \qquad (2\text{-}79b)$$

provided, once again, $\Delta \ll \nu_0$. Because of this condition, one may conveniently replace the lower limit in Eq. (2-79a) by $-\infty$ and set $\nu_0 = 0$.

AARC provides the user with a choice of several spectrometer lineshapes. Currently, four different lineshapes are included in the code and are available for use. If Δ is the full width at half-maximum (FWHM) of the lineshape function, then the lineshapes supported by AARC may be written as follows:

a) triangular lineshape

$$G(\delta\nu) = \begin{cases} \dfrac{\Delta - |\delta\nu|}{\Delta^2} & (\ |\delta\nu| \le \Delta) \\ 0 & (\ |\delta\nu| > \Delta) \end{cases} \ ; \qquad (2\text{-}80)$$

b) Gaussian lineshape

$$G(\delta\nu) = \frac{1}{\sigma_g\sqrt{2\pi}} \exp\left[-\frac{1}{2}\left(\frac{\delta\nu}{\sigma_g}\right)^2 \right] \ , \qquad (2\text{-}81)$$

where σ_g is the Gaussian standard deviation and is related to the FWHM by

$$\sigma_s = \frac{\Delta}{2\sqrt{2\ \ln 2}} \ ; \tag{2-82}$$

c) sinc lineshape

$$G(\delta\nu) = \frac{1}{\sigma_s}\ \mathrm{sinc}\left(\frac{\delta\nu}{\sigma_s}\right) = \frac{1}{\pi\ \delta\nu}\ \sin\left(\pi\ \frac{\delta\nu}{\sigma_s}\right) \ , \tag{2-83}$$

where

$$\sigma_s = \frac{\pi\Delta}{2X_0} = \frac{\Delta}{1.2067} \tag{2-84a}$$

and $X_0 = 1.8955$ is the smallest positive root of the transcendental equation

$$\sin X_0 = \frac{1}{2}\ X_0 \ ; \tag{2-84b}$$

d) Hamming lineshape

$$G(\delta\nu) = \frac{1}{\sigma_s}\ \left\{ c_0\ \mathrm{sinc}\frac{\delta\nu}{\sigma_s} + c_1\ \left[\ \mathrm{sinc}\left(\frac{\delta\nu\ -\ \sigma_s}{\sigma_s}\right) + \mathrm{sinc}\left(\frac{\delta\nu\ +\ \sigma_s}{\sigma_s}\right)\ \right]\right\} \ , \tag{2-85}$$

where $c_0 = 0.538357 \cdot 0.54$ and $c_1 = 0.230822 \cdot 0.23$;

e) rectangular lineshape

$$G(\delta\nu) = \begin{cases} \frac{1}{2\Delta} & (\ |\delta\nu| \le \Delta) \\ 0 & (\ |\delta\nu| > \Delta) \end{cases} \ . \tag{2-86}$$

The first two lineshapes (a and b) are, in general, appropriate for dispersive spectrometers while the latter two (c and d) are more suitable as unapodized and apodized two-beam interferometer spectral response functions. Lineshape c is a sinc function, obtained by

Fourier transformation of a square weighting function, or rect function, rect(x), while lineshape d, the Hamming lineshape, is the Fourier transform of the raised cosine weighting function,

$$w(x) = \begin{cases} c_0 + 2c_1 \cos\left(\pi \frac{x}{x_{max}}\right) & (|x| \leq x_{max}) \\ 0 & (|x| > x_{max}) \end{cases} \quad . \tag{2-87}$$

Notice that $c_0 + 2c_1 = 1.0000$, so that the Hamming weighting function w(x) takes on the value unity at the point of equal path difference $x = 0$; hence, the normalization condition, Eq. (2-79), is satisfied. The function w(x) drops cosinusoidally to a value of $c_0 - 2c_1 \approx 0.08$ at the point of maximum path difference $x = x_{max}$. Its transform, the Hamming lineshape, thus consists of the weighted sum of three sinc functions, one centered at $\delta\nu = 0$ and two centered at the displaced values $\pm\sigma_s$, where $\sigma_s = \pm(2x_{max})^{-1}$ is the half-width of the sinc function defined in Eq. (2-83). The Hamming function has a central peak twice as wide as the sinc function, but its sidelobes are much smaller than the those of the sinc. The power ratio in the Hamming sidelobes relative to the central peak is $\approx$ -41 dB, or a factor of 112.

Choices a - d for the spectrometer lineshape are only meant to represent a sample of the possible lineshape functions. A more extensive set of choices as well as a provision for user-specified lineshapes will be deferred to a later time.

In carrying out the sum of Eq. (2-77) to calculate the spectral

radiance $I'(\nu)$ at frequency ν, contributions from lines (ν_i, s_i) closest to ν are first summed, and the summation proceeds to larger and larger values of $|\nu - \nu_i|$ until ν reaches an upper limit specified by the user for the maximum number n_{max} of widths (FWHM) away from ν_i at which lines will contribute. A small value of n_{max} will increase execution speed at the risk of reducing the precision of the result.

The values of spectral radiance $I'(\nu)$ are written to a file for storage and may be read by plotting programs or used as input to further computations. A sample of the spectral radiance file is shown in Table 12.

2.8.5 PLOTTING SPECTRA

A plotting module is provided with AARC which calls modified CALCOMP plotting programs (AXIS, LINE, PLOT, SYMBOL, ...) available on the AFGL CYBER computer and at some other installations. It is designed to read the spectral radiance files generated by AARC and plot them under direction of the user through a menu-driven query system. The data entered by the user in response to menu prompts are used to update a default parameter file, which can then be saved for reuse. Alternatively, the user may use his favorite plotting programs to view the results of AARC computations. At AFGL we commonly plot the results on a VAX computer using plotting capabilities in the IDL (Interactive Data Language) package.

3. AARC PROGRAM DESCRIPTION AND USAGE

3.1 Main Modules

AARC consists of four distinct, interconnected program modules: DAARC, CO2, CONV, and AURGRAF (Figure 2). The first module, DAARC, begins by initializing user-defined program control parameters via a menu-driven procedure. The program then calculates the electron-ion pair production rate as a function of altitude, which is used for the calculation of NO emissions near 5.3 μm ($\Delta v = 1$) and 2.7 μm ($\Delta v = 2$) and NO^+ emissions near 4.3 μm later in the program. The pair production rate is also written to a file so that it may be used by the module CO2 to calculate the CO_2 emissions near 4.3 μm. The program then calculates the geometry of the line-of-sight and the emissions from NO and NO^+ fundamental and overtone bands. After summing the band emissions over the line-of-sight, the resulting band radiances are distributed among the individual lines among the individual lines making up the band. These line radiances are written to the file LNSPEC, making them accessible to the program module CONV. Because DAARC creates data files which are required by the other modules, the user must run DAARC first. A description of DAARC program flow is given in Appendix B.

The module CO2 calculates the CO_2 emissions from an aurorally disturbed atmosphere along the line-of-sight defined using the input procedure in the program DAARC. It performs a time-dependent calculation of the CO_2 vibrational temperatures and a line-by-line calculation of

subsequent infrared emissions, appending the line radiances to the end of file LNSPEC. This program module, which may be omitted if CO_2 emissions are not desired should be executed after DAARC but before CONV. A description of CO2 program flow is given in Appendix C.

CONV takes as input the line strengths of NO, NO^+ and CO_2 as calculated by DAARC and CO2 and convolves them to generate a synthetic spectrum. A description of CONV program flow is given in Appendix D. The program module AURGRAF uses the AFGL graphics library to plot the synthetic spectrum on an interactive graphics terminal.

Various input data files are needed by the program modules, and some intermediate files are used to communicate data between the modules (Figure 2). The file DEFLTS holds default values for the user-defined input parameters. These parameters are updated to the most recent values used each time the module DAARC is run. In addition, the parameters in DEFLTS may be changed directly by the user if the program is to be run non-interactively.

The data file ALLDAT contains data defining the model atmosphere such as temperature, density, and composition. The file also contains efficiencies required for the NO and NO^+ calculations.

The data file LINE25 contains the positions and Einstein A-coefficients of the appropriate NO and NO^+ lines, while LCO2 contains comparable data for CO_2 lines.

The file RELAY holds such data as line-of-sight information, electron-ion pair production profile, and time of observation relative to the start of auroral activity. These data are calculated in DAARC and

are used in the program CO2.

LNSPEC contains the line positions and intensities calculated by DAARC and CO2. A sample is shown in Table 12. These are read by the module CONV, which uses them to produce the synthetic spectrum.

3.2 Input, Output, and Program Communication

3.2.1 INPUT OF USER-DEFINED PROGRAM CONTROL PARAMETERS

The program DAARC will run in two possible modes depending upon the value of the first parameter stored in the file DEFLTS (Figure 2). If this has been set equal to one, the program will run in interactive mode, allowing the modification of any or all of the user-defined program control parameters via a series of menus. The default values of these parameters are taken from the file DEFLTS. (A zero for the first parameter in DEFLTS will cause the program to run in the batch mode.)

The interactive mode begins by presenting the user with the main menu, offering the user eight possible options. An example of program response to options 1-8 is shown in Table 13.

Option 1 at the main menu allows the user to alter the auroral energy parameters. If this option is chosen, the program presents the user with menu 1.0, allowing a choice of program-defined dosing or user-defined dosing. If the user chooses the program-defined dosing rate, the program goes to menu 1.1 offering a selection of three energy deposition profiles corresponding to auroras of intensity IBC II, IBC III, and IBC III^{+} and displaying the current value. Entering a

Table 12. Sample of LNSPEC File.

1	2	3	4	5	6	7	8
(Preface: approximately 64 lines of identifying information.)							
C $$$END3							
1736.6724	.1103987501E+06	1	0	P	35.5	46	NO
1741.1678	.2338593579E+06	1	0	P	34.5	46	NO
1745.6316	.4850611842E+06	1	0	P	33.5	46	NO
...		...					...
1969.1220	.1415501700E+10	1	0	R	32.5	46	NO
1971.2214	.1026515076E+10	1	0	R	33.5	46	NO
1973.2799	.7378481590E+09	1	0	R	34.5	46	NO
C $$$END NO$$$							
2230.0109	.2655262309E+03	00011	00001	P108		626	CO2
2232.8427	.4289189907E+03	00011	00001	P106		626	CO2
2235.6514	.6894373094E+03	00011	00001	P104		626	CO2
...		...					...
2383.5094	.9921045253E+02	01111	01101	R 99		626	CO2
2383.5736	.7867638783E+02	01111	01101	R100		626	CO2
2383.8070	.6452974842E+02	01111	01101	R101		626	CO2
C $$$END CO2$$$							

1. Line position (cm^{-1}).
2. Line radiance (photons/cm^2 sr sec).
3. Upper vibrational state.
4. Lower vibrational state.
5. Branch.
6. Lower-state angular momentum.
7. Isotope.[35]
8. Species.

Table 13. Input Parameter Menus for Example Shown.

```
1.0 REVIEW OR MODIFY AURORA ENERGY INFORMATION...

1. PROGRAM DEFINED DOSING
2. USER SUPPLIED DOSING

CURRENT SETTING: 1


1.1 REVIEW OR MODIFY IBC CLASS...

2. IBC II (ALPHA = 2.9, TOTAL FLUX = 12.9)
3. IBC III (ALPHA = 5.0, TOTAL FLUX = 100)
4. IBC III+ - IV (ALPHA = 10, TOTAL FLUX = 400)

CURRENT SETTING: 3


2.0 REVIEW OR MODIFY GEOGRAPHIC INFORMATION...

1. OBSERVER LATITUDE (+ = NORTH):  47.
2. OBSERVER LONGITUDE (+ = EAST):  -120.
3. OBSERVER ALTITUDE (KM):  300.
4. LOS NADIR ANGLE (DEGREES):  75.77
5. LOS AZIMUTH (DEGREES):  20.
6. MAXIMUM ALTITUDE OF INTEREST(KM):  158.


3.0 REVIEW OR MODIFY TIME INFORMATION...

1. UNIVERSAL TIME (HR):  0.
2. UNIVERSAL TIME (MIN):  0.
3. UNIVERSAL TIME (SEC):  0.
4. DAY OF THE YEAR:  79.
5. DURATION OF AURORA (SEC): 900.
6. TIME OF OBSERVATION, RELATIVE TO ONSET OF AURORA (SEC):    900.00
```

Table 13. (Continued)

```
4.0 CHOOSE NO DENSITY PROFILE:

1. HIGH DENSITY PROFILE
2. MEDIUM DENSITY PROFILE
3. BACKGROUND RADIANCE NOT CALCULATED.

CURRENT CHOICE: 1


5.0 REVIEW OR MODIFY SPECTRAL PARAMETERS:

1. LOWER BOUND OF SPECTRUM (CM ** -1):  1700.
2. UPPER BOUND OF SPECTRUM (CM ** -1):  2400.
3. FWHM OF SPECTROMETER RESPONSE FUNCTION (CM ** -1): .10000E+02
4. SPECTROMETER RESPONSE FUNCTION: HAMMING
5. NUMBER OF HALF WIDTHS: 20.
6. MAXIMUM NUMBER OF POINTS IN SPECTRUM: 2000


6.0 AURORAL ARC BOUNDARIES

1. GEOMAGNETIC BOUNDARY DEFINITION
2. GEOGRAPHIC BOUNDARY DEFINITION

CURRENT SETTING: 2


6.2 REVIEW OR MODIFY AURORAL GEOGRAPHIC BOUNDARIES

1. NORTHERN EDGE OF AURORA (DEG, + = NORTH):  58.
2. SOUTHERN EDGE OF AURORA (DEG, + = NORTH):  57.1
3. EASTERN EDGE OF AURORA (DEG, + = EAST):  -5.
4. WESTERN EDGE OF AURORA (DEG, + = EAST):  20.
```

zero at this menu causes a return to the main menu with no change in the default value.

If the user-defined dosing is chosen, the program then allows the user to choose either a Maxwellian or a Gaussian functional form for

the electron spectral number flux density at the top of the atmosphere. If a Maxwellian form is chosen, the user is presented with menu 1.21, allowing input of two parameters, the total energy flux and the characteristic energy, specifying the energy distribution. If the user chooses a Gaussian form, the user is presented with menu 1.22, allowing input of three input parameters. These are the total energy flux, position of the peak of the distribution, and the characteristic width of the distribution. Entering a zero at either of the menus 1.21 or 1.22 returns the user to the main menu.

Option 2 at the main menu allows the user to modify geographic information via menu 2.0. The parameters accessible via this menu include the observer geographic latitude, longitude and altitude, the nadir and azimuth angle of the line-of-sight, and the maximum altitude of interest. All values input from the terminal are checked for validity. Entering a zero at this menu returns the user to the main menu.

Option 3 at the main menu allows the user to access time information via menu 3.0. The user may change the time of the observation as given by the day of the year and the universal time-of-day. The user may also enter the time of the observation relative to the beginning of auroral dosing and the duration of auroral dosing. Entering a zero at this menu returns the user to the main menu.

Option 4 at the main menu allows the user to control the NO background calculation via menu 4.0. At this menu the user may choose to disable the NO background calculation, or may choose to have the back-

ground calculated using a medium or a high NO density profile. Entering a zero at this menu returns the user to the main menu.

Option 5 at the main menu allows the user to review or modify, via menu 5.0, the character of the synthetic spectrum generated. The user may choose the maximum and minimum wavenumber of the spectrum, the full-width-at-half-maximum (FWHM) of the spectrometer response function, the shape of the spectrometer response function, the number of half-widths of the response function to be used in the calculation of each point in the spectrum, and the maximum number of points in the spectrum. If the user selects option 4 in this menu, the program presents the user with menu 5.4, allowing a choice from five possible spectrometer response functions: triangular, Gaussian, sinc, Hamming, and rectangular. After the user enters a selection, the program returns to menu 5.0. Entering a zero at menu 5.0 returns the user to the main menu.

Option 6 at the main menu allows the user to input the boundaries of the auroral dosing zone. Menu 6.0 allows the user to choose either geomagnetic or geographic boundary definitions. Choosing geomagnetic boundaries presents the user with menu 6.1, allowing the user to input north, south, east and west boundaries of the auroral zone via uncorrected geomagnetic local time and latitude. Choosing geographic boundaries presents the user with menu 6.2, allowing the definition of the auroral zone using geographic coordinates. Entering a zero at the menus 6.0, 6.1, or 6.2 will return the user to the main menu.

Option 7 at the main menu will cause the program to update the

file DEFLTS with the most recent set of program control parameters and then halt. Entering a zero at the main menu causes the program to proceed with the calculation.

3.2.2 DEFLTS

If the value of the first parameter in the file DEFLTS is equal to zero, the program will run in batch mode, proceeding directly with the calculation using the values of the user-defined program control parameters, as stored in the file DEFLTS.

The file DEFLTS contains 10 lines of data, each line prefaced with a series of comments that facilitate direct modification of the data. These comment lines explain the data line and give the format of the data contained in the line.

During execution of DAARC, the program does not check to see if the input parameters in DEFLTS are within bounds. DEFLTS will be rewritten using the new values of parameters that may have been changed during the parameter input procedure. The comment lines in the file are preserved.

3.2.3 ALLDAT

The input data file ALLDAT contains three independent sections, each prefaced with a marker allowing a program to go directly to the section required. The first section of the file, prefaced by the marker "$$$MODELAT$$$", contains information defining the model atmosphere. This information includes, as a function of altitude, the temperature, atmosphoric mass density, mean molecular mass, number density of N_2, number density of O_2, number density of O, and two number

density profiles of NO. The data correspond to 100 altitudes from 30 to 300 kilometers.

The next section of the file, prefaced by the marker "$$$ARGEFF$$$", contains data giving the auroral production efficiencies for the four band systems: NO ($\Delta v = 1$), NO ($\Delta v = 2$), NO^+ ($\Delta v = 1$), and NO^+ ($\Delta v = 2$), in that order. Each set of data for a given band system begins with values for the array variable TBDEF(i, j), where TBDEF is the total band system production efficiency (that is, the number of photons emitted per electron-ion pair produced), i (i = 1, 4) is the band system, and j is the altitude slab. The data are given for the altitude slabs 31 through 66, corresponding to altitudes from 90 to 160 kilometers.

The next datum is NVL(i), the number of individual bands in the i^{th} band system. Following this are values for the fractional production efficiencies, FREF(i, k, j), where k is the particular band in the i^{th} band system. The data are ordered with the variable k varying more quickly than the variable j.

The last section of the file ALLDAT, prefaced by the marker "$$$SLOWDAT$$$", contains data used in the SLOWCO2 subroutine of the program CO2.

3.2.4 LINE25

Input file LINE25, a sample of which is shown in Table 8, contains the positions and Einstein A-coefficients for the NO fundamental and overtone lines and the NO^+ fundamental lines. The format of the data is similar to that found in the AFGL Atmospheric Absorption Line Com-

pilation[35] or HITRAN database with the exception that the Einstein A-coefficient has been substituted for the absorption line intensity, S.

LINE25 contains data on NO fundamental and overtone transitions, up to transitions with upper vibrational level, v', of 12, and NO^+ fundamental transitions up to v' = 14. The AARC input procedures allow comment lines to be included as part of the file LINE25.

3.2.5 LCO2

The input file LCO2, part of which is shown in Table 11, contains the positions and absorption line intensities of the CO_2 lines as recorded in the AFGL line compilation[35]. The data contained in this file are for the CO_2 00011 → 00001 transition for the isotopes 626, 636, 628, 627, 638, 637, and 828, though only the first four are involved in the AARC calculation. The file also contains lines for the CO_2 626 01111 → 01101 transition.

At the present time, AARC input procedures do not allow comment lines to be included as part of the file.

3.2.6 LNSPEC

The output file LNSPEC, shown in part in Table 12, contains the line positions in cm^{-1} and the line radiances in photons/cm^2 sec sr. This file, written by DAARC and appended to by CO2, is read as input by the program CONV (Figure 2). It is prefaced by a series of comment lines identifying the values of the input parameters to the calculation as well, as other calculational quantities. These are for the benefit of the user and are ignored by other programs.

The end of the identifying comment lines is signified by the file

marker "$$$END$$$". The series of NO lines then follows. The first and second field of each line is the position and intensity, respectively. The remainder of each line contains identification data for the benefit of the user. The end of the NO lines is indicated with the file marker "$$$END NO$$$". If the CO2 program is run, the output will be appended to the file at this point. The end of the CO_2 lines is indicated by the marker "$$$END CO2$$$".

3.2.7 BNDRAD

The output file BNDRAD, a sample of which is shown in Table 14, contains results pertaining to the bands as a whole and is similar in structure to the file LNSPEC. The file begins with the same series of comment lines found in LNSPEC, followed by the marker "$$$END$$$". Following that are a series of records giving the band radiances and effective temperatures for the NO and NO^+ bands as calculated by DAARC. The end of the NO and NO^+ band data is indicated by the marker "$$$END NO$$$". The CO_2 band radiances are then given, followed by the marker "$$$END CO2$$$". BNDRAD does not serve as input to any other AARC program module, but may be read by the user who desires band-related results or input to user-provided programs.

3.2.8 RELAY

The purpose of the file RELAY is to transfer data calculated in the program DAARC to the program CO2 (Figure 2). The first section of the file, indicated by the file marker "$$$LOSDAT$$$", has one line containing three parameters defining the geometry of the line-of-sight. The first field contains the tangent height of the line-of-

Table 14. BNDRAD File for Example Shown.

```
C
C
C*************** OBSERVER INFORMATION ***************
C
C LATITUDE:                                      47.00
C LONGITUDE:                                   -120.00
C ALTITUDE:                                      300.00
C NADIR ANGLE:                                    75.77
C AZIMUTH ANGLE:                                  20.00
C
C
C****************** TANGENT POINT ******************
C
C LATITUDE:                                      60.05
C LONGITUDE:                                   -110.31
C ALTITUDE:                                      100.09
C
C
C***************** AURORAL PARAMETERS ***************
C
C SOUTHERN BOUNDARY (GEOGRAPHIC LATITUDE):       57.10
C NORTHERN BOUNDARY (GEOGRAPHIC LATITUDE):       58.00
C EASTERN BOUNDARY (GEOGRAPHIC LONGITUDE):       -5.00
C WESTERN BOUNDARY (GEOGRAPHIC LONGITUDE):       20.00
C
C
C*************** BAND SYSTEMS CHOSEN ***************
C
C  NO DELTA V = 1
C  NO DELTA V = 2
C  NO+ DELTA V = 1
C  NO+ DELTA V = 2
C
C
C PROGRAM DEFINED IBC TYPE:  3 AURORA
C MAXWELLIAN FLUX DEFINED BY:
C          TOTAL FLUX =  100.0 (ERGS / CM ** 2 / S)
C          ALPHA      =    5.0 (KEV)
C
C DURATION OF AURORAL DOSING:  900.
C
C TIME OF OBSERVATION:  900.
C
C
```

Table 14. (Continued)

```
C************** START OF AURORAL ZONE **************
C
C LOS SEGMENT:                                   260
C ALTITUDE:                                   104.64
C LATITUDE:                                    57.99
C LONGITUDE:                                 -112.34
C GEOMAGNETIC LATITUDE:                        65.06
C GEOMAGNETIC TIME:                            15.40
C
C
C**************** END OF AURORAL ZONE ***************
C
C LOS SEGMENT:                                   285
C ALTITUDE:                                   109.62
C LATITUDE:                                    57.13
C LONGITUDE:                                 -113.12
C GEOMAGNETIC LATITUDE:                        64.10
C GEOMAGNETIC TIME:                            15.38
C
C LENGTH OF LINE OF SIGHT IN AURORA:          108.54
C $$$END$$$
C FILE  BNDRAD
C CONTAINS TOTAL BAND RADIANCES.
C
C BAND          BAND              EFFECTIVE     V'      V''      SPECIES
C ORIGIN        RADIANCE          TEMP
C (CM-1)        (PHOTONS /        (K)
C                SR - CM2 - S)
  1875.950      .46278E+12        219.097        1       0       NO
  1847.800      .56557E+12        219.097        2       1       NO
  1819.760      .55935E+12        219.097        3       2       NO
  1791.780      .50024E+12        219.097        4       3       NO
  1763.860      .43191E+12        219.097        5       4       NO
  1735.880      .35141E+12        219.097        6       5       NO
  1708.000      .26210E+12        219.097        7       6       NO
  1680.100      .18762E+12        219.097        8       7       NO
  1652.060      .12346E+12        219.097        9       8       NO
  1624.070      .66808E+11        219.097       10       9       NO
  1596.020      .32393E+11        219.097       11      10       NO
  1567.730      .13884E+11        219.097       12      11       NO
  3723.750      .19060E+11        219.007        2       0       NO
  3667.560      .19996E+11        219.007        3       1       NO
  3611.540      .42488E+11        219.007        4       2       NO
  3555.630      .49313E+11        219.007        5       3       NO
  3499.740      .52743E+11        219.007        6       4       NO
  3443.890      .47144E+11        219.007        7       5       NO
  3388.110      .40797E+11        219.007        8       6       NO
  3332.160      .31963E+11        219.007        9       7       NO
  3276.120      .20366E+11        219.007       10       8       NO
  3220.080      .11583E+11        219.007       11       9       NO
```

Table 14. (Continued)

```
  3163.750      .58328E+10          219.007        12        10      NO
  2344.170      .13312E+11          219.450         1         0      NO+
  2311.510      .17429E+11          219.450         2         1      NO+
  2278.770      .18289E+11          219.450         3         2      NO+
  2245.930      .17309E+11          219.450         4         3      NO+
  2213.000      .15195E+11          219.450         5         4      NO+
  2179.970      .12338E+11          219.450         6         5      NO+
  2146.850      .92048E+10          219.450         7         6      NO+
  2113.690      .51949E+10          219.450         8         7      NO+
  2080.340      .33242E+10          219.450         9         8      NO+
  2046.940      .30870E+10          219.450        10         9      NO+
  2013.440      .27464E+10          219.450        11        10      NO+
  1979.860      .17313E+10          219.450        12        11      NO+
  1946.180      .24056E+09          219.450        13        12      NO+
  1912.400      .40639E+08          219.450        14        13      NO+
  4655.680      .60126E+09          219.253         2         0      NO+
  4590.280      .12425E+10          219.253         3         1      NO+
  4524.700      .17591E+10          219.253         4         2      NO+
  4458.930      .21007E+10          219.253         5         3      NO+
  4392.970      .21803E+10          219.253         6         4      NO+
  4326.820      .20062E+10          219.253         7         5      NO+
  4260.540      .13577E+10          219.253         8         6      NO+
  4194.030      .10315E+10          219.253         9         7      NO+
  4127.280      .11155E+10          219.253        10         8      NO+
  4060.380      .11443E+10          219.253        11         9      NO+
  3993.300      .82542E+09          219.253        12        10      NO+
  3926.040      .13185E+09          219.253        13        11      NO+
  3858.580      .25357E+08          219.253        14        12      NO+
  1875.950      .66584E+13          472.581         1         0      NO
 NO  DELTA V = 1     .10216E+14 PHOTONS / CM2 - SR - S
 NO  DELTA V = 2     .34128E+12 PHOTONS / CM2 - SR - S
 NO+ DELTA V = 1     .11944E+12 PHOTONS / CM2 - SR - S
 NO+ DELTA V = 2     .15522E+11 PHOTONS / CM2 - SR - S
C $$$END NO$$$
C BAND          BAND                                V'      V''      SPECIES
C ORIGIN        RADIANCE
C (CM-1)        (PHOTONS /
C               SR - CM2 - S)
  2349.143      .82338E+12                        00011   00001     CO2(626)
  2283.488      .22733E+11                        00011   00001     CO2(636)
  2340.014      .16711E+10                        00011   00001     CO2(627)
  2332.113      .86057E+10                        00011   00001     CO2(628)
  2336.633      .17114E+11                        01111   01101     CO2(626)
C $$$END CO2$$$
```

sight in kilometers. The second and third parameters define the region of auroral dosing along the line-of-sight by giving the altitude of the line-of-sight when it enters and leaves the auroral arc. The second parameter is the lower altitude of the two points. A negative value for either of these two parameters indicates that that boundary lies between the tangent point and the observer. For instance, if both parameters are negative then the region of auroral dosing lies entirely on the observer's side of the tangent point.

The next section of the file, indicated by the marker "$$$QEDEP$$$", contains the electron-ion pair production profile. The production in pairs/cm^3 sec is given for each altitude listed in the file ALLDAT.

The last section of the file RELAY, prefaced by the file marker "$$$TIMDAT$$$", contains one line of data pertaining to the time-dependent calculation. The first field contains the parameter TS, which gives the initial value for the size of the time increments in the CO2 calculation. The second field contains the parameter DOSET, the time relative to the onset of auroral dosing that the observation is made. The third and fourth parameters are TSMIN and TSMAX, the lower and upper bounds of the time increment in the CO2 calculation, respectively. The fifth parameter is FRCO, the maximum allowed fractional change per time step in the densities of the species involved in the CO2 calculation. The sixth parameter, TEND, is the duration of the auroral dosing in seconds. The last two parameters give the multiplicative factor for adjustment of the time increment and the time

increment for writing output.

3.2.9 CO2OUT

The file CO2OUT is an informational file written by the program CO2. This file contains input data such as the model atmosphere density profiles, the pair production profile, the initial upper-state densities, and vibrational temperatures. It also contains intermediate results such as the densities and vibrational temperatures at the end of each iteration.

3.2.10 TAPE5

The output file TAPE5 is an informational file written by the program CO2. This file contains the line radiances and optical depths for the CO_2 lines involved in the calculation.

3.2.11 TAPE6

The output file TAPE6 is an informational file similar to the file TAPE5. In addition to the line radiances from the CO2 calculation, this file informs the user of the conditions along the line-of-sight, including data on the densities, kinetic temperatures, and vibrational temperatures both inside and outside the zone of auroral dosing. This file also contains data from the AFGL line file used in the CO2 calculation.

3.2.12 VIBTEMP, BACKDAT, and LOSDAT

The program module CO2 uses three temporary data files for internal communication. These files are rewritten for each species involved in the CO2 calculation. The first file, VIBTEMP, holds the vibrational temperatures as a function of altitude within the auroral

zone for the particular CO_2 band system being calculated.

The next file, BACKDAT, contains data on the background CO_2 parameters outside the dosing region for the particular band system being calculated. This data includes, as a function of altitude, the pressure, density, vibrational temperature outside the dosing region, and the ν_2 temperature.

The last file, LOSDAT, is used for communication between the two parts of the CO2 calculation, namely the SLOWCO2 vibrational temperature calculation and the line-by-line radiative transport code (NLTEA). This file contains three lines of control parameters. The first line contains data defining the molecule of interest, the isotope of interest, data on the vibrational energies involved in the transition, and data on the statistical weights involved in the transition. The second line contains parameters defining the branches to be calculated, the range of rotational lines, the upper and lower state indices, the lineshape option, and the lower and upper limits of the range in cm^{-1}. The third line of data defines the line-of-sight.

3.2.13 BLOCKDATA QEDEP

The block data section of the program DAARC contains the following data: values for the speed of light, Planck's constant, the second radiation constant, acceleration due to gravity, Boltzmann's constant, and Avogadro's number; three sets of data giving the elecron-ion pair production profiles for the standard built-in aurores of class IBC II, IBC III, and IBC III+; and NO and NO^+ band origins.

4. EXAMPLE

We present here a sample run of the AARC calculation. This example involves the calculation of the infrared radiance with dosing due to an IBC III aurora over approximately 108 km of the line-of-sight. The tangent height of the line-of-sight is approximately 100 km and the dosing is on the near side of the tangent point.

Table 13 shows the series of menus tabulating the data input to the program, and Table 14 presents the file BNDRAD, including the preface which summarizes the geometry, auroral energy and other data concerning the run, and the total band radiances calculated. Figure 22 shows a medium resolution (10 cm^{-1} FWHM) synthetic spectrum covering the entire range calculated.

Also shown is a second example (dashed line in Figure 22) with the dosing moved to the far side of the tangent point. The boundaries for auroral dosing in this example are from 61.8 to 62.65 degrees north geographic latitude. Care was taken to ensure that the dosing takes place over the same distance on the line-of-sight and over the same range of altitudes. From the figure, one can observe that over the spectral range from 1700 - 2000 cm^{-1} the spectral radiance is identical to the near side case. This is because the NO lines are optically thin. For the range from 2000 to 2400 cm^{-1} the far side aurora shows the effect of the optical thickness of the CO_2 lines. Figure 23 shows a higher resolution (1 cm^{-1} FWHM) spectrum of the range 2250 - 2400 cm^{-1}.

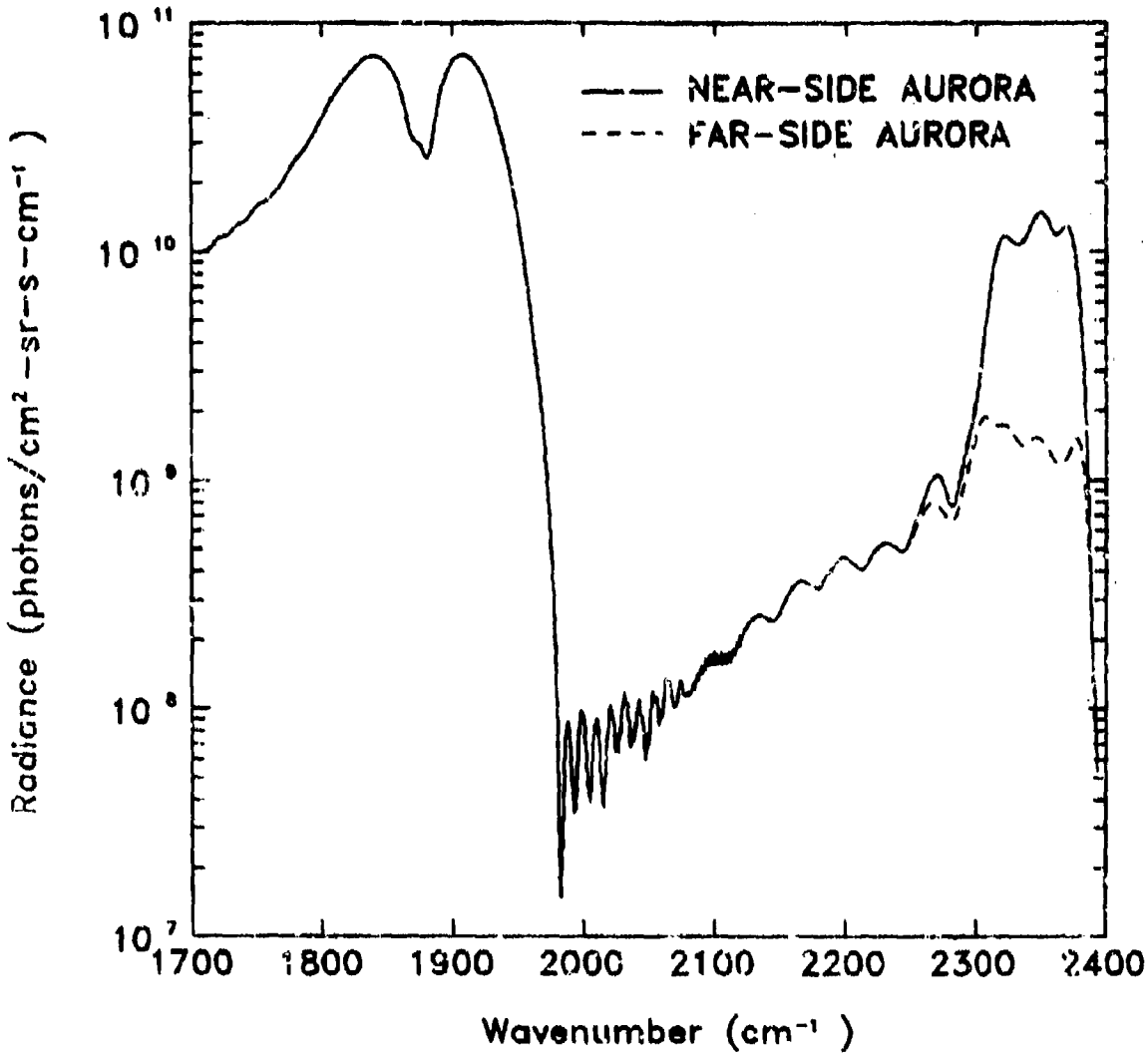

Figure 22. Synthetic Spectrum Generated by Example Using 10 cm^{-1} FWHM Hamming Function. Also shown is spectrum generated with aurora moved to far-side of tangent point.

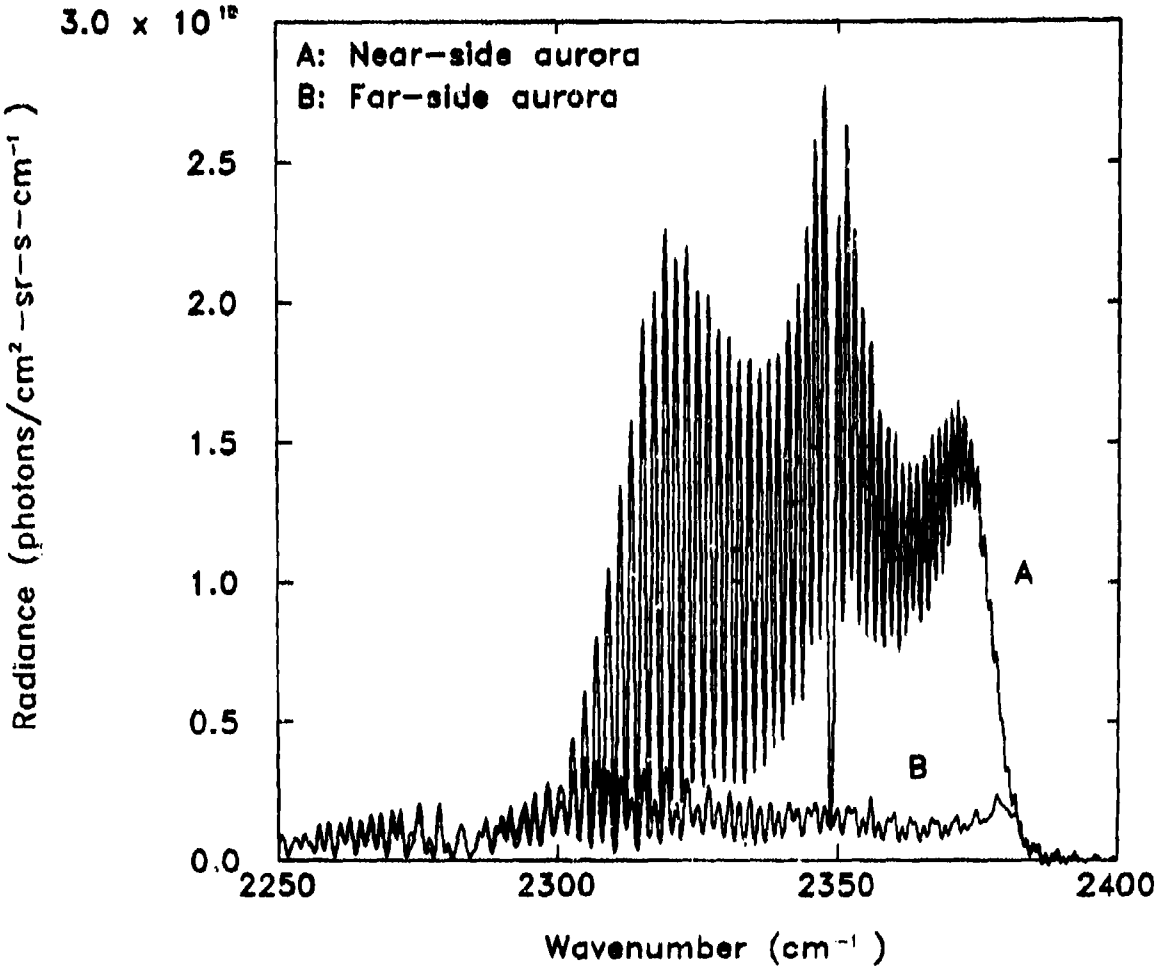

Figure 23. Higher Resolution Synthetic Spectra of Example Using 1 cm^{-1} FWHM Hamming Function.

References

1. Whalen, J.A., O'Neil, R.R., and Picard, R.H. (1985) "The Aurora," Chapter 12 of Handbook of Geophysics and the Space Environment, ADA 167000, A.S. Jursa, Editor. Air Force Geophysics Laboratory, Hanscom AFB, Massachusetts, pp. 12-1 to 12-42.

2. Stair, A.T., Jr., Ulwick, J.C., Baker, K.D., and Baker, D.J. (1975) Rocketborne observations of atmospheric infrared emissions in the auroral region, in Atmospheres of Earth and the Planets, B.M. McCormac, Editor. D. Reidel Publishing Co., Dordrecht, p. 335.

3. Gordiets, B.F., and Markov, M.N. (1977) Infrared radiation in the energy balance of the upper atmosphere, Kosm. Issled. 15: 725-35 [transl: (1976) Cosm. Res. 15: 633-41].

4. Kockarts, G. (1980) Nitric oxide cooling in the terrestrial thermosphere, Geophys. Res. Lett. 7: 137-40.

5. Gordiets, B.F., Kulikov, Yu.N., Markov, M.N., and Marov, M.Ya. (1982) Numerical modeling of the thermospheric heat budget, J. Geophys. Res. 87: 4504-14.

6. Zachor, A.S., and Sharma, R.D. (1985) Retrieval of non-LTE vertical structure from a spectrally resolved infrared limb radiance profile, J. Geophys. Res. 90: 467-75.

7. Baker, K.D., Baker, D.J., Ulwick, J.C., and Stair, A.T., Jr., (1977) Measurements of 1.5- to 5.3-μm infrared enhancements associated with a bright auroral breakup, J. Geophys. Res. 82: 3518.

8. Rawlins, W.T., Caledonia, G.E., Gibson, J.J., and Stair, A.T., Jr.(1981) Infrared emission from NO($\Delta\nu$ = 1) in an aurora: Spectral analysis and kinetic interpretation of HIRIS measurements, J. Geophys. Res. 86: 1313.

9. Reidy, W.P., Degges, T.C., Hurd, A.G., Stair, A.T., Jr., and Ulwick, J.C. (1982) Auroral nitric oxide concentration and infrared emission, J. Geophys. Res. 87: 3591-8.

10. Stair, A.T., Jr., Pritchard, J., Coleman, I., Bohne, C., Williamson, W., Rogers, J., and Rawlins, W.T. (1983) Rocketborne cryogenic (10° K) high-resolution interferometer spectrometer flight HIRIS: auroral and atmospheric IR emission spectra, Appl. Opt. 22: 1056.

11. Vallance Jones, A., and Gattinger, R.L. (1971) Infrared spectrum of aurora, in The Radiating Atmosphere, B.M. McCormac, Editor. D. Reidel, Dordrecht, pp. 176-84.

12. Baker, D., Pendleton, W., Jr., Steed, A., and Huppi, R. (1977) Near-infrared spectrum of an aurora, J. Geophys. Res. 82: 1601-9.

13. Gattinger, R.L., and Vallance Jones, A. (1981) Quantitative spectroscopy of the aurora. V. The spectrum of strong aurora between 10 000 and 16 000 Å, Can. J. Phys. 59: 480-7.

14. Huppi, R.J., and Stair, A.T., Jr. (1979) Aurorally enhanced infrared emissions, Appl. Opt. 18: 3394.

15. Vallance Jones, A. (1975) A model for the excitation of optical aurora and some of its applications, Can. J. Phys. 53: 2267-84.

16. Rees, M.H. (1975) Processes and emissions associated with electron precipitation, in Atmospheres of Earth and the Planets, B.M. McCormac, Editor. D. Reidel Publishing Co., Dordrecht, pp. 323-33.

17. Meier, R.R., Conway, R.R., Feldman, P.D., Strickland, D.J., and Gentieu, E.P. (1982) Analysis of nitrogen and oxygen far UV auroral emissions, J. Geophys. Res. 87: 2444.

18. Strickland, D.J., Jasperse, J.R., and Whalen, J.A. (1983) Dependence of auroral FUV emissions on the incident electron spectrum and neutral atmosphere, J. Geophys. Res. 88: 8051-62.

19. Degen, V. Private communication.

20. Tarr, P.W., Archer, D.H., and Utterback, N.G. (1974) Studies of Auroral Simulation, DNA Report No. 3297F.

21. Hurd, A.G., Carpenter, J.W., Degges, T.C., Grieder, W.F., Reidy, W.P., Shepherd, O., Stair, A.T., Jr., O'Neil, R.R., Ulwick, J.C., Baker, D.J., and Baker, K.D. (1977) Comparison of ICECAP and EXCEDE rocket measurements with computer code predictions, AFGL-TR-77-0060, AD-A047526.

22. Picard, R.H., Winick, J.R., Sharma, R.D., Zachor, A.S., Espy, P.J., and Harris, C.R. (1987) Interpretation of infrared measurements of the high-latitude thermosphere from a rocketborne interferometer, Adv. Space Res., 7(No. 10):23-30

23. Roble, R.G., and Rees, M.H. (1977) Time-dependent studies of the aurora: Effects of particle precipitation on the dynamic morphology of ionospheric and atmospheric properties, Planet. Space Sci. 25: 991-1010.

24. Kumer, J.B. (1977) Theory of the CO_2 4.3 μm aurora and related phenomena, J. Geophys. Res. 82: 2203.

25. Caledonia, G.E., and Kennealy, J.P. (1982) NO infrared radiation in the upper atmosphere, Planet. Space Sci. 30: 1043-56.

26. Sharma, R.D., Siani, R.D., Bullitt, M.K., and Wintersteiner, P.P. (1983) A computer code to calculate emission and transmission of infrared radiation through non-equilibrium atmospheres, AFGL-TR-83-0168, ADA137162.

27. Kennealy, J.P., Del Greco, F.P., Caledonia, G.E., and Green, B.D. (1978) Nitric oxide chemiexcitation occurring in the reaction between metastable nitrogen atoms and oxygen molecules, J. Chem. Phys. 69: 1574-84.

28. Smith, M.A., Bierbaum, V.M., and Leone, S.R. (1983) Infrared chemiluminescence from vibrationally excited NO^+: product branching in the $N^+ + O_2$ ion-molecule reation, Chem. Phys. Lett. 94:398-403.

29. Green, B.D., Caledonia, G.E., Blumberg, W.A.M., and Cook, F.H. (1984) Absolute production rates and efficiencies of NO in electron-irradiated N_2/O_2 mixtures, J. Chem. Phys. 80: 773-8.

30. U.S. Standard Atmosphere, 1976, NOAA-S/T 76-1562. National Oceanic and Atmospheric Administration, Washington, D.C.

31. Rees, M.H. (1964) Auroral ionization and excitation by incident energetic electrons, Planet. Space Sci. 111: 1209-18.

32. Grün, A.E. (1957) Luminescenz-photometrische Messungen der Energieabsorption im Strahlungsfeld von Elektronenquellen Eindimensionaler Fall im Luft, Z. Naturforsch. 112a: 89-95.

33. Rees, M.H. (1975) Magnetospheric substorm energy dissipation in the atmosphere, Planet. Space Sci. 23: 1589-1596.

34. Wintersteiner, P.P., and Sharma, R.D. (1985) Update of an Efficient Computer Code (NLTE) to Calculate Emission and Transmission of Radiation Through Non-Equilibrium Atmospheres, AFGL-TR-85-0240, AD A172556.

35. Rothman, L.S., Gamache, R.R., Barbe, A., Goldman, A., Gillis, J.R., Brown, L.R., Toth, R.A., Flaud, J.-M., and Camy-Payret, C. (1983) AFGL atmospheric absorption line parameters compilation: 1982 edition, Appl. Opt. 22: 2247.

36. Rothman, L.S., Goldman, A., Gillis, J.R., Gamache, R.R., Pickett, H.M., Poynter, R.L., Husson, N., and Chedin, A. (1982) AFGL trace gas compilation: 1982 version, Appl. Opt. 22: 1616-627.

37. Rothman, L.S., Gamache, R.R., Goldman, A., Brown, L.R., Toth, R.A., Pickett, H.M., Poynter, R.L., Flaund, J.-M., Camy-Payret, C., Barke, A., Husson, N., Rinsland, C.P., and Smith, M.A.H. (1987) The HITRAN database: 1986 edition, Appl. Opt. 26: 4058-4097.

38. Offermann, D., Friedrich, V., Ross, P., and Von Zahn, U. (1981) Neutral gas composition measurements between 80 and 120 km, Planet. Space Sci. 24: 747.

39. Sharp, W.E. (1985) Upper limits to [O] in the lower thermosphere from airglow, Planet. Space Sci. 33: 571.

40. Bethe, H. (1930) Zur Theorie des Durchgangs schneller Korpuskularstrahlen durch Materie, Ann. Phys. (Leipzig) 15: 325-400.

41. Bethe, H., and Heitler, W. (1934) On the stopping of fast particles and on the creation of positive electrons, Proc. Roy. Soc. (London) A146: 83-112.

42. Lewis, H.W. (1950) Multiple scattering in an infinite medium, Phys. Rev. 178: 526-9.

43. Spencer, L.V. (1955) Theory of electron penetration, Phys. Rev. 198: 1597-1615.

44. Chamberlain, J.W. (1961) Physics of the Aurora and Airglow, Academic Press, New York, pp. 284-92.

45. Jasperse, J.R., and Strickland, D.J. (1981) Approximate Analytic Solutions for the Primary Auroral Electron Flux and Related Quantities, AFGL-TR-81-0069, ADA102905.

46. Bethe, H. (1933) "Quantenmechanik der Ein- und Zwei-Elektronenprobleme," Chapter 3 of Handbuch der Physik, Vol. 24/1, H. Geiger and K. Scheel, Editors. Springer-Verlag, Berlin, pp. 273-560.

47. Green, A.E.S., and Barth, C.A. (1965) Calculations of ultraviolet molecular nitrogen emissions from the aurora, J. Geophys. Res. 170:1083-92.

48. Peterson, L.R., Sawada, T., Bass, J.N., and Green, A.E.S. (1973) Electron energy deposition in a gaseous mixture, Comp. Phys. Commun. 15: 239-62.

49. Maeda, K. (1965) Diffusion of low-energy auroral electrons in the atmosphere, J. Atm. Terr. Phys. 127: 259.

50. Berger, M.J., Seltzer, S.M., and Maeda, K. (1970) Energy deposition by auroral electrons in the atmosphere, J. Atm. Terr. Phys. 132: 1015-45.

51. Berger, M.J., Seltzer, S.M., and Maeda, K. (1974) Some new results on electron transport in the atmosphere, J. Atm. Terr. Phys. 136: 591-617.

52. Walt, M., MacDonald, W.M., and Francis, W.E. (1967) "Penetration of auroral electrons into the atmosphere," in Physics of the Magnetosphere, R.L. Carovillano, J.F. McClay, and H.R. Radoski, Editors. D. Reidel Publishing Company, Dordrecht, Netherlands, p. 354.

53. Banks, P.M., Chappell, C.R., and Nagy, A.F. (1974) A new model for the interaction of auroral electrons with the atmosphere: Spectral degradation, backscatter, optical emission, and ionization, J. Geophys. Res. 179: 1459-70.

54. Banks, P.M., and Nagy, A.F. (1970) Concerning the influence of elastic scattering upon photoelectron transport and escape, J. Geophys. Res. 175: 1902.

55. Strickland, D.J., Book, D.L., Coffey, T.P., and Fedder, J.A. (1976) Transport equation techniques for the deposition of auroral electrons, J. Geophys. Res. 181: 2755-64.

56. Stamnes, K. (1980) Analytic approach to auroral electron-transport and energy degradation, Planet. Space Sci. 28:427-441.

57. Stamnes, K. (1981) On the two-stream approach to electron transport and thermalization, J. Geophys. Res. 86:2405-2410.

58. Cohn, A., and Caledonia, G. (1970) Spatial distribution of the fluorescent radiation emission caused by an electron beam, J. Appl. Phys. 141: 3767-75.

59. Lazarev, V.I. (1967) Absorption of the energy of an electron beam in the upper atmosphere, Geomag. Aeron. 17: 219-23.

60. Barrett, J.L., and Hays, P.B. (1976) Spatial distribution of energy deposited in nitrogen by electrons, J. Chem. Phys. 164: 743-50.

61. Note, however, that Rees[31] calls distributions (b) and (c) "isotropic" while calling distribution (a) "cosine-dependent," as pointed out by Berger et al (1970).[49] Apparently, Rees defined isotropy, not as constant electron specific intensity Φ, but rather as constant angular flux $\Phi \cos\theta_0$. The angular flux falls in proportion to the projected area $dA \cos(\theta_0)$ as θ_0 increases, and consequently the source intensity must be increased with increased pitch angle to keep the angular flux constant. For case (b), the source intensity increases by a factor of 6 between pitch angles of 0° and 80°.

62. Valentine, J.M., and Curran, S.C. (1958) Average energy expenditure per ion pair in gases and gas mixtures, Rep. Progr. Phys. 21: 1.

63. Dalgarno, A. (1960) Range and energy loss, in Atomic and Molecular Processes, D.R. Bates, Editor. Academic Press, New York, pp. 622-42.

64. Fontheim, E.G., Stasiewicz, K., Chandler, M.O., Ong, R.S.B., Gombosi, E., and Hoffman, R.A. (1982) Statistical study of precipitating electrons, J. Geophys. Res. 187: 3469-80.

65. Wadzinski, H.T. and Jasperse, J.R. (1982) Low Energy Electron and Photon Cross Sections for O, N_2, and O_2, and Related Data, AFGL-TR-82-0008, AD A118921.

66. Jasperse, J. R. (1976) Boltzmann-Fokker-Planck model for the electron distribution function in the earth's ionosphere, Planetary Space Sci. 24: 33.

67. Jasperse, J.R., (1977) Electron distribution function and ion concentrations in the Earth's lower ionosphere from Boltzmann-Fokker-Planck theory, Planet. Space Sci., 28:743.

68. Swartz, W.E., Nisbet, J.S., and Green, A.E.S. (1971) J. Geophys. Res. 76:8425.

69. Opal, C.B., Peterson, W.K., and Beaty, E.C. (1971) Measurements of secondary-electron spectra produced by electron impact ionization of a number of simple gases, J. Chem. Phys. 55:4100-4106.

70. Rees, M.H., Stewart, A.I., and Walker, J.C.G. (1969) Secondary electrons in aurora, Planet. Space Sci. 17:1997-2008.

71. Rees, M.H. and Jones, R.A. (1973) Time dependent studies of aurora -II. Spectroscopic morphology, Planet. Space Sci. 21:1213-1235.

72. Vallance-Jones, A. and Gattinger, R.L. (1975) Quantitative spectroscopy of the aurora. III. The spectrum of medium intensity aurora between 3100 Å and 4700 Å, Can. J. Phys. 53:1806-1813.

73. Vallance-Jones, A. and Gattinger, R.L. (1976) Quantitative spectroscopy of the aurora. IV. The spectrum of medium intensity aurora between 8800 Å and 11400 Å, Can. J. Phys. 54:2128-2133.

74. Strickland, D.J. (1981) Electron transport, chemistry and optical emissions in the auroral E-layer, AFGL-TR-81-0042, AD/A102345

75. Kumer, J.B. (1975) Summary analysis of 4.3 μm data, in Atmospheres of Earth and the Planets, B.M. McCormac, Editor. D. Reidel Publishing Co., Dordrecht, p 347-358.

76. Kumer, J.B. (1979) Multidimensional time dependent structure and mechanisms for non-LTE CO_2 infrared emissions and 4.3μm aurora, AFGL-TR-79-0224, ADA084940, p 78-86.

77. Winick, J.R., Picard, R.H., Sharma, R.D., Joseph, R.A., and Wintersteiner, P.P. (1987) Radiative transfer effects on aurora enhanced 4.3 μm emission, Adv. Space Res. 7(No. 10):17.

78. Fuller-Rowell, T.J. and Rees, D. (1981) A three-dimensional time-dependent simulation of the global dynamical response of the thermosphere to a geomagnetic substorm, J. Atmos. Terr. Phys. 43:701.

79. Fuller-Rowell, T.J. (1984) A two-dimensional,high-resolution, nested grid model of the thermosphere. 1. Neutral response to an electric field "spike", J. Geophys. Res. 89, 2971-2990.

80. Fuller-Rowell, T.J. (1985) A two-dimensional,high-resolution, nested grid model of the thermosphere. 2. Response of the thermosphere to narrow and broad electrodynamic features, J. Geophys. Res. 90, 6567-6586.

81. Winkler, I.C., Stauhnik, R.A., Steinfeld, J.I., and Miller, S.M. (1986) Determination of NO(v=0-7) product distribution from the $N(^4S) + O_2$ reaction using two-photon ionization, J. Chem. Phys. 85:890-899.

82. Rahbee, A., and Gibson, J.J. (1981) Rate constants for formation of NO in vibrational levels $\nu = 2$ through 7 from the reaction $N(^4S) + O_2 \rightarrow NO^* + O$, J. Chem Phys. 74:5143-8.

83. Billingsley II, F.P. (1975) Calculated Vibrational-Rotational Intensities and Line Positions for Ground State Nitric Oxide, AFCRL-TR-75-0586, AD A019790.

84. Billingsley II, F.P. (1976) Calculated vibration-rotation intensities for $NO(X^2\Pi)$, J. Mol. Spectrosc. 61:53.

85. Gillis, J.R. and A. Goldman (1982) Nitric oxide IR line parameters for the upper atmosphere, Appl. Opt. 21:1161-1162.

86. Fernando, R.P., and Smith, I.W.M. (1979) Vibrational relaxation of NO by atomic oxygen, Chem. Phys. Lett. 66:218.

87. Glanzer, K., and Troe, J. (1975) Vibrational relaxation of NO in collisions with atomic oxygen and chlorine, J. Chem. Phys. 63:4352.

88. Murphy, R.E., Lee, E.T.P., and Hart, A.M. (1975) Quenching of vibrationally excited nitric oxide by molecular oxygen and nitrogen, J. Chem. Phys. 63:2919-2925.

89. Fernando, R.P., and Smith, I.W.M. (1981) Relaxation of NO(v=1) by radical species, J. Chem. Soc. Farad. Trans. II 77:459.

90. B.D. Green, Caledonia, G.E., Murphy, R.E., and Robert, F.X. (1982) The vibrational relaxation of NO(v=1-7) by O_2, J. Chem. Phys. 76:2441-2448.

91. Quack, M., and Troe, J. (1975) Complex formation in reactive and inelastic scattering: statistical adiabatic channel model of unimolecular processes. III, Ber. Bunsenges. Phys. Chem. 79: 170.

92. Kley, D., Lawrence, G.M., and Stone, E.J. (1977) The yield of $N(^2D)$ atoms in the dissociative recombination of NO+, J. Chem. Phys. 66:4157.

93. Werner, H.-J., and Rosmus, P. (1982) *Ab initio* calculations of radiative transition probabilities in the $^1\Sigma^+$ ground state of NO^+ ion, J. Molec. Spect. 96:362.

94. Dobler, W., Federer, W., Howorka, F., Lindinger, W., Durup-Ferguson, M., and Ferguson, E. (1983) Vibrational relaxation of $NO^+(v)$ ions in neutral collisions, J. Chem. Phys. 79:1543-1544.

95. Ferguson, E.E., Adams, N.G., Smith, D., and Alge, E. (1984) Rate coefficients at 300K for the vibrational energy transfer reactions from $N_2(v=1)$ to O_2^+ and $NO^+(v=0)$, J. Chem. Phys. 80: 6095-6098.

96. Stair, A.T., Sharma, R.D., Nadile, R.M., Baker, D.J., and Grieder, W.F. (1985) Observations of limb radiance with cryogenic spectral infrared rocket experiment, J. Geophys. Res. 90:9763-9775.

96. Kockart, G. (1980) Nitric oxide cooling in the terrestrial atmosphere, Geophys. Res. Lett. 7:137.

98. Gérard, J.-C., and Barth, C.A. (1977) High-latitude nitric oxide in the lower thermosphere, J. Geophys. Res. 82:674-680.

99. Cravens, T.E., Gérard, J.-C., LeCompte, M., Stewart, A.I., and Rusch, D.W. (1985) The global distribution of nitric oxide in the thermosphere as determined by the atmospheric Explorer D satellite, J. Geophys. Res. 90:9862-9870.

100. Kumer, J.B., and James, T.C. (1974) $CO_2(001)$ and N_2 vibrational temperatures in the $50 < z < 130$ km altitude range, J. Geophys. Res. 79:638.

101. Slanger, T.G., and Black, G. (1974) Electronic to vibrational energy transfer efficiency in the $O(^1D)$-N_2 and $O(^1D)$-CO systems, J. Chem. Phys. 60:468.

102. Link, R. (1983) A rocket observation of the 6300 Å/5200 Å intensity ratio in the dayside aurora: Implicastions for the production of $O(^1D)$ via the reaction of $N(^2D) + O_2 \rightarrow NO + O(^1D)$, Geophys. Res. Lett. 10:225-228.

103. Rusch, D.W., Gérard, J.-C., and Sharp, W.E. (1978) The reaction of $N(^2D)$ with O_2 as a source of $O(^1D)$ atoms in aurorae, Geophys. Res. Lett. 5:1043.

104. Langford, A.O., Bierbaum, V.M., and Leone, S.R. (1985) Auroral implications of recent measurements of $O(^1S)$ and $O(^1D)$ formation in the reaction of N^+ with O_2, Planet. Space Sci 33:1225-1228.

105. Taylor, R.L. (1974) Energy transfer processes in the stratosphere, Can. J. Chem. 52:1436-1451.

106. Penner, S.S. (1959) Chapter 2 of Quantitative Molecular Spectroscopy and Gas Emissivities. Addison-Wesley, Reading, Massachusetts, p. 21.

107. Reference 106, Chapter 3, p. 31.

108. Degges, T., and Smith, H.J.P. (1977) A High-Altitude Infrared Radiance Model, AFGL-TR-77-0271, AD A059242.

109. Feldstein, Y.I. (1964) Auroral morphology: I. Location of auroral zone, Tellus 16:252.

110. 1 kR = 1 kilo Rayleigh = 10^9 photons/cm^2-sec into 4π steradians.

111. Sandford, B.P. (1968) Variations of auroral emissions with time, magnetic activity and the solar cycle, J. Atmos. Terr. Phys. 30:1921.

112. Whalen, J.A., Buchau, J., and Wagner, R.A. (1971) Airborne ionospheric and optical measurements of noontime aurora, J. Atmos. Terr. Phys. 33:661.

113. Starkov, G.V. and Feldstein, Y.I. (1967) Variations of auroral oval zone boundaries, Geomagn. Aeron. 7: 62.

114. Whalen, J.A. (1983) A quantitative description of the spatial distribution and dynamics of the energy flux in the continuous aurora, J. Geophys. Res. 88:7155.

115. Akasofu, S.-I. (1968) Polar and Magnetospheric Substorms, D. Reidel, Dordrecht, Netherlands.

116. Reference 44, page 66.

117. Herzberg, G. (1950) Molecular Spectra and Molecular Structure I. Spectra of Diatomic Molecules. D. Van Nostrand Co., New York.

118. Billingsley II, F.P. (1973) Calculation of the absolute infrared intensities for the 0-1, 0-2, and 1-2 vibrational-rotational transitions in the ground state of NO^+, Chem. Phys. Lett. 23:160-166.

119. Huber, K.P. and Herzberg, G. (1979) Molecular Spectra and Molecular Structure IV. Constants of Diatomic Molecules, Van Nostrand Rienhold Co., New York.

Appendix A

Relation Between Eq. (2-14) and Rees' Ion-Pair Production Rate

We take $\rho(z)$ inside the E_0 integral in Eq. (2-14) and set

$$\frac{\rho(z)}{\rho(z_R)} = \frac{n(z)}{n(R)} \frac{\langle M(z)\rangle}{\langle M(R)\rangle} , \qquad \text{(A-1)}$$

where z_R is the altitude corresponding to the depth R, n(Z) and n(R) are number densities at depths Z and R, and $\langle M(Z)\rangle$ and $\langle M(R)\rangle$ are the corresponding mean molecular masses. Defining

$$r_0 = \frac{R}{\rho(R)} , \qquad \text{(cm)} \qquad \text{(A-2)}$$

we obtain

$$q(z) = \int_0^\infty dE_0 \frac{dF}{dE_0} \frac{E_0/r_0}{\Delta E_{ion}} \lambda\left(\frac{z}{R}\right) \frac{n(z)}{n(R)} \frac{\langle M(z)\rangle}{\langle M(R)\rangle} . \qquad \text{(A-3)}$$

If the mean molecular mass does not vary over the region of energy deposition and the electron flux is monoenergetic with energy E_1,

$$\frac{dF}{dE_0} = F\ \delta(E_0 - E_1) \ , \tag{A-4}$$

then we obtain Rees' expression

$$q(z) = F\ \frac{E_1/r_0}{\Delta E_{ion}}\ \lambda\left(\frac{z}{R}\right)\ \frac{n(z)}{n(R)} \ . \tag{A-5}$$

Appendix B

DAARC Program Flow

MAIN PROGRAM.

This is the driver for the other parts of the program. This part opens the input-output files, calls the proper subroutines that allow input of user-defined program control parameters, calls the subroutine AARCSUB, which performs the NO calculation, and calls the subroutine LINES which generates the synthetic spectrum.

1. Open the data files ALLDAT, LINE25, LNSPEC, BNDRAD, and RELAY. The input file ALLDAT contains parameters defining the model atmosphere and parameters giving the NO auroral emission efficiency. LINE25 contains the NO line positions and Einstein emission coefficients. LNSPEC is an output file containing the NO line radiances. BNDRAD is an output file containing the NO band radiances. RELAY is an output file which transfers results from the DAARC calculation to the CO2 program.

2. Call the subroutine LOADDE. This subroutine reads the input file DEFLTS, containing the default values of the input parameters, into the character array DFLTS. The array DFLTS acts as a buffer for the input and output of the user-defined input parameters.

3. Evaluate the function ACTIVE. This function returns a value of 1 if the first parameter in the file DEFLTS is equal to 1, and returns a value of 0 if the first parameter is 0. This first parameter determines whether or not the program is to run interactively. If the function ACTIVE is equal to 1 then do the following:

3.1 Print a message to the terminal.

3.2 Call the subroutine POLL. This subroutine presents the user with the main menu, allowing the user to choose which set of parameters are to be reviewed and modified. The subroutine returns the value of the variable N.

3.3 If N equals 1, call the subroutine INAUR. This subroutine allows the user to review or modify the auroral energy parameters.

3.4 If N equals 2, call the subroutine INGEO. This subroutine allows the user to review or modify the observer and line-of-sight information.

3.5 If N equals 3, call the subroutine INTIME. This subroutine allows the user to review or modify the time information.

3.6 If N equals 4, call the subroutine INBACK. This subroutine allows the user to review or modify the NO background information.

3.7 If N equals 5, call the subroutine INSPECS. This subroutine allows the user to review or modify the spectral parameters.

3.8 If N equals 6, call the subroutine MAGGEO. This subroutine allows the user to review or modify the definition of the auroral dosing zone.

3.9 If N is not equal to 0 or 7 then go back to step 3.2. Else continue with the rest of the program. If N is equal to 7, the program will terminate after updating the file DEFLTS.

4. Call the subroutine DUMPDE. This subroutine updates the file DEFLTS with the latest set of user-defined program control parameters.

5. If N equals 7, stop.

6. Call the subroutine AARCSUB. This subroutine calculates the NO band radiances over the line-of-sight, writing the radiances to the file BNDRAD.

7. Call the subroutine LINES. This subroutine distributes the band radiances over all the lines which make up the band.

8. Write the time information to the file RELAY. This information will be used by the SLOWCO2 calculation in the CO2 program module.

9. Close the files LINE25, LNSPEC, BNDRAD, and RELAY.

10. End.

SUBROUTINE LOADDE().

This subroutine loads parameter default values into the array DFLTS. It does this by first attempting to read the file DEFLTS. If this file is unavailable, the subroutine loads the array DFLTS with values hardwired into the program.

Parameters passed through common: DFLTS(10).

1. Open the input file DEFLTS.

2. If there is no error while opening the file (that is, the file exists) do the following:

2.1 Open the file SCRATCH for temporary storage.

2.2 For I equal 1 to 10, do the following:

2.2.1 Read a line from DEFLTS into the character variable DFLTS(I).

2.2.2 Write DFLTS(I) to the file SCRATCH.

2.2.3 If the first character of the line just read is the letter 'C' go to 2.2.1. This line is a comment line contained in the file and is ignored by the program.

2.2.4 Next I.

2.3 Close the file DEFLTS.

2.4 Return.

3. If an error occurred while attempting to open the file DEFLTS (that is, the file does not exist) then do the following:

3.1 Store into the array DFLTS values that are hard wired into the program.

3.2 Return.

4. End.

FUNCTION ACTIVE().

This function determines if the user has chosen the interactive mode.

Parameters passed through common: DFLTS(10).

1. Read the value of the integer ACTIVE from the string variable DFLTS(1).
2. Return.
3. End.

SUBROUTINE POLL(N).

This subroutine presents the user with the main parameter input menu. The subroutine returns in the variable N the option that the user has chosen.

1. Print the main menu to the terminal.
2. Input from the terminal the value of the integer variable N.
3. If N is less than 0 or is greater than 7, go to step 2.
4. Return.
5. End.

SUBROUTINE INAUR(IB, IBC, IFLG).

This subroutine allows the user to input parameters defining the rate of auroral energy deposition.

Parameters passed through common: DFLTS(10), IDGM, TEFLX, AG, ALPHA, DW, and E0.

1. Input, from the string variable DFLTS(5), the values of the variables IB, IDGM, TEFLX, ALPHA, E0, and DW.
2. If the value of the variable IFLG is not equal to 1, then return.
3. Print auroral energy information menu to the terminal.
4. Input from the terminal the value of the variable IBT.
5. If IBT is not equal to 1 or 2, go to 4.
6. Set IB equal to IBT.
7. If IB equals 1, the user has chosen program defined dosing. Call the subroutine INIBC.

8. If IB equals 2, the user has chosen user defined dosing. Call the subroutine MAXGAU.

9. Write the new values of the variables IB, IDGM, TEFLX, ALPHA, E0, and DW to the string variable DFLTS(5).

10. Return.

11. End.

SUBROUTINE INIBC(IBC).

This subroutine allows the user to input the IBC class of the aurora.

1. Print the IBC class menu to the terminal.

2. Input the variable IBCT from the terminal.

3. If IBCT is not equal to 0, 2, 3, or 4 then go to 2.

4. If IBCT is equal to 2, 3, or 4 do the following:

4.1 Set IBC = IBCT.

4.2 Go to 2.

5. Else if IBCT is equal to 0, then return.

6. End.

SUBROUTINE MAXGAU().

This subroutine allows the user to choose the functional form of the electron energy distribution at the top of the atmosphere.

Parameters passed through common: IDGM, TEFLX, AG, ALPHA, DW, and E0.

1. Print the auroral parameter menu to the terminal.

2. Input the value of the parameter IBT from the terminal.

3. If IBT is less than 0 or greater than 2, go to 2.

4. Set IDGM equal to IBT.

5. If IBT is equal to 1, the user has chosen a Maxwellian energy distribution. Call the subroutine INMAX to input the Maxwellian pa-

rameters.

6. If IBT is equal to 2, the user has chosen the Gaussian energy distribution. Call the subroutine INGAUS to input Gaussian parameters.

7. Return.

8. End.

SUBROUTINE INMAX().

This subroutine allows the user to define the electron energy distribution function using a Maxwellian functional form.

Parameters passed through common: IDGM, TEFLX, AG, ALPHA, DW, and EO.

1. Print the Maxwellian parameter menu to the terminal.

2. Input the value of the parameter N from the terminal.

3. If N is less than 0 or greater then 2, go to step 2.

4. If N is equal to 1, do the following:

4.1 Input, from the terminal, the value of TEFLX, the total energy.

4.2 If TEFLX is less than 0.0, go to 4.1.

5. If N is equal to 2, do the following:

5.1 Input, from the terminal, the value of ALPHA, the characteristic energy.

6. If N is equal to 0, return.

7. Go to 2.

8. End.

SUBROUTINE INGAUS().

This subroutine allows the user to define the electron energy distribution function using a Gaussian functional form.

Parameters passed through common: IDGM, TEFLX, AG, ALPHA, DW, and EO.

1. Print the Gaussian parameter input menu to the terminal.

2. Input the value of the parameter N from the terminal.

3. If N is less than 0 or greater than 3, go to 2.

4. If N is equal to 1, do the following:

4.1 Input from the terminal the value of TEFLX, the total energy flux.

4.2 If TEFLX is less than 0.0, go to 4.1.

5. If N is equal to 2, do the following:

5.1 Input from the terminal the value of E0, the characteristic energy.

5.2 If E0 is less than 0.0, go to 5.1.

6. If N is equal to 3, do the following:

6.1 Input the value of DW, the energy width.

6.2 If DW is less than 0.0, go to 6.1.

7. If N is equal to 0, then return.

8. Go to 2.

9. End.

SUBROUTINE INGEO(HAMX, IGEOFLG)

This subroutine allows the user to input parameters defining the observational geometry.

Parameters passed through common: OBLAT, OBLONG, OBLAT, RNADIR, AZIM, and DFLTS.

1. Set PI = 2.0 * ASIN(1.0).

2. Set RAD = 180.0 / PI. This constant is used to convert from degrees to radians.

3. Input, from the string variable DFLTS(3), the default values of the parameters ZPA, SPA, OBALT, GPA, AZA, and HMAX.

4. Convert the parameters ZPA, SPA, GPA, and AZA from degrees to ra-

dians, storing the results in the variables OBLAT, OBLONG, RNADIR, and AZIM, respectively.

5. If IGEOFLG is not equal to 1, then return.

6. Print the geographic information menu to the terminal.

7. Input the value of N from the terminal.

8. If N is less than 0 or greater than 6, go to 7.

9. If N is equal to 1, do the following:

9.1 Input from the terminal the value of ZPA, the observer latitude.

9.2 If ZPA is less than -90.0 or greater than 90.0, go to 9.1.

9.3 Set OBLAT = ZPA / RAD.

10. If N is equal to 2, do the following:

10.1 Input from the terminal the value of SPA, the observer longitude.

10.2 If SPA is less than -180 or greater than 180, go to 10.1.

10.3 Set OBLONG = SPA / RAD.

11. If N is equal to 3, do the following:

11.1 Input from the terminal the value of OBALT, the altitude of the observer.

11.2 If OBALT is less than 0.0, go to 11.1.

12. If N is equal to 4, do the following:

12.1 Input from the terminal the value of GPA, the observer nadir angle.

12.2 If GPA is greater than 90.0 or less than 0.0, go to 12.1.

12.3 Set RNADIR = GPA / RAD.

13. If N is equal to 5, do the following:

13.1 Input from the terminal the value of AZA, the azimuth of the line-of-sight.

13.2 If AZA is greater than 360.0 or less than 0.0, go to 13.1.

13.3 Set AZIM = AZA / RAD.

14. If N is equal to 6, do the following:

14.1 Input from the terminal the value of HMAX, the maximum altitude of interest.

14.2 If HMAX is less than 0.0, go to 14.1.

15. If N is equal to 0, do the following:

15.1 Write the values of the parameters ZPA, SPA, OBALT, GPA, AZA, and HMAX to the string variable DFLTS(3).

15.2 Return.

16. Go to 7.

17. End.

SUBROUTINE INTIME(HR, MIN, DOY, DOSET, TEND, IFLG).

This subroutine allows the input of time information.

Parameters passed through common: DFLTS(10).

1. Input from the string variable DFLTS(2) the values of the variables HR, MIN, SEC, DOY, DOSET, and TEND.

2. If the value of the parameter IFLG is not equal to 1, then return.

3. Print the time information menu to the terminal.

4. Input from the terminal the value of N.

5. If N is less than 0 or greater than 6, go to 4.

6. If N is equal to 1, do the following:

6.1 Input from the terminal the value of HR, the hour part of the universal time of observation.

6.2 If HR is less than 0 or greater than 23, go to 6.1.

7. If N is equal to 2, do the following:

7.1 Input from the terminal the value of MIN, the minute part of

the universal time of the observation.

7.2 If MIN is less than 0 or greater than or equal to 60, go to 7.1.

8. If N is equal to 3, do the following:

8.1 Input from the terminal the value of SEC, the seconds part of the universal time of observation.

8.2 If SEC is less than 0 or greater than or equal to 60, go to 8.1.

9. If N is equal to 4, do the following:

9.1 Input from the terminal, the value of DOY, the day of the year of the observation.

9.2 If DOY is greater than 366 or less than 0, go to 9.1.

10. If N is equal to 5, do the following:

10.1 Input from the terminal the value of DOSET, the duration of the aurora in seconds.

10.2 If DOSET is less than 0, go to 10.1.

11. If N is equal to 6, do the following:

11.1 Input from the terminal the value of TEND, the time of the observation relative to the beginning of the auroral dosing.

11.2 If DOSET is less than 0, go to 11.1.

12. If N is equal to 0, do the following:

12.1 Write the values of the parameters HR, MIN, SEC, DOY, DOSET, and TEND to the string variable DFLTS(2).

12.2 Return.

13. Go to 4.

14. End.

SUBROUTINE INBACK(IBACK, LOHI, IFLG).

This subroutine allows the input of parameters defining the background calculation.

Parameters passed through common: DFLTS(10).

1. Read the values of IBACK and LOHI from the string variable DFLTS(7).

2. If IFLG is not equal to 1, then return.

3. Print to the terminal the NO density profile menu.

4. Input from the terminal the value of N.

5. If N is less than 0 or greater than 3, go to 4.

6. If N is equal to 3, the user has disabled the background calculation. Set IBACK = 0.

7. Else if N is not equal to 3 and is not equal to 0, the user has chosen an NO profile. Do the following:

7.1 Set IBACK = 1.

7.2 Set LOHI = N.

8. Write the values of IBACK and LOHI to the string variable DFLTS(7).

9. Return.

10. End.

SUBROUTINE INSPECS(GMIN, GMAX, IFLG).

This subroutine allows the input of parameters determining the character of the synthetic spectrum.

Parameters passed through common: DFLTS(10), ISHAPE, FWHM, DELMAX, and MXDLS.

1. Read from the string variable DFLTS(8), the values of GMIN, GMAX, FWHM, ISHAPE, DELMAX, and MXDLS.

2. If IFLG is not equal to 1, then return.

3. Print the spectral parameter menu to the terminal.

4. Input the value of N from the terminal.

5. If N is less than 0 or greater than 6, go to 4.

6. If N is equal to 1, do the following:

6.1 Read from the terminal the value of GMIN, the lower bound of the sythetic spectrum to be generated.

6.2 If GMIN is less than 0, go to 6.1.

7. If N is equal to 2, do the following:

7.1 Input from the terminal the value of GMAX, the upper bound of the synthetic spectrum.

7.2 If Gmax is less than 0, go to 7.1.

8. If N is equal to 3, do the following:

8.1 Input from the terminal the value of FWHM, the full-width-half-maximum of the synthetic spectrum.

8.2 If FWHM is less than 0, go to 8.1.

9. If N is equal to 4, call the subroutine INSHAPE, which allows the user to input the spectrometer response function.

10. If N is equal to 5, do the following:

10.1 Input from the terminal the value of DELMAX, the maximum number of half widths calculated within each line.

10.2 If DELMAX is less than 0, go to 10.1.

11. If N is equal to 6, do the following:

11.1 Input from the terminal, the value of MXDLS, the maximum number of points to be calculated for the spectrum.

11.2 If MXDLS is less than 0, go to 11.1.

12. If N is equal to 0, do the following:

12.1 Write the values of GMIN, GMAX, FWHM, ISHAPE, DELMAX, and MXDLS to the string variable DFLTS(8).

12.2 Return.

13. Go to 4.

14. End.

SUBROUTINE INSHAPE(ISHAPE).

This subroutine allows the user to choose the character of the spectrometer response function for the synthetic spectrum.

1. Print the spectrometer response function menu to the terminal.

2. Input from the terminal the value of ISHAPE. ISHAPE is the user's choice for the spectrometer response function. The available choices are : 1. Triangular, 2. Gaussian, 3. Sinc, 4. Hamming, and 5. Rectangular.

3. If ISHAPE is less than 1 or greater than 5, go to 2.

4. Return.

5. End.

SUBROUTINE MAGGEO(IFLG).

This subroutine allows the user to choose the manner by which the auroral dosing zone is defined.

Parameters passed through common: MORG, ARLAT2, ARLAT1, ARLONG1, ARLONG2, and DEFLTS.

1. Set PI = 2.0 * ASIN(1.0).

2. Set RAD = 180.0 / PI. This constant is used to convert from degrees to radians.

3. Input from the string variable DFLTS(6), the values of MORG, Z1, Z2, Z3, Z4, Z5, Z6, Z7, and Z8.

4. If MORG is equal to 1, the auroral dosing zone is defined via geomagnetic coordinates. Do the following:

4.1 Set ARLAT1 = Z1 / RAD.

4.2 Set ARLAT2 = Z2 / RAD.

4.3 Set ARLONG1 = Z3.

4.4 Set ARLONG2 = Z4.

5. Else if MORG is equal to 2, the auroral dosing zone is defined using geographic coordinates. Do the following:

5.1 Set ARLAT1 = Z5 / RAD.

5.2 Set ARLAT2 = Z6 / RAD.

5.3 Set ARLONG1 = Z7 / RAD.

5.4 Set ARLONG2 = Z8 / RAD.

6. If IFLG is not equal to 1, then return.

7. Print the auroral boundary menu to the terminal.

8. Input from the terminal the value of N.

9. If N is less than 0 or greater than 2, go to 8.

10. If N is equal to 1, do the following:

10.1 Set MORG = N.

10.2 Call the subroutine MAGAUR(Z1, Z2, Z3, Z4). This subroutine allows input of the magnetic boundaries of the aurora.

11. If N is equal to 2, do the following:

11.1 Set MORG = N.

11.2 Call the subroutine GEOAUR(Z5, Z6, Z7, Z8). This subroutine allows input of the geographic boundaries of the aurora.

12. Write to the string variable DFLTS(6), the values of MORG, Z1, Z2, Z3, Z4, Z5, Z6, Z7, and Z8.

13. Return.

14. End.

SUBROUTINE MAGAUR(Z1, Z2, Z3, Z4).

This subroutine allows the user to define the zone of auroral dosing using geomagnetic coordinates.

Parameters passed through common: MORG, ARLAT2, ARLAT1, ARLONG1, and ARLONG2.

1. Set PI = 2.0 * ASIN(1.0).

2. Set RAD = 180.0 / PI. This constant is used to convert from degrees to radians.

3. Set ARLAT1 = Z1 / RAD.

4. Set ARLAT2 = Z2 / RAD.

5. Set ARLONG1 = Z3.

6. Set ARLONG2 = Z4.

7. Print to the terminal the auroral geomagnetic boundary menu.

8. Input from the terminal the value of N.

9. If N is less than 0 or greater than 4, go to 8.

10. If N is equal to 1, do the following:

10.1 Input from the terminal the value of Z2, the geomagnetic latitude of the northern edge of the aurora.

10.2 If Z2 is greater than 90 or less than -90, go to 10.1.

10.3 Set ARLAT2 = Z2 / RAD.

11. If N is equal to 2, do the following:

11.1 Input from the terminal the value of Z1, the geomagnetic latitude of the southern edge of the aurora.

11.2 If Z1 is greater than 90 or less than -90, go to 11.1.

11.3 Set ARLAT1 = Z1 / RAD.

12. If N is equal to 3, do the following:

12.1 Input from the terminal the value of ARLONG1, the geomagnetic time at the eastern edge of the aurora.

12.2 If ARLONG1 is greater than 24 or less than 0, go to 12.1.

12.3 Set Z3 = ARLONG1.

13. If N is equal to 4, do the following:

13.1 Input from the terminal the value of ARLONG2, the geomagnetic time at the western edge of the aurora.

13.2 If ARLONG2 is greater than 24 or less than 0, go to 13.1.

13.3 Set Z4 = ARLONG2.

14. If N is equal to 0, then return.

15. Go to 8.

16. End.

SUBROUTINE GEOAUR(Z5, Z6, Z7, Z8)

This subroutine allows the user to define the zone of auroral dosing using geographic boundaries.

Parameters passed through common: MORG, ARLAT2, ARLAT1, ARLONG1, and ARLONG2.

1. Set PI = 2.0 * ASIN(1.0).

2. Set RAD = 180.0 / PI. This constant is used to convert from degrees to radians.

3. Set ARLAT1 = Z5 / RAD.

4. Set ARLAT2 = Z6 / RAD.

5. Set ARLONG1 = Z7 / RAD.

6. Set ARLONG2 = Z8 / RAD.

7. Print the geographic auroral boundary menu to the terminal.

8. Input the value of N from the terminal.

9. If N is less than 0 or greater than 4, go to 8.

10. If N is equal to 1, do the following:

10.1 Input from the terminal the value of Z6, the geographic latitude of the northern edge of the aurora.

10.2 If Z6 is greater than 90 or less than -90, go to 10.1.

10.3 Set ARLAT2 = Z6 / RAD.

11. If N is equal to 2, do the following:

11.1 Input from the terminal the value of Z5, the geographic latitude of southern edge of the aurora.

11.2 If Z5 is greater than 90 or less than -90, go to 11.1.

11.3 Set ARLAT1 = Z5 / RAD.

12. If N is equal to 3, do the following:

12.1 Input from the terminal the value of Z7, the geographic longitude of the eastern edge of the aurora.

12.2 If Z7 is greater than 180 or less than -180, go to 12.1.

12.3 Set ARLONG1 = Z7 / RAD.

13. If N is equal to 4, do the following:

13.1 Input from the terminal the value of Z8, the geographic longitude of the western edge of the aurora.

13.2 If Z8 is greater than 180 or less than -180, go to 13.1.

13.3 Set ARLONG2 = Z8 / RAD.

14. If N is equal to 0, then return.

15. Go to 8.

16. End.

SUBROUTINE DUMPDE().

This subroutine updates the file DEFLTS using the most recent values of the user-defined program control parameters.

Parameters passed through common: DFLTS(10).

1. Attempt to open the file DEFLTS as a pre-existing file. If successful then do the following:

1.1 Rewind DEFLTS.

1.2 Rewind the file SCRATCH, a temporary file holding a copy of the old version of DEFLTS.

1.3 For I equal 1 to 10, do the following:

1.3.1 Read one line from the file SCRATCH.

1.3.2 If the first character of that line is 'C', the line is a comment line. Do the following:

1.3.2.2 Go to 1.3.1

1.3.3 If the first character of the line is not 'C', then the line is a data line, and should be updated. Write the string variable DFLTS(I) to the file DEFLTS.

1.3.4 Next I.

1.4 Close the file DEFLTS.

1.5 Delete the file SCRATCH.

1.6 Return.

2. If an error occurred while attempting to open the file DEFLTS (the file did not exist), do the following:

2.1 Create the file DEFLTS.

2.2 For I equal 1 to 10, do the following:

2.2.1 Write the value of the string variable DFLTS(I) to the file DEFLTS.

2.2.2 Next I.

2.3 Close the file DEFLTS.

2.4 Return.

3. End.

SUBROUTINE AARCSUB(NBS, NVL, VIELOS, TEFF, DOSET, TEND).

This subroutine calculates the geometry of the line-of-sight, divides the line-of-sight into segments, and calculates the observed radiance for the NO bands.

Parameters passed through common: Q2(100), Q3(100), Q4(100), BANDOR(5, 15), H(100), T(100), RHOV(100), ATW(100), AIRM(100), DOX2(100), DOX(100), and DNO(2, 100).

1. Initialize constants.

2. Initialize user-defined program control variables by calling the subroutines INAUR, INGEO, INTIME, INBAND, INBACK, and MAGGEO.

3. Call the subroutine POSIT(1, '$$$MODELAT$$$'). This subroutine positions the file ALLDAT at the beginning of the model atmosphere

3. Call the subroutine POSIT(1, '$→ODELAT$|). This subroutine positions the file ALLDAT at the beginning of the model atmosphere data.

4. For I equal 1 to NSTP, the number of altitude steps, do the following:

4.1 Call the subroutine FETCH(1, BUFFER,EOF). This subroutine reads the file ALLDAT, returning in the string BUFFER the next line of ALLDAT for which the first character of the string is not 'C'.

4.2 Read from the string BUFFER, the values of the parameters H(I), T(I), RHOV(I), ATW(I), DN2, DOX2(I), DOX(I), DNO(1, I) and DNO(2,I). These variables are altitude, temperature, mass density, atomic weight, and number densities of N2, O2, O, and NO, respectively.

4.3 Next I.

5. Call the subroutine POSIT(1, '$$$ARCEFF$$$'). This subroutine positions the file ALLDAT at the beginning of the auroral emission production efficiencies.

6. Input from the file ALLDAT the values of TBDEF(J, N), NVL(J), and FREF(J, K, M).

7. Set P0 = (PI / 2.0) - RNADIR, where RNADIR is the nadir angle of the line-of-sight. P0 is the angular separation between the observer and the tangent point as measured at the earth's center.

8. Call the subroutine CALCTN(TNLAT, TNLONG, DUMMY, P0). CALCTN calculates the geographic latitude, TNLAT, and geographic longitude, TNLONG, of the tangent point.

9. Set OBRAD = RY(OBLAT) and TNRAD = RY(TNLAT). RY is a function which returns the radius of the earth at a particular latitude. Thus OBRAD is the radius at the observation point and TNRAD is the radius at the tangent point.

10. Calculate TNALT, the altitude of the tangent point.

11. If the altitude of the tangent point is less than 0.0, the line-of-sight intersects earth surface. Print a message and stop.

12. If the altitude of the tangent is less than H0, the line-of-sight passes through altitudes for which the program does not have data. Print a message and stop.

13. If the altitude of the tangent height is greater than HMAX, the

line-of-sight passes through altitudes for which the program does not have data. Print a message and stop.

14. Call the subroutine INITQ(Q, IB, IBC, NSTP, TNRAD). This subroutine calculates the elements of the array Q, where Q(I) is the electron-ion pair production rate per unit volume at the altitude H(I).

15. Calculate DEC, the declination of the sun based on the value of DOY, the day of the year for the observation.

16. Calculate SLONG, the geographic longitude of the sun point, based on the values of HR, MIN, and SEC, the universal time of day of the observation.

17. Call the subroutine GEOM(DEC, SLONG, SLATM, SLONGM). This subroutine calculates SLATM, the magnetic latitude of the sun point, and SLONGM, the magnetic longitude of the sun point.

18. Calculate PS, the angle intersected at earth center by the part of the line-of-sight going from the tangent point to the point where the line-of-sight passes through the altitude HMAX, the effective atmospheric ceiling.

19. Set DP = PS / (NT - 1). DP is the angular size of each segment of the line-of-sight.

20. Set variables. Set JS = 0, set JE = 0, and set FLAG = FALSE. JS records the number of the first segment of the line-of-sight to lie within the auroral dosing zone and JE records the last segment of the line-of-sight to lie within the zone. The logical variable FLAG is set to true when and if the line-of-sight crosses into the auroral dosing zone.

21. For each segment of the line-of-sight, identified by the index J, do the following, starting from the far end of the line-of-sight:

21.1 Calculate P(J), the angular separation of the segment from the tangent point.

21.2 Set ANGLE = P0 + P(J). This is the angular separation between the observer and the segment, J.

21.3 Call the subroutine CALCTN(ZL(J), SL(J), DUMMY, ANGLE). CALCTN calculates the geographic latitude, ZL(J), and geographic longitude, SL(J), of the segment, J.

21.4 Call the subroutine GEOM(ZL(J), SL(J), ZLG(J), RLONGM). GEOM calculates, ZLG(J), the geomagnetic latitude, and RLONGM, the geomagnetic longitude of the segment, J.

21.5 Set TLG(J) = GMTIME(SLONGM, RLONGM). GMTIME is a function which returns the geomagnetic time of a point having geomagnetic longitude RLONGM, given that the geomagnetic longitude of the sun point is SLONGM.

21.6 Calculate HL(J), the altitude of the segment, J.

21.7 Calculate L(J), the distance from the observer to the segment, J.

21.8 If MORG is equal to 1, then the aurora has been defined using geomagnetic coordinates. Set DLONG = TLG(J), the magnetic longitude of the segment, and DLAT = ZLG(J), the magnetic latitude of the segment.

21.9 If MORG is equal to 2, then the aurora has been defined using geographic coordinates. Set DLONG = SL(J), the geographic longitude of the segment, and set DLAT = ZL(J), the geographic latitude of the segment.

21.10 Is the segment outside the auroral zone? If it is do the following:

21.10.1 If the variable FLAG has been set to true and the variable JE is equal to 0, then this is the first segment to lie outside the auroral zone. In this case, set JE = J. If JE is not equal to zero, then this was not the first segment outside the auroral zone, and no action is taken.

21.10.2 If the variable FLAG is not equal to true, then the line-of-sight has not yet entered the auroral zone. Set JS = J. This keeps track of the last segment to lie outside the auroral zone.

21.11 If the segment is inside the auroral zone, set FLAG = TRUE.

21.12 Next J.

22. If DOSET is less than TEND, then the time of observation is after the end of the auroral dosing. Print a message to the terminal. In this case the NO calculation will be disabled.

23. If the variable FLAG is equal to false, then the line-of-sight never intersected the auroral zone. Print a message to the terminal. In this case the NO calculation will be disabled.

24. If either of the conditions in steps 22 or 23 hold, then disable the NO calculation by setting the array NVL(J), for J equal to 1...NBS, = 0. NVL is the number of bands in a band system, for

which the calculation is performed.

25. For all segments in the line-of-sight, calculate the length of each segment.

26. Set the arrays STEFF(K), TBINLOS(K) and VIBLOS(K, I) equal to 0. STEFF(K) is an accumulator used for the calculation of the effective temperature of the K th band system over the line-of-sight, TBINLOS(K) is the total radiance of the K th band system, and VIBLOS(K, I) is the radiance of the I th band in the K th band system.

27. If the variable IBACK is equal to 1, then include the background contribution to the NO emissions. Do the following:

27.1 Increment by the variable NBS by one. NBS is the number of band systems in the calculation. The background contribution is treated as a seperate contribution.

27.2 Set NVL(NBS) = 1. There is only one band in the background band system.

27.3 Store the value of the band origin of the background band in the variable BANDOR(NBS, NVL(NBS)).

27.4 Call the subroutine AIRGLO(PHEMNO, NSTP, ANO10, BANDOR, LOHI). This subroutine calculates the background NO emissions as a function of altitude, storing the values in the array PHEMNO.

27.5 For each segment of the line-of-sight, J, do the following:

27.5.1 Use linear interpolation to find the background volume emission rate at the altitude of the segment, J.

27.5.2 Interpolate to find the temperature at the altitude of the segment, J.

27.5.3 Multiply the volume emission rate by the length of the segment and add to the accumulator, VIBLOS(NBS, 1).

27.5.4 Multiply the temperature of the segment by the emission from the segment and add to the accumulator, STEFF(NBS).

27.5.5 Next J.

27.6 Set TBINLOS(NBS) = VIBLOS(NBS, 1).

28. Here the program calculates the emissions due to auroral excitation. For each segment of the line-of-sight, J, lying inside the auroral zone, do the following:

28.1 Interpolate to find the electron-ion pair production rate and the temperature for the altitude of the segment, J.

28.2 For each band system, K, except for the background band system, NBS, do the following:

28.2.1 Interpolate to find TBDEFHL, the band production efficiency appropriate for the altitude of the segment.

28.2.2 Use TBDEFHL to calculate TVBIN(K, J), the contribution of the J th segment to the K th band system radiance.

28.2.3 For all bands which make up the band system K, do the following:

28.2.3.1 Interpolate to find FREFHL, the fractional efficiency appropriate for the altitude of the segment.

28.2.3.2 Use FREFHL to calculate calculate the emission in the band I, of the K th band system from the J th segment. Add this contribution to the accumulator VIBLOS(K, I).

28.2.4 Set TBINLOS(K) = TBINLOS(K) + TVBIN(K, J). TBINLOS(K) contains a running sum of the emissions of all segments inside the auroral zone.

28.2.5 Add the kinetic temperature, THL, weighted by the band emission, to STEFF(K).

28.2.6 Next K. Go on to the next band system.

28.3 Next J. Go on to the next segment.

29. For all K, set TEFF(K) = STEFF(K) / TBINLOS(K). TEFF(K) is the band temperature for the band system K. It is the weighted average of the kinetic temperature over the line-of-sight.

30. Call the subroutines RYT1, RYT6, RYT2, RYT7, and RYT4. These subroutines write information to the files LNSPEC, BNDRAD, and RELAY.

31. Return.

32. End.

SUBROUTINE POSIT(IFILE, STRIG).

This subroutine positions the data file with unit number IFILE to the record just after the record containing the string STRIG.

1. Rewind the file.

2. Input a record from the file, placing it in the string variable, BUFFER.

3. If an error occurred while attempting to read the file, print a message to the terminal and terminate.

4. If the string STRIG does not occur within BUFFER, go to 2.

5. Return.

6. End.

SUBROUTINE FETCH(F, BUFFER, EOF).

This subroutine returns in the string BUFFER, the first record of the file F which does not have a character 'C' as its first character. This allows comment statements to be inserted into the data file.

1. Input a record from the file with unit number F, placing it in the string variable, BUFFER.

2. If an error occured while reading the file, do the following:

2.1 Set EOF = 0. This indicates to the calling routine that an error has occurred.

2.2 Return.

3. If the first character of the string BUFFER is equal to 'C', go to 1.

4. Set EOF = 0. This indicates to the calling program that the search was successful.

5. Return.

6. End.

SUBROUTINE CALCTN(TNLAT, TNLONG, AT, PO).

This subroutine calculates the geographic latitude, TNLAT, and longitude, TNLONG, of a point lying on the line-of-sight displaced from the observer by an angular distance, PO.

Parameters passed through common: OBLAT, OBLONG, OBALT, RNADIR, and

AZIM.

1. Set PI = 2.0 * ASIN(1.0).

2. Set QS = SIN(OBLAT) * COS(P0) + COS(OBLAT) * SIN(P0) * COS(AZIM), where OBLAT is the latitude of the observer, P0 is the angular separation between the observer and the point in question, and AZIM is the azimuth angle of the line-of-sight.

3. Set TNLAT = ASIN(QS), where TNLAT is the latitude of the latitude in question. This result is easily shown by examining the triangle formed on the surface of the earth with vertices at the observation point, at the point in question and at the north pole.

4. If TNALT is equal to 90.0 degrees or -90.0 degrees then the point is over one of the poles. In this case the longitude is undefined. Set TNLONG = OBLONG and return.

5. Set QC = (SIN(OBLAT) - COS(P0) * SIN(TNLAT)) / (SIN(P0) * COS(TNLAT)).

6. If QC is greater than 1.0, set QC = 1.0. If QC is less than -1.0, set QC = -1.0. These conditions may result from roundoff error.

7. Set AT = ACOS(QC). AT is the angle formed by the lines connecting the point in question with the observation point and the north pole.

8. If AZIM is less than PI, set AT = 2.0 * PI - AT. This ensures that AT is in the correct quadrant.

9. Set QC = RNUM / DEN , where RNUM = COS(P0) - SIN(OBLAT) * SIN(TNLAT) and DEN = COS(TNLAT) * COS(OBLAT)

10. If QC is greater than 1.0, set QC = 1.0. If QC is less than -1.0, set QC = -1.0. These conditions may result from roundoff error.

11. Set DELL = ACOS(QC). DELL is the angle formed by the lines running from the north pole to the point in question and from the north pole to the observation point.

12. If AZIM is less than PI, set TNLONG = OBLONG + DELL, else set TNLONG = OBLONG - DELL.

13. If TNLONG is less than -PI, add 2.0 * PI to TNLONG. If TNLONG is greater than PI, subtract 2.0 * PI from TNLONG.

14. Return.

15. End.

SUBROUTINE INITQ(Q, IB, IBC, NSTP, TNRAD).

This subroutine calculates the electron-ion pair production rate as a function of altitude, placing the rate into the array Q().

Parameters passed through common: IDGM, TEFLX, AG, ALPHA, DW, EO, Q2(100), Q3(100), Q4(100), BANDOR(5, 15), H(100), T(100), RHOV(100), ATW(100) and AIRM(100).

1. If IB is equal to 1, then the user has chosen a pre-defined production profile. Use one of the profiles stored in Q2, Q3 or Q4:

1.1 For N equal 1 to NSTP, the number of altitude steps, do the following:

1.1.1 If IBC is equal to 2, set Q(N) = Q2(N).

1.1.2 If IBC is equal to 3, set Q(N) = Q3(N).

1.1.3 If IBC is equal to 4, set Q(N) = Q4(N).

1.1.4 Next N.

2. If IB is equal to 2, the user has chosen a user defined electron energy distribution. Do the following:

2.1 Call the subroutine CAIRM(NSTP). This subroutine calculates the airmass above each altitude slab in gm/cm^2.

2.2 Call the subroutine CALAG(). This subroutine calculates the coefficient AG in the equation defining the electron energy distribution.

2.3 For N equal 1 to NSTP, do the following:

2.3.1 Set Q(N) = QED(H(N)). The function QED calculates the electron-ion pair production rate at the altitude H(N).

2.3.2 Next N.

3. Return.

4. End.

SUBROUTINE CAIRM(NALT).

This subroutine calculates the air mass above a certain altitude, and

stores it in the array, AIRM().

Parameters passed through common: H(100), T(100), RHOV(100), ATW(100), AIRM(100), C, HPL, C2, G0, and AVGN.

1. Set RE = 6378.116. RE is the radius of the earth.

2. For I equal 1 to NALT, the number of altitude steps, do the following:

2.1 Set G = G0 * (RE / (RE + H(I))) ** 2. G is the local acceleration due to gravity.

2.2 Set SCHT = BK * T(I) * AVGN / (ATW(I) * G), where BK is Boltzmann's constant, T(I) is the temperature, ATW(I) is the mean atomic weight, and AVGN is Avogadro's number. SCHT is the local density scale height.

2.3 Set AIRM(I) = RHOV(I) * SCHT, where RHOV(I) is the air density.

2.4 Next I.

3. Return.

4. End.

SUBROUTINE CALAG().

This subroutine calculates the value of the parameter AG, the normalization factor in the definition of the electron energy distribution function.

Parameters passed through common: IDGM, TEFLX, AG, ALPHA, DW, and E0.

1. Set ERFDKEV = 1.602E-09. This is a conversion factor between kilo-electron volts and ergs.

2. Set PI = 2.0 * ASIN(1.0).

3. If IDGM is equal to 1, then the user has chosen a Maxwellian definition of the electron energy distribution function. Set AG = TEFLX / (2.0 * ERFDKEV * ALPHA ** 3).

4. Else if IDGM is equal to 2, then the user has chosen a Gaussian definition of the electron energy distribution function. Do the following:

4.1 Set X = E0 / DW, where E0 is energy at the peak of the distri-

bution and DW is the characteristic width of the distribution.

4.2 Set TOENFL = 0.5 * (DW ** 3) * (SQRT(PI) * 0.5 * (1.0 + 2.0 * X ** 2) * (1.0 + ERF(X)) + X * EXP(-(X ** 2))). TOENFL integral over the energy distribution for unit flux.

4.3 Set AG = TEFLX / (TOENFL * ERFDKEV), where TEFLX is the total energy flux specified by the user.

5. Return.

6. End.

SUBROUTINE QED(ALT).

This subroutine calculates the electron-ion pair production per second per cubic centimeter at the altitude ALT.

Parameters passed through common: H(100), T(100), RHOV(100), ATW(100), AIRM(100).

1. Set ENPION = 0.035. This is the energy loss in electron volts per electron-ion pair formed.

2. Set ELOWST = 0.4. This is the minimum lower bound for the integration over energy.

3. Set PWR = 1.75. This is the exponent of the energy in the equation for the range.

4. Set RMF = 1.35. This is the width of the integration panel.

5. Set CGRUN = 4.57E-06. This is the coefficient in the equation for the range.

6. Set EMAXX = 200.0. This is the upper bound for the integration over energy.

7. Call the subroutine INTERP(ALT, H, M, IFALL, NSTP). This subroutine finds the two altitude intervals H(M - 1) and H(M) which lie below and above the altitude of interest.

8. If the INTERP failed, print a message to the screen and stop.

9. Interpolate to find RHOZ, the mass density at the altitude ALT.

10. Interpolate to find ATWZ, the mean atomic weight at the altitude of interest.

11. Interpolate to find Z, the altitude in units of g/cm^2.

12. Set FACT1 = RHOZ / (CGRUN * ENPION).

13. Calculate EMINN, the minimum energy that an electron must have in order to penetrate to the altitude ALT.

14. Set QED = 0.0.

15. If EMINN is greater than EMAXX, there is no pair production at this altitude. Return.

16. If EMINN is less than ELOWST, set EMINN = ELOWST.

17. Set TQ = 1.0 - PWR.

18. Set E2 = EMINN. The energy range from EMINN to EMAXX is divided into panels and then each panel is integrated.

19. For each integration panel do the following:

19.1 Set E1 = E2. Set E2 = RMF * E1. E1 is the lower bound and E2 is the upper bound of the integration panel.

19.2 If E2 is greater than EMAXX, set E2 = EMAXX.

19.3 Call the subroutine SVALUE(E1, E2, ASQ, ASWT) to determine the six points, ASQ(i), and the six weights, ASWT(i), for the Gaussian quadrature integration over the panel.

19.4 Set FN = (E2 - E1) / 2.

19.5 For L equal 1 to 6, for each of the Gaussian points do the following:

19.5.1 Set ENERG = ASQ(L).

19.5.2 Set RANGE = CGRUN * ENERG ** PWR.

19.5.3 Call the subroutine INTERP(RANGE, AIRM, M, IFALL, NSTP). This will determine the two points which lie above and below RANGE.

19.5.4 Interpolate to find the altitude in km which corresponds to RANGE.

19.5.5 Interpolate to find ATWR, the mean atomic weight at that altitude.

19.5.6 Calculate TERM, the contribution to the integral from the

energy, ENERG.

19.5.7 Set QED = QED + TERM.

19.5.8 Next L.

19.6 If the there are more integration panels to be included go back to step 19.1.

20. Set QED = FACT1 * QED.

21. Return.

22. End.

SUBROUTINE INTERP(H0, H, M, IFALL, NSTP).

This subroutine searches through array H to find the index M such that H(M) is greater than H0, but H(M - 1) is less than H0. If the search fails, the variable IFALL is set equal to 1.

1. Set IFALL = 1.

2. Is H(NSTP) greater than H(1)? If it is, the array is in order of increasing value. Do the following:

2.1 Is H(1) greater than H0. If it is, the variable H0 is outside the range of the array. Return.

2.2 For M equal 2 to NSTP, the number of elements of the array, do the following:

2.2.1 If H(M) is greater than or equal to H0, do the following:

2.2.1.1 Set IFALL = 0.

2.2.1.2 Return.

2.2.2 Next M.

3. If H(NSTP) is less than H(1), the array is in decreasing order. Do the following:

3.1 If H(1) is less than H0, the variable H0 is outside the range of the array. Return.

3.2 For M equal 2 to NSTP, do the following:

3.2.1 If H(M) is less than or equal to H0, do the following:

3.2.1.1 Set IFALL = 0.

3.2.1.2 Return.

3.2.2 Next M.

4. End.

SUBROUTINE SVALUE(AS1, AS2, ASQ, ASWT).

This program returns to the calling module six positions, ASQ(6), within the interval from AS1 to AS2, and the weights associated with those positions, ASWT(6), to be used for for a Gaussian quadrature integration.

1. Set CA = (AS2 - AS1) / 2.0 and set CB = (AS1 + AS2) / 2.0.

2. For J equal 1 to 6, do the following:

2.1 The six zeros of the Legendre polynomial of degree six are in the interval from -1 to 1 are symmetric about zero and are stored in the array ZZ(3). We wish to map that interval onto the interval from AS1 to AS2. If J is less than or equal to 3, do the following:

2.1.1 Set ASQ(J) = -CA * ZZ(4 - J) + CB.

2.1.2 Set ASWT(J) = WEIGHT(4 - J), where WEIGHT(I) is the coefficient corresponding to the position ZZ(I) is the Gaussian quadrature sum.

2.2 If J is greater than 3, do the following:

2.2.1 Set ASQ(J) = CA * ZZ(J - 3) + CB.

2.2.2 Set ASWT(J) = WEIGHT(J - 3).

2.3 Next J.

3. Return.

4. End.

FUNCTION FUNCT(X).

This function interpolates to find the value of the normalized energy dissipation function corresponding to the value of X. The dissipation

function is stored in the set of variables XA(23) and YA(23), the abscissa in XA and the ordinate in YA. The XA are in ascending order from 1 to 23.

1. For J equal 23 to 1, step -1, do the following:

1.1 If X is greater than XA(J), do the following:

1.1.1 Interpolate to find the value of FUNCT, based upon the values of YA(J) and YA(J + 1).

1.1.2 Return.

1.2 Next J.

2. If the program has fallen through this loop without finding an appropriate value of J, send a message to the terminal and stop.

3. End.

FUNCTION DFDE(ENERGY).

This function returns the number of electrons incident on the top of the atmosphere per square centimeter per erg per second according to the electron energy distribution function input by the user.

Parameters passed through common: IDGM, TEFLX, AG, ALPHA, DW, E0.

1. If the parameter IDGM is equal to 1, the user has specified the distribution function to be a Maxwellian. Do the following:

1.1 Set DFDE = AG * ENERGY * EXP(-ENERGY / ALPHA). Here AG is the normalization parameter to ensure that the total rate of deposition is the proper value, and ALPHA is the characteristic energy in kev.

2. Else if the parameter IDGM is equal to 2, the user has specified the distribution function to be a Gaussian. Do the following:

2.1 Calculate the argument of the exponential, arg = ((ENERGY - E0) / DW)**2, where E0 is the characteristic energy and DW is the width of the distribution function. If this exceeds 80, set the argument to 80 to avoid numerical underflow.

2.2 Set DFDE = AG * ENERGY * EXP(-arg).

3. Return.

4. End.

SUBROUTINE GEOM(RLAT, RLONG, RLATM, RLONGM).

This function calculates the geomagnetic latitude, RLATM, and the geomagnetic longitude, RLONGM, of a point having geographic latitude and longitude, RLAT and RLONG.

1. Set DELONG = RLONG0 - RLONG, where RLONG0 is the geographic longitude of the north magnetic pole.
2. Set RLATM = arcsin(sin(RLAT0) * sin(RLAT) + cos(RLAT0) * cos(RLAT) * cos(DELONG)).
3. Set RLONGM = arcsin(cos(RLAT) * sin(-DELONG) / cos(RLATM)).
4. Check that RLONGM is in the right quadrant and correct if necessary.
5. Return.
6. End.

FUNCTION GMTIME(SLONGM, RLONGM).

This function calculates the local geomagnetic time based on the local geomagnetic longitude, RLONGM, and the geomagnetic longitude of the subsolar point, SLONGM.

1. Set GMTIME = (RLONGM - SLONGM) * RAD / 15 + 12.
2. Check that the GMTIME is greater than or equal to 0, but less than or equal to 24. Correct if necessary.
3. End.

SUBROUTINE AIRGLO(PHEMNO, NSTP, ANO10, BNDORG, LOHI).

This subroutine calculates the background NO radiance as a function of altitude using a method from Caledonia and Kennealy(1982).

Parameters passed through common: DOX2(100), DOX(100), DNO(2, 100), T(100), and C2.

1. For N equal 1 to NSTP, the number of altitude steps do the following:

1.1 Set RNO01 = RNO10 * exp(-BNDORG * C2 / T(N)), where RNO01 is the rate of NO v = 0 to v = 1 excitation via collision with atomic oxygen, RNO10 is the coresponding relaxation rate,

BNDORG is the energy of the v = 1 state relative to v = 0, C2 is the second radiative constant, and T(N) is the kinetic temperature at the altitude N.

1.2 Set RBO2 = RO2 * exp(-BNDORG * C2 / T(N)), where RBO2 is the rate of excitation of NO v = 1 via collision with molecular oxygen and RO2 is the corresponding relaxation rate.

1.3 The density of NO(v = 1) is then given by: DNOV1 = (ERTHSH + RNO01 * DOX(N) + RBO2 * DOX2(N)) * DNO(N) / (ANO10 + RNO10 * DOX(N) + RO2 * DOX2(N)), where ERTHSH is the rate of v = 1 excitation due to earthshine, DOX(N) is the atomic oxygen density, DOX2(N) is the molecular oxygen density, DNO(N) is the NO density and ANO10 is the Einstein coefficient for radiation from NO v = 1 to v = 0.

1.4 Set PHEMNO(N) = ANO10 * DNOV1, where PHEMNO(N) is the volume rate of background radiation at the altitude N.

1.5 Next N.

2. Return.

3. End.

SUBROUTINE RYT1(F, TNLAT, TNLONG, TNALT, GSPEC, NBS).

This subroutine writes the following information to unit F: observer position and line-of-sight geometry, tangent point of the line-of-sight, auroral boundaries, and the band systems involved in the calculation.

Parameters passed through common: OBLAT, OBLONG, OBALT, RNADIR, AZIM, MORG, ARLAT2, ARLAT1, ARLONG1, and ARLONG2.

SUBROUTINE RYT6(F, IB, IBC, DOSET, TEND).

This subroutine writes the following information to unit F: the energy parameters of the aurora, duration of auroral dosing, and time of observation relative to the beginning of auroral dosing.

Parameters passed through common: IDGM, TEFLX, AG, ALPHA, DW, and EO.

SUBROUTINE RYT2(F, JS, JE, HL, XL, SL, ZLG, TLG, L).

This subroutine writes the following information to unit F: the coordinates of the point where the line-of-sight enters the auroral zone,

the coordinates of the point where the line-of-sight exits the auroral zone, and the length of the line-of-sight lying inside the auroral zone.

SUBROUTINE RYT7(TNALT, BD1, BD2, Q, NSTP).

This subroutine writes the following information to the file RELAY: the altitude of the tangent point of the line-of-sight, the lower altitude of the points where the line-of-sight enters or leaves the auroral zone, and the higher altitude of the points where the line-of-sight enters or leaves the auroral zone. The file RELAY is used to transfer line-of-sight information to the program CO2.

SUBROUTINE RYT4(NBS, NVL, VIBLOS, TEFF).

This subroutine writes the following information to the file BNDRAD: band identifiers, band origins, band radiances, and effective temperatures.

SUBROUTINE LINES(NBS, NVL, VIBLOS, TEFF).

This subroutine distributes the band radiances as calculated in AARCSUB to all the lines which make up the bands, according to the line strengths given in the file LINE25.

Parameters passed through common: RNU(500), EMISH(500), N, and IDENT(500).

1. Call the subroutine INBACK. This determines the value of the variable IBACK. If IBACK is equal to 1, then background radiances will be included in the output.

2. For K1 equal to 1 to NBS, where NBS is the number of band systems included in the calculation, do the following:

2.1 If K1 is equal to 2 or 4, then we are dealing with one of the overtone bands. The smallest v' is then 2. Set the variable ISTART to 2.

2.2 Otherwise we are considering a fundamental band, in which case set the value of ISTART to 1.

2.3 If K1 is not equal to NBS or IBACK is equal to 0, then we are not dealing with the background band. Set K = K1.

2.4 Otherwise, we are dealing with the background band. Rewind the file LINE25 to get back to the v = 1 --> v = 0 NO data and

set K equal to 1.

2.5 For I equal ISTART to NVL(K1), where NVL(K1) is the number of bands in the K1 band system, do the following:

2.5.1 Call the subroutine LOAD. This subroutine reads the appropriate data from the file LINE25 for the band system with upper vibrational state equal to ISTART. It uses this data and the value of the effective band temperature to calculate the relative intensity of all of the lines which make up the band. These relative intensities are stored in the array EMISH while the line positions are stored in the array RNU. A string identifying the particular line is stored in the elements of the array IDENT. The variable N is set to the number of lines in the band.

2.5.2 Set TEMISH equal to 0.

2.5.3 For J equal 1 to N, do the following:

2.5.3.1 Set TEMISH = TEMISH + EMISH(J).

2.5.3.2 Next J.

2.5.4 Calculate the renormalization constant, RENORM = VIBLOS(K1, I) / TEMISH, where VIBLOS is the total band radiance as calculated in AARCSUB.

2.5.5 For J equal 1 to N, do the following:

2.5.5.1 Set EMISH(J) = EMISH(J) * RENORM.

2.5.5.2 Write the line positions, intensities and identification to the file LNSPEC.

2.5.5.3 Next J.

2.5.6 Next I.

2.6 Next K1.

3. Return.

4. End.

SUBROUTINE LOAD(K, I, TEFF, EOF).

This subroutine inputs data from file LINE25 appropriate for the K band with upper vibrational state I. The subroutine stores the line

positions in the array RNU and calculates the relative intensities, storing them in the array EMISH. The number of lines in the band is stored in N.

Parameters passed through common: RNU(500), EMISH(500), N, IDENT(500), C, HPL, C2, GO, BK, and AVGN.

1. Set SV1 = I, where SV1 is the upper state vibrational number.

2. If K is equal to 1 or 3, we are dealing with a fundamental band. Set SV2 = SV1 - 1, where SV2 is the lower state vibrational number.

3. Otherwise we are dealing with an overtone band. Set SV2 = SV1 - 2.

4. If K is equal to 3 or 4, we are dealing with an NO^+ band. Set M1 = 'NO+'.

5. Otherwise we are dealing with an NO band. Set M1 = 'NO'.

6. Do the following:

6.1 Call the subroutine FETCH. This subroutine will return the next non-comment line from the file LINE25.

6.2 Read the values of RNU(N + 1), EINT, ALPHA, E2, V1, V2, ETRANS, BRANCH, AM, S, and D from the line returned by FETCH.

6.3 If V1 is not equal to SV1 or V2 is not equal to SV2, then the line does not belong to the band in question. Do the following:

6.3.1 Backspace on the file LINE25. This effectively returns the line retrieved so that it may be gotten on the next read.

6.3.2 Return.

6.4 Set E1 = E2 + RNU(N + 1), where E1 is the energy of the upper state, E2 is the energy of the lower state, and RNU(N + 1) is the energy of the transition.

6.5 Set EMISH(N + 1) = EINT * G * exp(-E1 * C2 / TEFF), where EINT is the Einstein emission coefficient, G is the degeneracy of the upper state, C2 is the second radiative constant, and TEFF is the effective band temperature.

6.6 Copy the identifying information into the string IDENT(N + 1).

6.7 Increment N.

6.8 Loop back to 6.

7. End.

Appendix C

CO2 Program Flow

MAIN PROGRAM.

1. Open the four data files. VIBDAT is an output file containing intermediate results from the SLOWCO2 calculation. RELAY is an input file containing results calculated by the program DAARC needed for the CO_2 calculation. ALLDAT is an input file containing parameters defining the model atmosphere and parameters important for the SLOWCO2 calculation. CO2OUT is another output file containing intermediate results from the SLOWCO2 calculation.

2. Read in model atmosphere data from the file ALLDAT. The subroutine POSIT positions the input file to the beginning of the model atmosphere data.

3. Read in the electron-ion pair production profile from the file RELAY. The subroutine POSIT positions the input file to the beginning of the profile data.

4. Read in data defining the line of sight from the file RELAY. Again, the subroutine POSIT positions the file to this information.

5. Call the subroutine DENSITY. This subroutine writes the model atmosphere input data to the file CO2OUT.

6. Call the subroutine SLOWCO2. This subroutine calculates the CO_2 vibrational temperature profile in the zone of auroral dosing.

7. Close files VIBDAT, RELAY, ALLDAT, and CO2OUT.

8. Open files TAPE5, TAPE6, BNDRAD, and LNSPEC. The files TAPE5 and TAPE6 contain output from the NLTEA calculation. BNDRAD is an output file created by DAARC, to which the CO_2 band radiances will be appended. LNSPEC is an output file created by DAARC, to which the CO_2 line radiances will be appended.

9. Call POSIT to position the two files BNDRAD and LNSPEC to the end of the NO information.

10. For the five bands CO_2 bands calculated by the SLOWCO2 routine do the following:

10.1 Call the subroutine RYT1. This subroutine writes the vibrational temperature profile in the auroral zone to the file VIBTEMP. This file is used to transfer data from the main program to the NLTEA routine.

10.2 Call the subroutine RYT2. This subroutine writes the vibrational temperature profile outside the auroral zone to the file BACKDAT. This file is used to transfer data from the main program to the NLTEA routine.

10.3 Call the subroutine RYT3. This subroutine writes the file LOSDAT. This file contains parameters controlling the execution of the NLTEA routine.

10.4 Call the subroutine NLTEA. This subroutine performs a line by line calculation of the CO_2 radiance over the line of sight. During the calculation the line radiances are written to the file LNSPEC.

10.5 Write the CO_2 band radiances to the file BNDRAD.

11. Close the files TAPE5, TAPE6, BNDRAD, and LNSPEC.

12. End

SUBROUTINE SLOWCO2(QE, TIMS, TDVIDT, KT, N1, N2, TEND).

This subroutine performs a time-dependent calculation of the CO_2 vibrational temperature due to auroral excitation.

Parameters passed through common: DN2(100), DO2(100), DCO2(100), H(100), T(100), SNO(100), CO2V2T(100), and TVIBO(100).

1. Initialize the following variables:

A43	425.0	Einstein coefficient for CO_2 emission in the 4.26-μm band.
A104	0.357	Einstein coefficient for CO_2 emission in the 10.4-μm band.
A94	0.372	Einstein coefficient for CO_2 emission in the 9.4-μm band.
SIG0	2.47E-14	000 → 001 band cross section, from Penner.[108]

FRI(1)	0.9889	626 isotopic fraction.
FRI(2)	0.0111	636 isotopic fraction.
FRI(3)	0.00074	627 isotopic fraction.
FRI(4)	0.00408	628 isotopic fraction.
FRI(5)	0.9889	626 isotopic fraction.
FRI(6)	1.00	N_2 isotopic fraction.
ECM(1)	2349.14	Transition energy for 626 001 → 000.
ECM(2)	2283.49	Transition energy for 636 001 → 000.
ECM(3)	2340.01	Transition energy for 627 001 → 000.
ECM(4)	2332.11	Transition energy for 628 001 → 000.
ECM(5)	2336.63	Transition energy for 626 011 → 010.
ECM(6)	2331.00	Transition energy for N_2^*.

2. Read the values of N1 and N2 from the file ALLDAT. N1 and N2 are the lower and upper indices of the array H giving the lower and upper bound of the atmosphere used in the calculation.

3. Read the values of the array FMXRCO2(J) from the data file ALLDAT, for J equal N1 to N2. FMXRCO2 is the CO_2 mixing ratio as a function of altitude.

4. Read the values of the array CO2V2T(J) from the data file ALLDAT), for J equal N1 to N2. CO2V2T is the CO_2 010 vibrational temperature.

5. Read the values of the array EN2VPQE(J) from the data file ALLDAT, for J equal N1 to N2. EN2VPQE is the total N_2 excitation rate per electron-ion pair.

6. For I equal N1 to N2, do the following:

6.1 Calculate DCO2(I) using the value of FMXRCO2(I). DCO2(I) is the number density of CO_2 as a function of altitude.

6.2 Calculate DCO2V2(I) using the value of FMXRCO2(I). DCO2V2(I) is the number density of CO_2 in the 010 state as a function of altitude.

6.3 Calculate DM(I). DM(I) is the total number density of the

species N_2, O_2, and O as a function of altitude.

6.4 Calculate RCO2N2(I). RCO2N2(I) is the rate coefficient for the reaction:

$$N_2^* + CO_2 \rightarrow N_2 + CO_2(001).$$

6.5 Calculate RN2O2(I). This is the rate coefficient for the reaction:

$$N_2^* + O_2 \rightarrow N_2 + O_2.$$

6.6 Calculate RCO2M(M). This is the rate coefficient for the reaction:

$$CO_2(001) + M \rightarrow CO_2(000) + M.$$

6.7 Calculate RN2O(I). This is the rate coefficient for the reaction:

$$N_2^* + O \rightarrow N_2 + O.$$

6.8 Calculate PRODN2V(I), where PRODN2V is the rate of excitation of N_2 due to auroral dosing.

6.9 For J equal 1 to 4, do the following:

6.9.1 Set DCO2LST(J, I) = FRI(J) * DCO2(I), where DCO2LST is the number density of CO_2 in the lower state for the J^{th} species.

6.9.2 Next J.

6.10 Set DCO2LST(5, I) = FRI(5) * DCO2(I).

6.11 Next I

7. Set NLO = N1 - 5, where NLO is the "bottom side".

8. Calculate GO, the acceleration due to gravity at the altitude H(NLO).

9. Calculate BTSCHT, the bottomside atmospheric scale height.

10. Read NPT, the number of escape function data points stored on the data file ALLDAT.

11. Read in the values of SIGNO(I), for I equal 1 to NPT, where SIGNO are the values of the cross section multiplied by the column density for the set of values of the band transmission function

stored on the data file.

12. Read in the values of EBP(I), for I equal 1 to NPT, where EBP are the values of the plane parallel band transmission function as tabulated by Kuner.

13. Calculate CO2TSCH, the CO_2 scale height at the top of the atmosphere, H(N2), assuming an ideal atmosphere. Set CO2TSCH = [H(N2) - H(N2 - 1)] / log[DCO2(N2 - 1) / DCO2(N2)].

14. Calculate CO2CLDN(N2), the column density at the top of the atmosphere, assuming an ideal, isothermal atmosphere. Set CO2CLDN(N2) = 1.0e+05 * CO2TSCH * DCO2(N2).

15. Set SIGNI(N2) = CO2CLDN(N2) * SIGO.

16. For K equal to N2 - 1 to N1, do the following:

16.1 Calculate CO2CLDN(K), the column density for the altitude slab, K. Set CO2CLDN(K) = CO2CLDN(K + 1) + 1.0e+05 * [H(K + 1) - H(K)] * sqrt[DCO2(K + 1) * DCO2(K)].

16.2 Set SIGNI(K) = CO2CLDN(K) * SIGO.

16.3 Next K.

17. Calculate the column density above the lower boundary, H(NL0). Set CO2CDN0 = CO2CLDN(N1) + 3.2e-04 * [DN2(NL0) + DO2(NL0)] * BTSCHT.

18. For I = N1 to N2, do the following:

18.1 Interpolate to determine the value of EBPNU(I), the plane parallel band transmission function, giving the probability that a photon will travel from the altitude H(I) to the top of the atmosphere without being absorbed.

18.2 Interpolate to determine the value of EBPNL(I), the value of the transmission function for photon transmission through a distance from the altitude H(I) to the altitude of the lower boundary of the atmosphere.

18.3 Set ESCF(I) = EBPNU(I) + EBPNL(I), where ESCF(I) is the escape function for the altitude H(I).

18.4 Next I.

19. For all bands, I = 1,..., 5 and all altitudes N = N1, ..., N2, do the following:

19.1 Calculate the radiative loss factor, AESCF(I, N) = A43 * ESCF(N) + A104 + A94, if I is equal to 1, or AESCF(I, N) = A43 + A104 + A94, otherwise.

19.2 Next N, next I.

20. Read in the value of the parameter IVIBT.

21. If IVIBT is equal to 0, all initial vibrational temperatures, TVIB0, are set equal to the kinetic temperature and the background production rate, PRDN2V0, is set equal to 0.

22. If IVIBT is equal to 1, do the following:

22.1 Read in the values of the vibrational temperatures, TVIB0, from the file ALLDAT.

22.2 For N equal N1 to N2, do the following:

22.2.1 Calculate DVIB0(1, N), the excited state density of CO_2 001, at the altitude H(N): DVIB0(1, N) = DCO2LST(1, N) * EXP(-1.439 * ECM(1) / TVIB(1,N)).

22.2.2 Set DVIB(1, N) equal to DVIB0(1, N).

22.2.3 Calculate the background production term: PRDN2V0(N) = - RCO2N2(N) * DN2(N) * DVIB0(1, N) + DVIB(1, N) * DENOM * [RCO2N2(N) * DCO2LST(1, N) + RN2O(N) * DO(N)] / [RCO2N2(N) * DCO2(N)], where DENOM is equal to RCO2M(N) * DM(N) + RCO2N2(N) * DN2(N) + AESCF(1, N). The value of PRDN2V0 will cause the excited N_2 population to relax to the proper value after the end of auroral excitation as dictated by the density of the excited CO_2 population.

22.2.4 If N is less than 40, that is if H(N) is less than 110 km, then do the following:

22.2.4.1 Set DVIB0(6, N) = [PRDN2V0(N) + RCO2N2(N) * DN2(N) * DVIB0(1, N)] / [RCO2N2(N) * DCO2(N) + RN2O(N) * DO(N)]. DVIB0(6, N) is the density of vibrationally excited N_2.

22.2.5 Else if N is greater than 40 do the following:

22.2.5.1 Set DVIB0(6, N) = DN2(N) * EXP[-1.439 * ECM(6) / TVIB(6, N)].

22.2.6 Set DVIB(6, N) = DVIB0(6, N).

22.2.7 For I equal 2 to 5, do the following:

22.2.7.1 For the four weak bands, calculate the upper-state density. Set DVIBO(I, N) = RCO2N2(N) * DCO2LST(I, N) * DVIB(6, N) / [RCO2N2(N) * DN2(N) + RCO2M(N) * DM(N) + AESCF(I, N)].

22.2.7.2 Set DVIB(I, N) = DVIBO(I, N).

22.2.7.3 Calculate the corresponding vibrational temperature. Set TVIBO(I, N) = 1.439 * ECM(I) / log[DCO2LST(I, N) / DVIB(I, N)].

22.2.7.4 Next I.

22.2.8 Next N.

23. Set TIMS(1) = 0.0. The array TIMS(I) holds the time in seconds corresponding to the Ith time step.

24. For I equal 1 to 6, do the following:

24.1 For N equal to N1 to N2, do the following:

24.1.1 Set TDVIBT(I, N - N1 + 1, 1) = TVIBO(I, N). The array TDVIBT(I, J, K) holds the value of the vibrational temperature for the Ith band, at the altitude H(J), at the K^{th} time step.

24.1.2 Next N.

24.2 Next I.

25. Set KT = 1. The counter KT keeps track of the data sets stored. Conditions for storage of data sets is the same as the conditions for writing to the output file.

26. Read the values of the following parameters from the file RELAY:

TS Initial length in seconds of the time step. The value of TS is adjusted during execution.

DOSET Duration of auroral dosing. Aurora is assumed to begin at time equal zero.

TSMIN Minimum length of time step.

TSMAX Maximum length of time step.

FRCO Maximum allowed fractional change in excited state density.

TEND — Time of observation relative to the commencement of auroral dosing.

TSMULT — Multiplicative factor by which TS is increased.

TIMINC — Maximum time between output of intermediate results.

27. Read the values of the parameters ITW and ITEND from the file ALLDAT. ITW is the number of iterations between output of intermediate results and ITEND is the maximum number of iterations calculated.

28. Set TIMES = 0.0, where TIMES is the time in seconds since the beginning of the calculation.

29. Set PDOSE = 1.0, where PDOSE is a flag indicating that auroral dosing is on.

30. Set N110 = N1 + 10. The calculation checks the magnitude of the fractional changes in excited state for altitudes less than H(N110).

31. Set IT = 1, where IT is the number of iterations calculated.

32. While TIMES is less than TEND and IT is less than ITEND, do the following:

32.1 For N equal N1 to N2, calculate the production and loss rates of the excited species. Do the following:

32.1.1 Set PROD(6, N) = PDOSE * PRODN2V(N) + PRDN2V0(N) + RCO2N2(N) * N2 * DVIB(1, N), where PROD(6, N) is the excitation rate of N_2.

32.1.2 Set XLOSS(6, N) = RN2O(N) * DO(N) + RN2O2(N) * DO2(N) + RCO2N2 * [DCO2LST(1, N) + DCO2LST(2, N) + DCO2LST(3, N) + DCO2LST(4, N) + DCO2LST(5, N)], where XLOSS(6, N) is the rate of de-excitation of excited N_2.

32.1.3 For I equal 1 to 5, calculate the rate of production and loss of the Ith CO_2 isotope. Do the following:

32.1.3.1 Set PROD(I, N) = RCO2N2(N) * DCO2LST(I, N) * DVIB(6, N).

32.1.3.2 Set XLOSS(I, N) = AESCF(I, N) + RCO2N2(N) * DN2(N) + RCO2M(N) * DM(N).

32.1.3.3 Next I.

32.1.4 Next N.

32.2 For N equal N1 to N2, using the production and loss rates just calculated, calculate the values of the excited-state densities after the time step TS. Do the following:

32.2.1 For I equal 1 to 6, do the following:

32.2.1.1 Calculate the new vibrational density, DVIB, based on the value of the old vibrational density, DVIBO. Set DVIB(I, N) = [DVIBO(I, N) + TS * PROD(I, N)] / [1.0 + TS * XLOSS(I, N)].

32.2.1.2 If N is not greater than N110 and I is equal to either 1 or 6, and the fractional change in DVIB is greater than FRCO, then do the following:

32.2.1.2.1 Set ITSMULT = 0, where ITSMULT is a flag indicating whether or not a later step should increase the value of the time step, TS.

32.2.1.2.2 Calculate a new value for the time step TS. If the new value is less than TSMIN, retain the old value and continue. Otherwise, replace the value of TS and go back to the beginning of the altitude loop, step 32.2.

32.2.1.3 Next I.

32.2.2 Next N.

32.3 If TIMES is greater than TIMEW + TIMINC, where TIMEW is the time of the last output of data, or if TIMES is approximately equal to DOSET, the time of auroral shutoff, or if IT is a multiple of ITW, then output the current values of the vibrational densities. Do the following:

32.3.1 Set TIMEW = TIMES.

32.3.2 Increment KT.

32.3.3 Set TIMS(KT) = TIMES + TS.

32.3.4 For N equal N1 to N2, do the following:

32.3.4.1 Set NL = N - N1 + 1.

32.3.4.2 For I equal 1 to 6, do the following:

32.3.4.2.1 Using the value of DVIB(I, N), calculate the vibrational temperature TVIB(I, N).

32.3.4.2.2 Set TDVIBT(I, NL, KT) = TVIB(I, N).

32.3.4.2.3 Next I.

32.3.4.3 Next N.

32.3.5 Write to the output file TAPE6 the values of the vibrational densities and temperatures, and also the production and loss rates.

32.4 For N equal N1 to N2, do the following:

32.4.1 For I equal 1 to 6, do the following:

32.4.1.1 Set DVIBO(I, N) = DVIB(I, N).

32.4.1.2 Next I

32.4.2 Next N.

32.5 If ITSMULT is equal to 1, then set TS = TS * TSMULT.

32.6 If TS is greater than TSMAX, set TS = TSMAX.

33. Return.

34. End.

Appendix D

Program CONV

MAIN PROGRAM.

Parameters passed through common: RNU(8000), EMISH(8000), NLINES, ISHAPE, FWHM, DELMAX, MXDLS, C, HPL, C2, GO, BK, and AVGN.

1. Initialize C, the speed of light, HPL, Planck's constant, GO, the acceleration due to gravity, BK, Boltzmann's constant and AVGN, Avogadro's number.

2. Call the subroutine LOADDE. This subroutine reads the input file DEFLTS, containing the default values of the input parameters, into the character array DFLTS. The array DFLTS acts as a buffer for the input and output of the user-defined input parameters.

3. Call the subroutine INSPECS. This subroutine reads the value of the parameters ISHAPE, FWHM, DELMAX, and MXDLS from the array DFLTS.

4. Open the output file SPECT and the input file LNSPEC.

5. Transfer the informational preface from the input file LNSPEC to the output file SPECT. These lines, running from the beginning of the file to a line containing the string $$$END$$$, contain information defining the observation conditions. Do the following:

5.1 Read a line from the file LNSPEC.

5.2 Write that line to SPECT.

5.3 If that line does not contain the string $$$END$$$, go to step 5.

6. Set DEL = DELMAX * FWHM, where DEL is maximum distance away from the line center in wavenumbers for which the line shape is calculated and included in the synthetic spectrum, FWHM is the full-width-at-half-maximum of the spectrometer response function, and DELMAX is the maximum distance in units of FWHM.

7. Set I = 1.

8. The file LNSPEC contains line positions and strengths which are to be read into the arrays RNU and EMISH. Do the following:

8.1 Call the subroutine FETCH. This subroutine reads the file, placing the next line which does not begin with the character 'C' (comment lines) into the string BUFFER.

8.2 If we have reached the end of the file, go to step 9.

8.3 Read the values of RNU and EMISH from the string BUFFER.

8.4 If RNU is within the wavenumber bounds of the synthetic spectrum requested by the user, set I = I + 1.

8.5 Go the step 8.

9. Call the subroutine LOADGL. This subroutine initializes the array GL, which will hold a set of wavenumber values, regularly spaced from the lower bound of the spectrum to the upper bound of the spectrum.

10. Call the subroutine LOADR. This subroutine calculates values for the array R, the spectral radiance corresponding to the wavenumber value of GL.

11. Set PMAX = ARMAX(R, NG), where the function ARMAX determines the maximum value in the array R.

12. Set PMIN = ARMIN(R, NG), where the function ARMIN determines the minimum value in the array R.

12. Write the values of GL and R to the file SPECT. Do the following:

12.1 Write the minimum and maximum values of GL., the total number of points in the spectrum, the increment in wavenumber between different points in the spectrum, and the minimum and maximum values of the spectral radiance.

12.2 Write the values of GL and R to the file using a compressed format with every tenth value of GL in the left column followed by 10 successive values of R.

13. End.

SUBROUTINE LOADDE().

This subroutine loads parameter default values into the array DFLTS.

It does this by first attempting to read the file DEFLTS. If this file is unavailable, the subroutine loads the array DFLTS with values hardwired into the program.

Parameters passed through common: DFLTS(10).

1. Open the input file DEFLTS.

2. If there is no error while opening the file (that is, the file exists) do the following:

2.1 Open the file SCRATCH for temporary storage.

2.2 For I equal 1 to 10, do the following:

2.2.1 Read a line from DEFLTS into the character variable DFLTS(I).

2.2.2 Write DFLTS(I) to the file SCRATCH.

2.2.3 If the first character of the line just read is the letter 'C' go to 2.2.1. This line is a comment line contained in the file and is ignored by the program.

2.2.4 Next I.

2.3 Close the file DEFLTS.

2.4 Return.

3. If an error occured while attempting to open the file DEFLTS (that is, the file does not exist) then do the following:

3.1 Store into the array DFLTS values which are hard-wired into the program.

3.2 Return.

4. End.

SUBROUTINE INSPECS(GMIN, GMAX, IFLG).

This subroutine allows the input of parameters determining the character of the synthetic spectrum.

Parameters passed through common: DFLTS(10), ISHAPE, FWHM, DELMAX, and MXDLS.

1. Read from the string variable DFLTS(8), the values of GMIN, GMAX,

FWHM, ISHAPE, DELMAX, and MXDLS.

2. If IFLG is not equal to 1, than return.

3. Print the spectral parameter menu to the terminal.

4. Input the value of N from the terminal.

5. If N is less than 0 or greater than 6, go to 4.

6. If N is equal to 1, do the following:

6.1 Read from the terminal the value of GMIN, the lower bound of the sythetic spectrum to be generated.

6.2 If GMIN is less than 0, go to 6.1.

7. If N is equal to 2, do the following:

7.1 Input from the terminal the value of GMAX, the upper bound of the synthetic spectrum.

7.2 If GMAX is less than 0, go to 7.1.

8. If N is equal to 3, do the following:

8.1 Input from the terminal the value of FWHM, the full-width-at-half-maximum of the synthetic spectrum.

8.2 If FWHM is less than 0, go to 8.1.

9. If N is equal to 4, call the subroutine INSHAPE, which allows the user to input the spectrometer response function.

10. If N is equal to 5, do the following:

10.1 Input from the terminal the value of DELMAX, the maximum number of half-widths calculated within each line.

10.2 If DELMAX is less than 0, go to 10.1.

11. If N is equal to 6, do the following:

11.1 Input from the terminal, the value of MXDLS, the maximum number of points to be calculated for the spectrum.

11.2 If MXDLS is less than 0, go to 11.1.

12. If N is equal to 0, do the following:

12.1 Write the values of GMIN, GMAX, FWHM, ISHAPE, DELMAX, and MXDLS to the string variable DFLTS(8).

12.2 Return.

13. Go to 4.

14. End.

SUBROUTINE FETCH(F, BUFFER, EOF).

This subroutine returns, in the string BUFFER, the first record of the file F which does not have a character 'C' as its first character. This allows comment statements to be inserted into the data file.

1. Input a record from the file with unit number F, placing it in the string variable, BUFFER.

2. If an error occured while reading the file, do the following:

2.1 Set EOF = 0. This indicates to the calling routine that an error has occurred.

2.2 Return.

3. If the first character of the string BUFFER is equal to 'C', go to 1.

4. Set EOF = 0. This indicates to the calling program that the search was successful.

5. Return.

6. End.

SUBROUTINE LOADGL(GL, NG, GMIN, GMAX, DEL)

This subroutine initializes the array GL. This array holds a set of evenly spaced points spanning the limits of the spectrum requested.

1. Set NG = 1.

2. Call the subroutine CALDEL. This subroutine calculates a suitable value for the spacing in wavenumber between the elements in the array GL.

3. Do the following:

3.1 Set GL(NG) = GMIN + DEL * (NG - 1).

3.2 If GL(NG) is greater than GMAX, set NG = NG - 1 and return.

3.3 Else set NG = NG + 1.

3.4 Go to step 3.

4. End.

SUBROUTINE CALDEL(GMIN, GMAX, DEL)

This subroutine determines the value of the increment parameter DEL, such that the interval from GMIN to GMAX is divided into less than MXDLS intervals and DEL is convenient (0.01, 0.02, 0.04, or 0.05, for example). The subroutine uses trial and error to determine DEL.

Parameters passed through common: ISHAPE, FWHM, DELMAX, and MXDLS.

1. Set DEL = 0.0001.

2. Set G = GMAX - GMIN.

3. Do the following:

3.1 Set DEL = 10 * DEL.

3.2 For J equal 1 to 4, do the following:

3.2.1 Set K = J + J / 3. As J takes on the values 1 through 4, K will assume the integer values 1, 2, 4, and 5.

3.2.2 Set ITEST = G / (K * DEL), where ITEST is the number of increments required to span the limits of the spectrum.

3.2.3 If ITEST is less than or equal to MXDLS, do the following:

3.2.3.1 Set DEL = K * DEL.

3.2.3.2 Set GMIN = INT(GMIN / DEL) * DEL + DEL.

3.2.3.3 Return.

3.2.4 Else next J.

3.3 Go to step 3.

4. End.

SUBROUTINE LOADR(R, GL, NG).

This subroutine calculates the values for the array R, the spectral radiance at the value of wavenumber GL.

Parameters passed through common: RNU, EMISH, NLINES, ISHAPE, FWHM, DELMAX, and MXDLS.

1. Set DELINC = GL(2) - GL(1), where DELINC is the increment between the wavenumber points.

2. Set the elements of the array R to 0.

3. Set DEL = DELMAX * FWHM. The algorithm calculates for a particular wavenumber, GL, the spectral radiance, R, due to all emission lines in the file LNSPEC. Since not all lines contribute to the emission at GL, DEL will provide a cutoff, giving the maximum displacement away from GL for a line to be included in the calculation.

4. Loop over all individual emission lines read from the file LNSPEC and stored in the arrays RNU and EMISH. For I equal 1 to NLINES, where NLINES is the number of lines read in, do the following:

4.1 The emission line at RNU contributes to the synthetic spectrum at points displaced from the line by an amount less than DEL. Calculate the lower and upper indices of the array GL to which the line will contribute. Do the following:

4.1.1 Set J1 = INT((RNU(I) - DEL - GL(1)) / DELINC) - 1, where J1 is to be the lower index. If J1 is less than 1, set J1 equal to 1.

4.1.2 Set J2 = 2 * INT(DEL / DELINC) + J1 + 3, where J2 is to be the upper index. If J2 is greater than NG, set J2 equal to NG.

4.2 If J1 is less than NG and J2 is greater than 1, do the following:

4.2.1 For J equal J1 to J2, do the following:

4.2.1.1 Set DELTA = ABS(GL(J) - RNU(I)), where DELTA is the displacement of the emission line from the point in the spectrum, GL, being calculated.

4.2.1.2 If DELTA is less than DEL, set R(J) = R(J) + LNSHAPE(EMISH(I), DELTA), where the function LNSHAPE calculates the contribution of the emission line to

the spectrum at GL, according to the spectrometer response function chosen.

4.2.1.3 Next J.

4.3 Next I.

5. Return.

6. End.

REAL FUNCTION LNSHPE(EMISH, DELTA).

This function returns the spectral radiance at a point displaced a distance DELTA from line center, folding in the spectrometer response function.

Parameters passed through common: ISHAPE, FWHM, DELMAX, and MXDLS.

1. If the parameter ISHAPE is equal to 1, the user has requested a triangular spectrometer response function. Do the following:

1.1 If DELTA is greater than FWHM, set LNSHPE = 0.

1.2 Else set LNSHPE = (FWHM - DELTA) / FWHM ** 2.

2. Else if the parameter ISHAPE is equal to 2, the user has requested a Gaussian response function. Do the following:

2.1 Set LNSHPE = exp(- 0.5 * X ** 2) / (sqrt(2 * PI) * SIGMA), where SIGMA = FWHM / sqrt(2 * log(2)) and X = DELTA / SIGMA.

3. Else if the parameter ISHAPE is equal to 3, the user has requested a sinc response function. Do the following:

3.1 Set LNSHPE = SINC(X) / SIGMA, where the function SINC returns the value of the sinc function for X, X = DELTA / SIGMA, and SIGMA = FWHM / 1.2067.

4. Else if the parameter ISHAPE is equal to 4, the user has requested a Hamming lineshape. Do the following:

4.1 Set LNSHPE = HAMM(X) / SIGMA, where the function HAMM returns the value of the Hamming function for the argument X, X = DELTA / SIGMA, and SIGMA = FWHM / 1.8218.

5. Else if the parameter ISHAPE is equal to 5, the user has requested a rectangular lineshape. Do the following:

5.1 If DELTA is greater than FWHM set LNSHPE = 0, else set LNSHPE = 0.5 / FWHM.

6. Set LNSHPE = EMISH * LNSHPE.

7. Return.

8. End.

FUNCTION SINC(A).

This function returns the value of the sinc function = sin(x) / x.

1. Set ARG = abs(A).

2. If ARG is greater than 0.2, set SINC = sin(A) / A.

3. Else approximate with a series. Do the following:

3.1 Set Z2 = ARG ** 2.

3.2 Set SINC = 1 + Z2 * (C1 + Z2 * (C2 + C3 * Z2)), where C1 = - 1/6, C2 = 1/120, and C3 = - 1/5040.

4. Return.

5. End.

FUNCTION HAMM(A).

This function returns the value of the Hamming function.

1. Set HAMM = (SINC(A) + A1 * (SINC(A + 1) + SINC(A - 1))) / A0, where A0 = 1.857504 and A1 = 0.428752.

2. Return.

3. End.

FUNCTION ARMIN(ARRAY, N).

This function returns the value of the smallest element in the array ARRAY.

1. Set ARMIN = ARRAY(1).

2. For I equal 2 to N, where N is the number of elements in the ar-

ray, do the following:

2.1 If ARRAY(I) is less than ARMIN, set ARMIN = ARRAY(I).

2.2 Next I.

3. Return.

4. End.

FUNCTION ARMAX(ARRAY, N).

This function returns the value of the largest element in the array ARRAY.

1. Set ARMIN = ARRAY(1).

2. For I equal 2 to N, where N is the number of elements in the array, do the following:

2.1 If ARRAY(I) is less than ARMIN, set ARMIN = ARRAY(I).

2.2 Next I.

3. Return.

4. End.

☆ U.S. GOVERNMENT PRINTING OFFICE: 1988— 501-737/80077